UNIVERSITAT DE
BARCELONA

Analysis of the contribution of Barrier-to-Autointegration Factor (BAF) to centromere function and mitosis progression

Paula Escudero Ferruz

Analysis of the contribution of Barrier-to-Auotintegration Factor (BAF) to centromere function and mitosis progression

Paula Escudero Ferruz
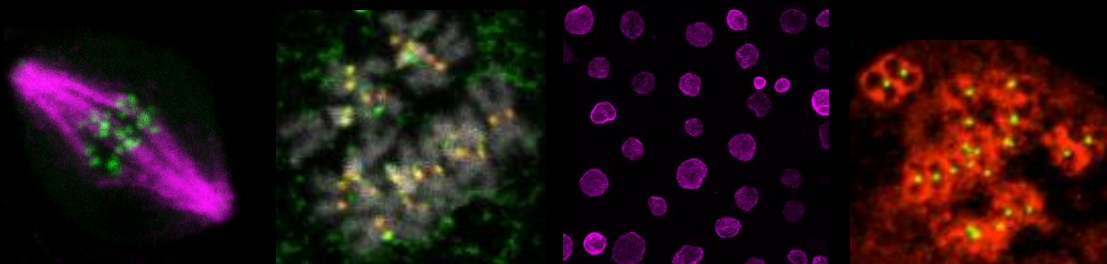
Barcelona, 2021

Tesi Doctoral
Universitat de Barcelona

Analysis of the contribution of Barrier-to-Autointegration Factor (BAF) to centromere function and mitosis progression

Memòria presentada per
Paula Escudero Ferruz

Per optar al grau de
Doctora per la Universitat de Barcelona
Programa de Genètica
Institut de Biologia Molecular de Barcelona, CSIC
Institut de Recerca Biomèdica de Barcelona, IRB

Directors de la tesis

AZORIN MARIN FERNANDO - DNI 37655533W
Firmado digitalmente por AZORIN MARIN FERNANDO - DNI 37655533W
Fecha: 2021.04.23 10:50:57 +02'00'

MONICA TORRAS LLORT - DNI 39346756N
Digitally signed by MONICA TORRAS LLORT - DNI 39346756N
Date: 2021.04.23 10:38:17 +02'00'

Dr. Ferran Azorín Marin   Dra. Mònica Torras Llort

Tutor de la tesis

Dr. Pere Martínez Serra

Doctoranda

Paula Escudero Ferruz

Barcelona 2021

ACKNOWLEDGEMENTS

Aquests quatre anys i mig de tesis han sigut un aprenentatge personal i professional d'un valor incalculable i no podria estar més agraïda de l'afecte, respecte i suport que tothom m'ha ofert.

Primer de tot, moltes gràcies, Ferran, per depositar la teva confiança en mi i haver-me donat l'oportunitat de treballar en el teu laboratori i gràcies per la bona supervisió durant aquests 4 anys.

Mònica, no hagués pogut tenir una millor supervisora que tu. He gaudit moltíssim treballant "mano a mano" al teu costat, disposada a ensenyar-me tot el que fes falta i sempre amb un tracte de luxe. Si em sento preparada per continuar la meva carrera científica és gràcies a la bona formació que m'has donat, al bon ambient que generes i a la confiança que sempre has depositat en mi. No t'imagines com et trobaré a faltar!!!

Als sèniors del *lab* Ali, Albert, Lluïsa, Jordi, Sri, Olga i Guillermo, gràcies per sempre estar disposats a oferir-me la vostra ajuda amb un somriure, per les discussions i per les xerrades informals. M'heu fet molt amens aquests quatre anys. Per a qualsevol cosa que mai necessiteu, podeu comptar amb mi.

Paula Climent, Gianmarco, Maria i Anna, gràcies per la bona acollida des de el moment zero, per la infinitat d'hores que hem passat en el PBA33, per la bonica amistat que hem forjat i per cuidar-me tant. *¡Gracias por venir, sois unos dioses!*

Paula Bujosa, gràcies per valorar-me tant, no sé com haurien sigut aquests dos últims anys sense tu. Si us plau, truca'm cada dia, fas que els meus dies siguin més bonics i t'has convertit en un suport indispensable.

Uxue, Alba i Oriol, encara sort que existiu i us he trobat. Perquè tenir un grup d'amics que està vivint la mateixa experiència que tu i que amb quatre paraules t'entenguin a la perfecció és extremadament valuós. *Cómo de diferentes somos, pero qué bien nos hemos*

complementado. Hagués estat molt perduda en el grup de *PhD students* sense vosaltres.

No puc deixar d'agrair tot el suport rebut fora del *lab*. Lau, ni pandèmies, ni mentides, ni distàncies han pogut amb la nostra amistat, sinó que l'han enfortida. Ets indispensable. Irina, et trobo molt a faltar, torna ja que t'esperem amb els braços oberts. Mariona, has passat de ser la *twin* de la Laura a ser una molt bona amiga. *Paminins, your calls and your hugs are healing. Our partnership in crime is a life term contract and I could not be happier about it. Also thanks for introducing me Sandra. San, como echo de menos nuestras escapaditas, ¡ojalá verte pronto!* Núria, ets la persona amb millor gust musical del IRB, gràcies per les xerrades pels passadissos. Ens veiem aviat en la primera fila d'algun concert. Carme i Núria, que per molt lluny que visquem no perdem l'esperit *"vesinas"*, sou un regal. Marina i Aina, quina sort saber que puc comptar amb vosaltres per passejades al costat del mar i bones xerrades. Jud, *merci* per endolcir-me els dies. *Elvira de mi corazón, eres y serás siempre mi manchega favorita.* Mele, Irene, Ania i Jordi, amb vosaltres, pizza i vi; no necessito res més. Que guai seguir creixent junts. Dalmo, el Nobel no ha arribat però gràcies per sempre creure que puc arribar tan lluny com vulgui. Des de sempre i per sempre. *Anna, you and your sweetness have become truly good friends to me. And, Katrin and Ewelina, you are a great example of the beauty of long distance friendship. Cannot wait to celebrate, my girls!*

Per últim, no puc oblidar-me de la meva família. Bel, Fina i família de Galícia, gràcies per preocupar-vos per saber com estan «els meus *bitxitus»* i per alegrar-vos infinitament dels meus èxits. I, papa i mama, sou la meva bombolla preferida, el meu màxim suport, un exemple de bones persones i, si us estimés més, rebentaria.

Cada final és un nou començament

Anònim

ABSTRACT

Abstract

This work is focused on Barrier-to-Autointegration Factor (BAF) protein. BAF is a nuclear envelope (NE) component that binds chromatin and is required for NE reassembly (NER) at mitosis exit. Previous work in our group showed that, in *Drosophila,* a small fraction of BAF (cenBAF) associates with the centromere*.* BAF function is regulated by cycles of phosphorylation and dephosphorylation. At the entry of mitosis, BAF is phosphorylated by VRK1/NHK1 kinase and is released from chromatin and the NE. At mitosis exit, protein phosphatase 2A (PP2A) dephosphorylates BAF, which resumes binding to chromatin and promotes NER. Here, we find that cenBAF remains bound to the centromere during mitosis by the action of protein phosphatase 4 (PP4), which is recruited to the centromere by the constitutive centromere component CenpC. At the same time, BAF stabilizes CenpC and PP4 at the centromere forming a functional centromeric network essential for faithful chromosome segregation. Disrupting centromeric localization of PP4 destabilizes cenBAF at centromeres and induces ectopic PP2A-mediated dephosphorylation of free phosphoBAF (pBAF) in mitosis, which results in the accumulation of BAF in a perichromosomal layer surrounding the chromosomes. Concomitantly, NE disassembly/reassembly during mitosis is altered resulting in micronuclei formation and cells with altered NE morphology. This suggests that CenpC, PP4 and cenBAF form a centromeric network that signals pBAF dephosphorylation at mitosis exit by regulating PP2A activity. We also identify T4 and S5 as the main BAF phosphosites in *Drosophila* and study the actual contribution of PP4 and PP2A to pBAF dephosphorylation.

El present treball se centra en l'estudi de la proteïna Barrier-to-Autointegration Factor (BAF). BAF és una proteïna de la membrana nuclear (MN) que s'uneix a la cromatina i té un paper essencial en el reassemblatge de la MN al final de la mitosi. BAF ha estat descrit per primer cop en el nostre grup com una nova proteïna centromèrica (cenBAF) a *Drosophila.* La localització de BAF durant el cicle cel·lular està regulada per cicles de fosforilació i defosforilació. A l'entrada de mitosi BAF és fosforilat per la kinasa VRK1/NHK1 perdent la seva afinitat per unir cromatina i la MN. Aquesta situació es manté fins que PP2A desfosforila BAF al final de la mitosi, retornant al seu estat inicial. En el present treball es mostra que BAF es manté al centròmer durant la mitosi degut a l'acció de PP4 que és reclutada al centròmer per CenpC. Al seu torn cenBAF estabilitza la localització de CenpC i PP4 al centròmer formant un entramat centromèric responsable de garantir la correcta segregació dels cromosomes. L'alteració d'aquest entramat centromèric desemboca en la desregulació de l'activitat de PP2A sobre phosphoBAF (pBAF) soluble, observant-se com a resultat una acumulació de BAF defosforilat envoltant els cromosomes a metafase i com conseqüència, provocant la formació de micronuclis i alteracions en la morfologia nuclear. També hem identificat T4 i S5 com els principals residus implicats en la fosforegulació de BAF a *Drosophila* i hem estudiat la contribució de PP4 i PP2A sobre la defosforilació de BAF.

TABLE OF CONTENTS

LIST OF ABBREVIATIONS

List of abbreviations

A	alanine
APC/C	anaphase promoting complex
BAF	Barrier-to-Autointegration Factor
CAF-1	Chromatin assembly factor 1
CAL-1	Chromosome alignment defect 1
CATD	CenpA centromere targeting domain
CCAN	Constitutive centromere associated network
CDK	cyclin-dependent kinase
CenBAF	centromeric BAF
CenpA	centromeric protein A
CenH3	centromeric histone H3 variant
CenpC	centromeric protein C
CID	centromere identifier protein
E	Glutamic acid
Endos	endosulfine
ER	endoplasmic reticulum
EVH1	enabled/VASP homology 1
FHA	fork-head associated
Flfl	Falafel
FIM	CenpC Flfl-interacting motif
Gwl	Greatwall kinase
HhH	helix-hairpin-helix motif
INM	inner nuclear membrane
LAD	lamina associated domain
LEM-d	Lap2, emerin, MAN 1-domain
LINK	linker of the nucleoskeleton and cytoskeleton
MAP	microtubule associated protein
MCC	mitotic checkpoint complex
MTOC	microtubule organizing centre
MN	micronuclei
MTS	microtubule star

MPF	maturation-promoting factor
NE	nuclear envelope
NEB	nuclear envelope breakdown
NER	nuclear envelope reassembly
NGPS	Néstor-Guillermo progeria syndrome
NHK1	nucleosomal histone kinase 1
NIFK	nucleolar protein interacting with the FHA domain of Ki-67
NUP	nucleoporin
NPC	nuclear pore complex
OA	okadaic acid
ONM	outer nuclear membrane
PES1	pescadillo ribosomal biogenesis factor 1
PIC	pre-integration complex
PP1	protein phosphatase 1
PP2A	protein phosphatase 2A
PP4	protein phosphatase 4
PP6	protein phosphatase 6
PPM	metallodependent phosphatases
PPP	phosphoprotein phosphatases
PSTP	serine/threonine-specific phosphatases
PTP	protein tyrosine phosphatases
SAC	Spindle Assembly Checkpoint
SLiM	Short Lineal interaction Motifs
SMC	Structural Maintenance Chromosomes
TWS	Twins
VRK1	Vaccinia-Related kinase 1
WDB	Widerbroast

LIST OF FIGURES AND TABLES

INTRODUCTION

1. THE CELL CYCLE

Cell cycle is the progression of events that a cell undergoes in order to give rise to two daughter cells. It consists of a long interphase (S phase) in which the DNA material is duplicated and a mitosis (M phase) where the genetic content is faithfully segregated into the two daughter cells. S and M phases are separated by two gap phases (G1 and G2 phases) where the cell grows and prepares for DNA synthesis or division (fig 1).

Cell cycle progression is monitored by the activation of cyclin-dependent kinases (CDKs). CDKs levels are stable during cell cycle but CDK activity requires binding of regulatory cyclin subunits. Cyclins are synthesized and degraded in a timely manner in order to activate CDKs at specific times during cell cycle (fig 1). Active CDKs phosphorylate and regulate the activity of target proteins that are relevant for cell cycle progression.

A series of checkpoints control cell cycle progression (fig 1). When sensing an alteration, a specific signalling pathway is activated in order to inhibit CDK activity and arrest cell cycle progression to allow proper repair of the defects. The G1-S or restriction checkpoint senses if there are enough nutrients and growth factors to properly undergo cell cycle and it also senses DNA damage. At the end of G2, the replication checkpoint detects and repairs DNA damage and senses correct cell size to enter mitosis. Later, during mitosis, the spindle assembly checkpoint (SAC) controls correct chromosome alignment and attachment to the mitotic spindle at the metaphase/anaphase transition and ensures faithful segregation of the DNA material into the daughter cells[1] (fig 1).

Alteration of the checkpoints leads to deregulated CDK activation, which promotes uncontrolled cell division and the accumulation of

mutations that eventually may cause genomic and chromosomal instability, a characteristic feature of cancer cells[2].
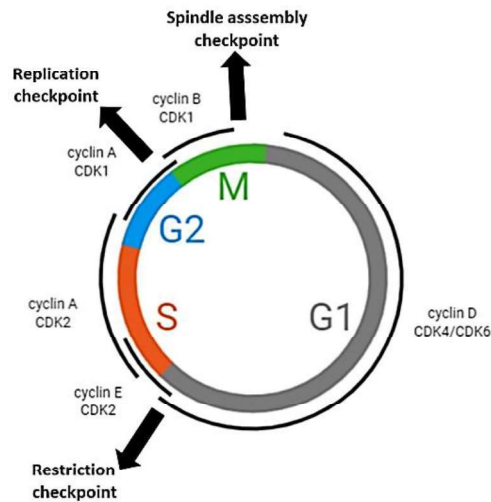
Figure 1. The cell cycle. Schematic representation of the different phases of the cell cycle (G1-S-G2-M). Cyclin-CDK complexes that are activated at specific timings are specified as well as checkpoints that control cell cycle progression (restriction checkpoint, replication checkpoint, spindle assembly checkpoint).

Mitosis is a dynamic and complex process that involves an extensive and coordinated remodelling of the nucleus. Mitosis is divided in five phases depending on the level of DNA condensation and the morphology of the cytoskeleton structure and the nuclear envelope (NE) (fig 2).
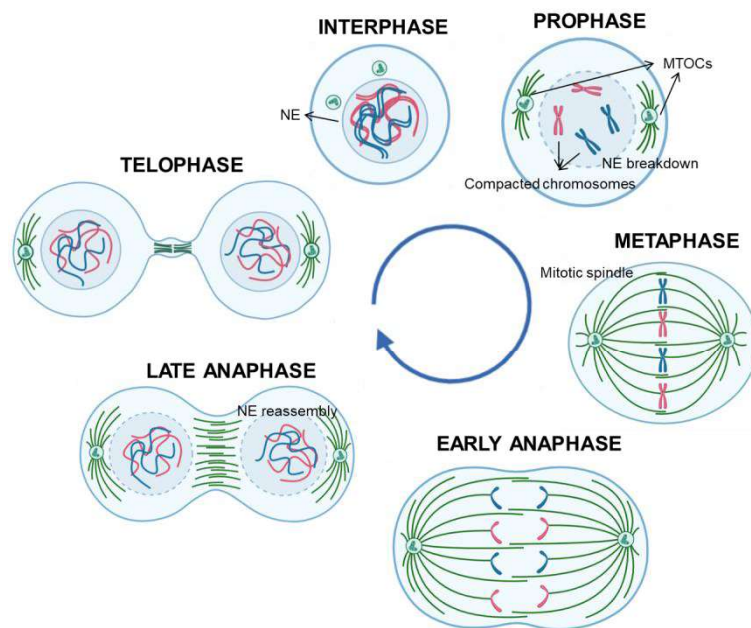
Figure 2. Mitotic phases: Schematic representation of the changes that the DNA, the cytoskeleton structure and the nuclear envelope (NE) undergo during the different phases of mitosis.

Prophase is the first step in mitosis. During prophase, the DNA material is compacted into individualized chromosomes (fig 2). There are two main mechanisms responsible for that, the formation of loops by condensing complexes and a cascade of histone modifications that involves increasing H3 phosphorylation at S10 (PS10), which is an epigenetic modification usually used to identify mitotic cells[3,4]. In addition, during prophase microtubules start to polymerase to form the mitotic spindle structure and the NE disassembles during the open mitosis of most metazoan (fig 2)[5,6].

All these processes continue during prometaphase leading to metaphase when chromosomes are found aligned at the metaphase plate. At this point, the NE is completely disassembled and the mitotic spindle is able to access and bind chromosomes (fig 2). Only when each sister chromatid is attached to opposite poles of the spindle, SAC

is satisfied and anaphase takes place (fig 1). Proper SAC function is essential to ensure faithful chromosome segregation and equal partition of the DNA material into the daughter cells.

During anaphase, centromeric cohesins, which are essential to keep sister chromatids together and generate tension, are degraded and spindle microtubules depolymerisation pulls sister chromatids to opposite poles of the cell[7]. At late anaphase, chromosomes start to decondense and the NE reassembles surrounding the bulk of decondensing chromatin (fig 2). Mitosis ends at telophase when chromatin is fully decondensed and cytokinesis takes place (fig 2)[8].

During mitosis, many cellular organelles and molecules are also remodelled and redistributed between daughter cells to ensure they are functional and capable of synthesising new proteins, metabolise nutrients, grow and response to internal and external signals[8].

2. THE NUCLEAR ENVELOPE

2.1 Structure of the NE

The NE is a highly specialized extension of the endoplasmic reticulum (ER) that acts as boundary between the nucleus and the cytoplasm. It is formed by two membranes, the outer nuclear membrane (ONM) and the inner nuclear membrane (INM). A distinct set of membrane proteins in the INM link the NE to chromatin and the nuclear lamina, providing mechanical support and contributing to genome organization. ONM and INM are connected at numerous sites creating nuclear pores where specific nuclear pore complexes (NPCs) regulate nuclear-cytoplasm transport. Moreover, the nucleoskeleton and cytoskeleton (LINC) complex anchors the NE to the actin cytoskeleton (fig 3).
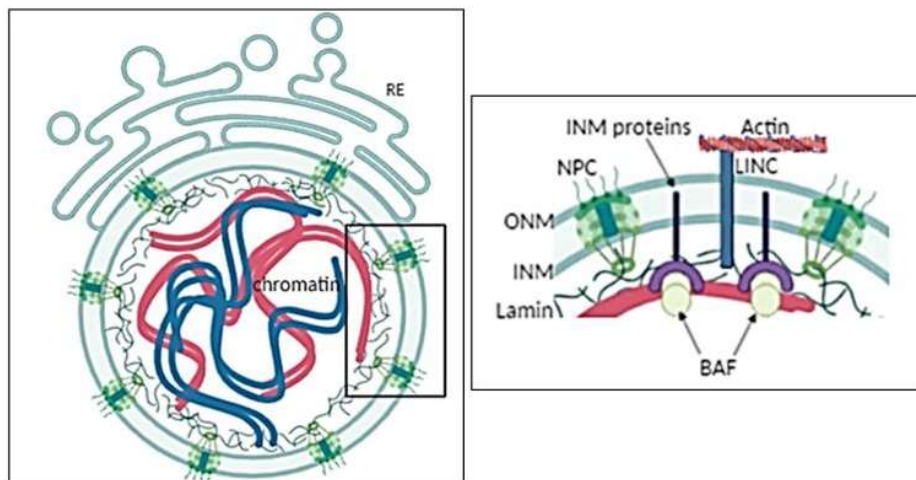
Figure 3. Structure of the NE: The left panel shows a schematic view of the NE and the right panel shows the main NE components. RE: endoplasmic reticulum, INM: inner nuclear membrane, ONM: outer nuclear membrane, NPC: nuclear pore complex, LINC: linker of the nucleoskeleton and cytoskeleton complex, BAF: Barrier-to-Autointegration Factor.

2.1.1 Nuclear pore complexes

The ONM and the INM are separated by the perinuclear space and at many sites both membranes are fused creating holes containing NPCs (fig 3). NPCs are huge multi-subunit protein complexes structured in the cytoplasmic and nuclear ring and the central pore. Cytoplasmic filaments extend from the cytoplasmic ring and a nuclear basket complex extends from the nuclear one. The central channel is composed by nucleoporins (NUPs) that control the transport between the nucleoplasm and cytoplasm (fig 4). It allows the trafficking of small proteins but restrict the passive diffusion of molecular exceeding 30kDa. More than 500 nucleoporins have been described being usually named by its predicted molecular weight[9].
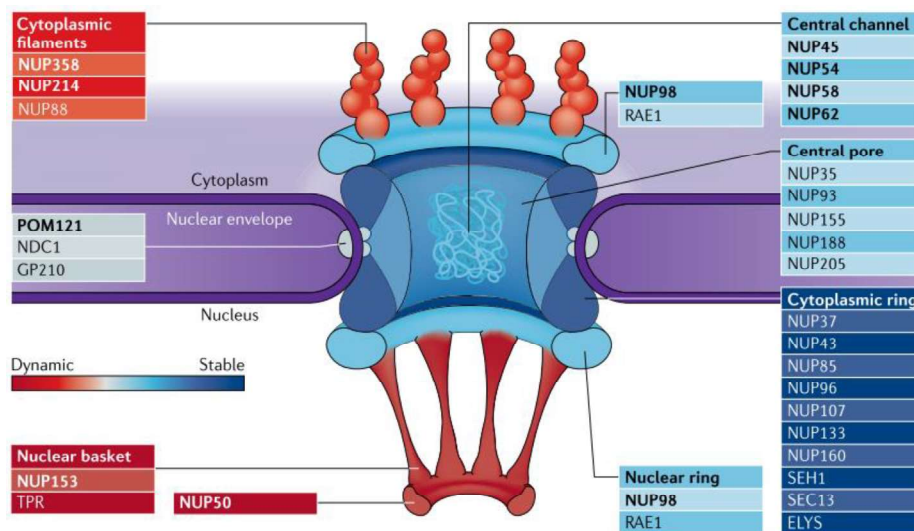
Figure 4. An NPC overview. Schematic representation of the NPC structure. NUP proteins composing each structural part of the NPC are indicated. Taken from[10].

2.1.2 LEM-d proteins

LEM-d proteins bind lamins and this interaction provides mechanical support to the NE. LEM-d proteins also bridge chromatin to the NE since the LEM-domain has the capability of binding Barrier-of-Autointegration Factor protein (BAF), a chromatin binding protein. BAF also interacts with lamins, which additionally contributes to anchor chromatin to the NE. The interaction of LEM-d proteins with lamins and BAF is regulated by phosphorylation and plays an important contribution in both NE breakdown (NEBD) and NE reassembly (NER) during mitosis. LEM-d proteins also interact with signalling effectors. For example Emerin regulates the flux of β-catenin and MAN1 regulates TGF-β signalling by its interaction with receptor associated Smads. LEM-d proteins have differential expression depending on the tissue and their loss causes specific defects[11,12]. For example, loss of function of Emerin is responsible for the Emery–Dreifuss muscular dystrophy (EDMD), mutations in Lap2 cause dilated cardiomyopathy and MAN 1 deficiency leads to bone density disorders[13–15].

LEM-d proteins are classified in three groups (Table 1). Group I proteins (Emerin, LAP2β and LEMD1) have a single transmembrane domain and a long N-terminal region facing the nucleoplasm that contains the LEM-domain. Group II proteins (MAN1 and LEMD2) have two transmembrane regions and, in addition to the N-terminal LEM-domain, they contain a C-terminal Man1-SRC1 (MSC) facing also the nucleoplasm. Finally, group III (LAP2α, Ankle1 and Ankle2) proteins contain Ankyrin (ANK) repeats and they lack a transmembrane domain, being localized in the nucleoplasm and/or cytoplasm (fig 5)[12,16].
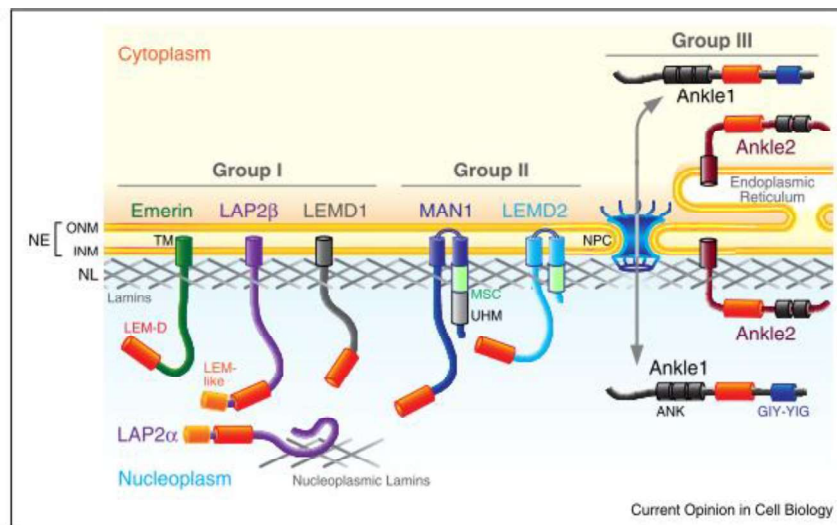
Figure 5. The human LEM-D protein family. Schematic representation of the main features and subcellular localization of the 3 differents LEM-d proteins structural groups. Taken from[11].

Drosophila expresses 4 LEM-d proteins (table 1)[12]. Otefin and Bocksbeutel are group I proteins and they are homologous to human Emerin[17]. Otefin is highly expressed in embryos and in first-instar larvae and it is crucial for stem cell homeostasis in the female germline[18]. The *Bocksbeutel* gene expression is uniform throughout development and encodes two different isoforms originated by alternative splicing, resulting in lack of the transmembrane domain in isoform β[19]. dMAN1 and dLEM3 are the group II and III LEM-d proteins of *Drosophila*, respectively. dMAN1 is involved in the regulation of the TGF-β signalling impacting decapentaplegic(Dpp)-mediated patterning along the embryonic dorsoventral axis[20,21]. Finally dLEM3 is the single protein composing group III LEM-d protein of *Drosophila*.

Organism	LEM-domain protein group	Proteins	A-type lamins	B-type lamins	BAF	Type of mitosis
Schizosaccharo-myces pombe (Fission yeast)	II	Lem2 Man1	Absence	Absence	Absence	Closed
Saccharomyces cerevisiae	II	Heh1 (Src1) Heh2	Absence	Absence	Absence	Closed
Caenorhabditis elegans	I	Ce-emerin	Ce-lamin (single gene)		Presence	Semi-closed
	II	MAN1				
	III	LEM3 LEM-4L				
Drosophila melanogaster	I	Otefin Bocksbeteul (α, β)	C	Dm	Presence	Open
	II	dMAN1				
	III	dLEM3				
Homo Sapiens	I	Emerin LAP2 (α, β, γ, δ, ε, ζ) LEMD1 (CT50, LEMP-1)	A and C	B1 and B2	Presence	Open
	II	MAN1 (NET25)				
	III	Ankl1 (LEM3, ANKRD41) Ankle2 (LEM4)				

Table 1. LEM-d proteins. List of the LEM-d proteins of the indicated species. A and B type lamins, BAF and type of mitosis are also indicated. Adapted from[16].

2.1.3 Nuclear lamina

The nuclear lamina is the underlying structure of the NE and is found in metazoan (Table 1). The nuclear lamina is formed by a dense meshwork of intermediate filaments called lamins and a large number of lamin binding partners. Lots of proteins localized at the INM are retained at the NE due to its direct binding to lamins, providing mechanical rigidity and stability to the nucleus. Lamins associate with chromatin, either directly or indirectly, and contribute to chromatin organization, gene regulation, genome stability and cell differentiation[22].

Lamins are classified as an independent group V of intermediate filaments. Mammals encode 4 main types of lamins: two A-type (A and C) and two B-type (B1 and B2). Lamins A and C are encoded by the

LMNA gene by alternative splicing and they are mainly found in differentiated cell types. Lamins B1 and B2, which are products of the *LMNB1* and *LMNB2* genes respectively, are constitutively expressed in most somatic cells[23].

Lamins are formed by an N-terminal head domain, a coiled-coil central road domain and a C-terminal domain. Post-translational modifications are key for its correct functioning. Processing of pre-lamins to functional lamins involves methylation and farnesylation, as well as cleavage, of the C-terminal CaaX motif (C: cysteine, a: aliphatic reside; X: any residue). Regarding its organization, single lamin proteins form dimers which in turn assemble into polymers that interact laterally to form protofilaments. Phosphorylation is a reversible post-translational modification crucial for the dynamic properties of lamin protofilaments and to regulate binding of associated factors. Importantly, CDK1 phosphorylates lamins at the entry of mitosis causing their depolymerisation and disruption of the nuclear lamina network[22–24].

Lamins contact chromatin either directly or indirectly, through lamin binding factors. Chromatin regions tethered to the periphery of the nucleus by the lamina are known as lamina associated domain (LADs) and they mainly correspond to transcriptionally silent heterochromatic regions (fig 6). Instead, the transcriptionally active and gene-rich euchromatic regions locate at the centre of the nucleus. LADs are cell type specific and invariant and have a global impact on the 3D structure of the genome and in the regulation of cell type-specific features of gene positioning and expression[25]. Nuclear lamina changes are related with aging and senescence[26].
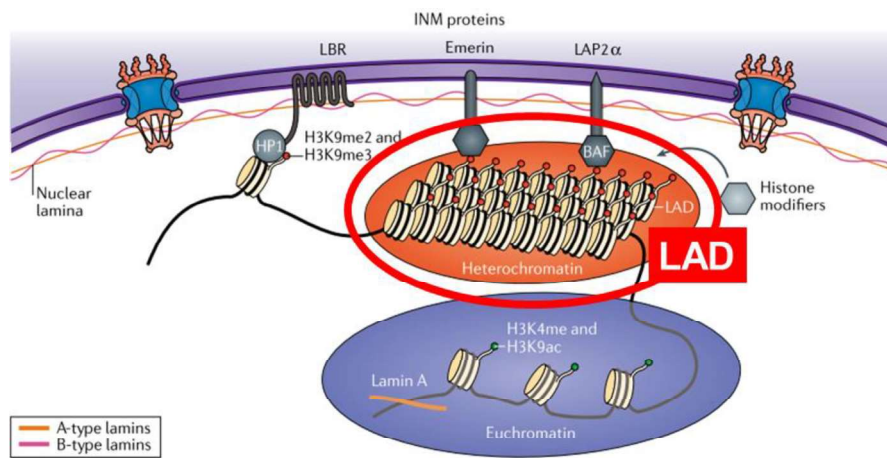
Figure 6. Schematic representation of LADS. LADs are heterochromatic regions located at the nuclear periphery by the interaction with lamin and lamin associated factors. Euchromatic regions are found in the centre of the nucleus. Adapted from [25].

Drosophila encodes for both a B-type (lamin Dm) and an A-type (lamin C) lamins, which is in contrast with most invertebrates that express only B-type lamins (Table 1), making *Drosophila* a good model organism to study NE[27]. Lamin Dm is phosphorylated by CDK1 at the entry of mitosis.

Laminopathies is the termed assigned to the group of diseases caused by mutations in lamin genes (Table 2) and their main features are severe nuclear morphology defects. Most mutations associated with laminopathies mapped to the *LMNA* gene, affecting A-type lamins. These mutations disrupt LADs formation and 3D genome organization. Generally, laminopathies affect specific cell types (Table 2). Hutchinson-Gilford progeria syndrome is the best understood laminopathy. It is characterized by premature aging in childhood and involves symptomatology that affects skin, bones and the cardiovascular system. Myocardial infarction is the most frequent cause of death and the average life span of these patients is 13 years old[26,28].

Disease	Mutated gene(s)[a]	Affected tissues
Emery–Dreifuss muscular dystrophy	*LMNA* (181350 AD; 616516 AR); *EMD* (310300 XR); *SYNE1* (612998 AD), *SYNE2* 612999 AD), *TMEM43* (614302 AD), *FLH1* (300696 XR)	Striated muscle
Cardiomyopathy dilated 1A	*LMNA* (115200 AD)	Striated muscle
Limb girdle muscular dystrophy type 1B	*LMNA* (159001 AD)	Striated muscle
Congenital muscular dystrophy	*LMNA* (613205 AD)	Striated muscle
Heart–hand syndrome	*LMNA* (610140 AD)	Striated muscle
Torsion dystonia-1	*TOR1A* (128100 AR)	Striated muscle
Greenberg dysplasia	*LBR* (215140 AR)	Skeleton
Buschke-Ollendorf syndrome	*LEMD3* (166700 AD)	Skeleton
Familial partial lipodystrophy type 2	*LMNA* (151660 AD)	Adipose
Mandibuloacral dysplasia with lipodystrophy	*LMNA* (248370 AR); *ZMPSTE24* (608612 AR)	Adipose
Acquired partial lipodystrophy	*LMNB2* (608709 AD)	Adipose
Adult-onset demyelinating leukodystrophy	*LMNB1* (169500 AD)	Central nerve system
Spinocerebellar ataxia-8	*SYNE1* (610743 AR)	Central nerve system
Charcot–Marie–Tooth disease type 2B1	*LMNA* (605588 AR)	Peripheral nerve system
Pelger–Huët anomaly	*LBR* (169400 AD)	Blood system
Restrictive dermopathy	*LMNA* (275210 AD); *ZMPSTE24* (275210 AR)	Skin
Hutchinson–Gilford progeria syndrome	*LMNA* (176670 AD)	Multiorgan disease
Nestor-Guillermo progeria syndrome	*BANF1* (614008)	Multiorgan disease

[a]Numbers in parentheses refer to OMIM entries (http://omim.org), XR X-linked recessive, AD autosomal dominant, AR autosomal recessive.

Table 2. Laminopathies. The mutated genes and affected tissues are presented. Adapted from [29].

2.1.4 BAF

Barrier-to-Autointegration Factor (BAF) is named after its ability to prevent autointegration of the Moloney Murine Leukaemia Virus (MoMLV)[30,31]. Upon entering the host cell, the viral RNA is retrotranscribed in the cytoplasm and forms the pre-integration complex (PIC) that enters the nucleus and promotes integration into the host genome. In this process, viral DNA must not autointegrate since this leads to its destruction. BAF was identified as a host factor that prevents MoMLV autointegration by compacting the viral DNA within the PIC and assembling higher nucleoproteins complexes[32,33]. BAF has also been reported to be a component of PICs derived from HIV-1 infected cells[34,35]. Paradoxically, BAF also plays a protective role against viruses that, like vaccinia virus, express their own replication and transcriptional machinery and replicate in the cytoplasm of the host cell. In these cases, BAF re-localizes to the cytoplasm and interferes with viral DNA replication and transcription. To overcome BAF blockage, the vaccinia virus encodes the B1 kinase that phosphorylates BAF to prevent its binding to viral DNA[36,37]. Apart from its role in defence against foreign DNA, BAF has also been proposed

to participate in multiple processes from the regulation of chromatin structure and gene expression to DNA repair and, through the interaction with LEM-d proteins and lamins, the regulation of NEB and NER during mitosis[38].

BAF is a small protein of 10kDa that, absent in unicellular eukaryotes, is highly conserved in Metazoan (Table 1 and fig 7). BAF is ubiquitously expressed in all cell types and tissues, except in thymus and peripheral blood leukocytes[39]. Regarding subcellular localization, BAF is found both in the cytoplasm and the nucleus, being enriched at the NE. Viral infection and stresses, including heat shock and caloric restriction, alter the subcellular distribution of BAF[40]. BAF localization is highly dynamic, changing during cell cycle progression, which is important for BAF function and varies depending on the cell type[41]. BAF localization is regulated by phosphorylation and the interaction with specific partners[42].

Figure 7. BAF conservation. Amino acid sequences of BAF from human (hBAF), mouse (mBAF), zebrafish (zBAF), *Xenopus* (xBAF), *Drosophila* (dBAF) and *Caenorhabditis elegans* (CeBAF). Non-conserved residues are shown in red. In hBAF, residues involved in phosphorylation (T3 and S4) are indicated in green. K6 and the HhH motif (from 20-35), which mediate DNA binding, are indicated in orange. Residues 39 to 62, which are involved in homodimerization, are highlighted with blue. Adapted from[43].

BAF has been reported to interact with a large number of factors (Table 3), of which the NE LEM-d proteins and lamins are the best studied[44,45]. BAF has also been shown to interact with histones and bind DNA. Because of its interaction with NE proteins and its ability to bind chromatin, BAF plays a critical role in the dynamics of the NE during mitosis[46], a topic that will be further discussed in following chapters. The interaction of BAF with transcription factors and chromatin modifiers has an impact on gene expression. For instance, BAF directly interacts with the transcription factor cone-rod homeobox (Crx) in differentiating retinal cells[47]. BAF also affects gene expression indirectly through its interaction with LEM-d proteins that, in their turn, interact with transcription factors. It has been proposed that the interaction of transcription factors with LEM-d proteins induces their re-localisation to the NE, antagonizing their transcriptional activity. For example, BAF competes with the transcriptional repressor germ cell-less (GCL) for binding to Emerin and lamin A complexes[48]. In addition, BAF is also involved in chromatin remodelling. BAF overexpression reduces global histone H3 acetylation and alters different histone marks[49,50]. However, BAF has not been described to directly associate with chromatin modifiers/remodellers. Instead, it appears to act as an epigenetic regulator that alters chromatin structure and, thus, the recruitment of chromatin modifiers/remodellers[49,50]. BAF also interacts with factors involved in DNA repair, such as poly ADP-ribose polymerase 1 (PARP1) enzyme. Upon oxidative stress, BAF increases its binding to PARP and blocks NAD^+, which negatively regulates PARP activity[51].

BAF has also been reported to interact with BAF-like (BAF-L), a highly related protein that, contrary to BAF, does not bind DNA or LEM-d proteins and modulates BAF function *in vivo*. BAF-L expression is limited to pancreas and testis, suggesting that it has a specific role in regulating BAF function in the male germline[52].

Protein group	Protein	Function	References
LEM-d proteins	Emerin	Mitosis, inner NE component, transcriptional regulation.	46,53–57
	LAP2	Mitosis, inner NE component, transcriptional regulation.	58–61
	Man1	Inner NE component.	62
	LEMD2	Inner NE component, DNA damage repair.	63
	Ankl1/ LEM3	DNA damage repair, resolution of chromatin bridges.	64
	Ankle2/ LEM4	Recruits PP2A for BAF phosphorylation.	65
	Nemp1	Inner NE component, neural development.	66
Lamins	Lamin A	Mitosis, NE structural component, cell signalling.	55,56,67
	Prelamin A	Precursor form of lamin A.	68,69
	Progerin	Truncated and permanently farnesylated form of lamin A.	69
Histones	H1.1	Linker histone.	50
	H3	Core histone.	50,67
	H4	Core histone.	49
Transcription	EFF-1	Somatic cell fusion in *C. elegans*.	70
	P15/SUB1/PC4	Chromatin remodelling,	67

regulators		transcription, DNA repair.	
	Requiem	Transcription factor in myeloid cells, apoptosis.	67
	Crx	Organ morphogenesis	47,71
	Sox2	Embryonic stem cell differentiation.	72
	Oct4	Embryonic stem cell differentiation.	72
	Nanog	Embryonic stem cell differentiation.	72
DNA damage repair proteins	PARP1	DNA repair, chromatin structure and remodelling, transcription.	51,67
	DDB1, DDB2	DNA repair, protein degradation.	67
	CUL4	Protein ubiquitination.	67
Kinases	Vaccinia related kinases	Ser-Thr kinases, mitosis, protein phosphorylation.	73–75
	B1	Vaccinia kinase for viral DNA replication.	36,42,73
Phosphatases	PP2A	Ser-Thr phosphatase, mitosis, protein phosphorylation.	65
	PP4	Ser-Thr phosphatase, mitosis, protein phosphorylation.	76
Others	BAF-L	Regulator of BAF DNA binding	52

Table 3. List of BAF interactors. Adapted from [77] and [38].

Important for its function, BAF forms homodimers. Dimerization involves a hydrophobic interface (residues 39 to 62 in hBAF) that creates a central pocket (fig 7 and 8)[78]. This hydrophobic pocket is the binding site of LEM-domain proteins[45,53,79].

BAF binds DNA in a non-sequence specific manner. DNA binding is mediated by the helix-hairpin-helix (HhH) motives of each monomer that, in the dimer, occupy opposite positions (fig 8). K6 in the N-terminal region has also been reported to contribute to DNA binding (fig 7 and 8)[80]. These DNA binding properties are fundamental for the ability of BAF to bridge DNA fragments, either intra or inter-molecularly, and condenses DNA by a looping mechanism[78,80,81]. The DNA bridging activity of BAF has been recently reported to play a crucial role during NER by binding DNA distant sites to maintain the bulk of decondensing chromosomes as a single entity and prevent nuclear fragmentation[82].
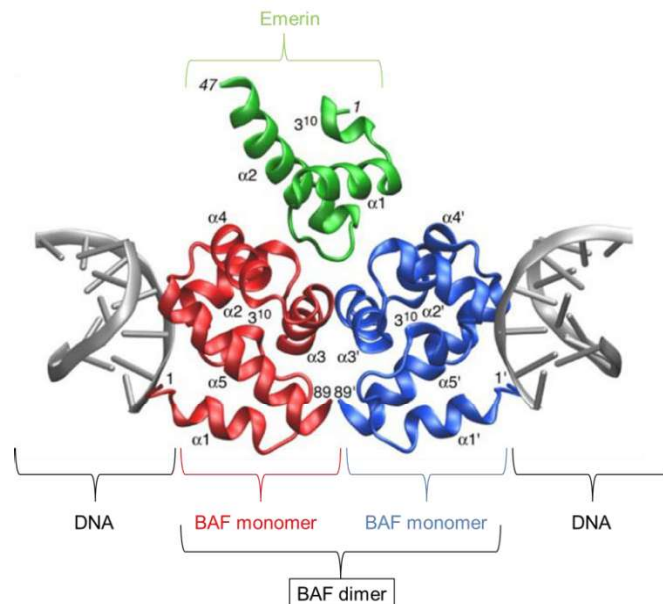
Figure 8. DNA – BAF – Emerin complex structure. BAF monomers (blue and red) interact to DNA (grey) thanks to the K6 residue and the HhH domain found at its N-terminal. Residues 39-62 from both monomers are involved in BAF dimerization creating a central pocket where LEM-d proteins (green) bind. Adapted from[53].

BAF mutations associate with some rare laminopathies. A recessive A12T mutation was reported to cause Néstor-Guillermo progeria syndrome (NGPS), an atypical chronic progeria syndrome that partially shares the same phenotype with the Hutchinson-Gilford progeria syndrome (Table 2), though patients show milder symptoms and longer life spam[83]. Fibroblasts from Néstor-Guillermo patients exhibit nuclear lamina abnormalities that are rescued by the ectopic expression of a wild type BAF[84]. This mutation impairs binding of BAF to DNA and lamins[45,85], while the interaction with PARP1 upon oxidative stress is increased leading to defective DNA repair. In fact, defective DNA repair of oxidative damage is observed in fibroblast from NGPS patients[51]. Overexpression of BAF has also been observed in certain oesophageal, gastric and breast cancers, correlating with malignancy, metastasis and poor prognosis[86–88]. However, the link between high BAF levels and cancer progression is not well understood.

As mentioned above BAF is highly conserved in Metazoan. In this regard, *Drosophila* BAF shows 69% identity to human BAF (fig 7). In *Drosophila,* BAF is essential for viability since BAF null mutants are lethal at the larval-pupal transition. Moreover, BAF is essential for germ stem cells maintenance since its depletion leads to germ stem cells loss. These phenotypes have been proposed to reflect the contribution of BAF to NE[89,90]. BAF is also essential for karyosome formation in the female germline[91]. Finally, work in our group identified BAF as a new centromere associated protein in *Drosophila*[92].

2.2 The NE in cell division

The NE is continuously being remodelled during cell cycle progression and the most dramatic changes occur during mitosis. NE remodelling during mitosis allows spindle microtubules to gain access and attach to chromosomes ensuring their equal segregation into daughter cells.

The mitotic spindle forms early in mitosis. Centrosomes are microtubule organizing centres (MTOCs) from which the spindle assembles. The centrosome duplicates during S phase and each copy locates on opposite sides at the spindle poles. There are two main types of microtubules: astral microtubules, which are short and radiate out from the centrosome and play a role in anchoring and stabilizing the centrosome at the correct localization, and kinetochore microtubules, which are polymers made by α and β tubulin heterodimers bound by microtubule associated proteins (MAPs) that regulate their dynamics[5].

In eukaryotes, centrosomes and chromosomes are located in different cellular compartments, the cytoplasm and the nucleus respectively. The NE constitutes a barrier that prevents spindle microtubules to reach the chromosomes. During evolution, different mechanisms have been implemented to solve this problem, involving always more or less extensive remodelling of the NE. There are basically two extreme scenarios: open and closed mitosis. Most Metazoan undergo open mitosis (fig 9a), in which the NE disassembles and retracts into the ER at the beginning of mitosis (NEBD) to reassemble around the bulk of decondensing chromosomes after chromosome segregation is completed (NER). On the other extreme, budding and fission yeasts undergo closed mitosis (fig 9b), in which the NE remains more or less intact and the spindle assembles in the nucleus. This is achieved by the integration into the NE of the spindle pole bodies that act as the

MTOCs to assemble the spindle. Between these two extreme possibilities, there are different forms of semi-closed mitosis (fig 9c and d). For example, in the filamentous fungus *Aspergillus nidulans*, the NE remains functional until anaphase when it partially breaks allowing the spindle microtubules to access the DNA material[93,94]. Semi-closed mitosis has also been observed in Metazoan, such as during early embryogenesis in *Drosophila* and in *Caenorhabditis elegans* early embryos[95,96].
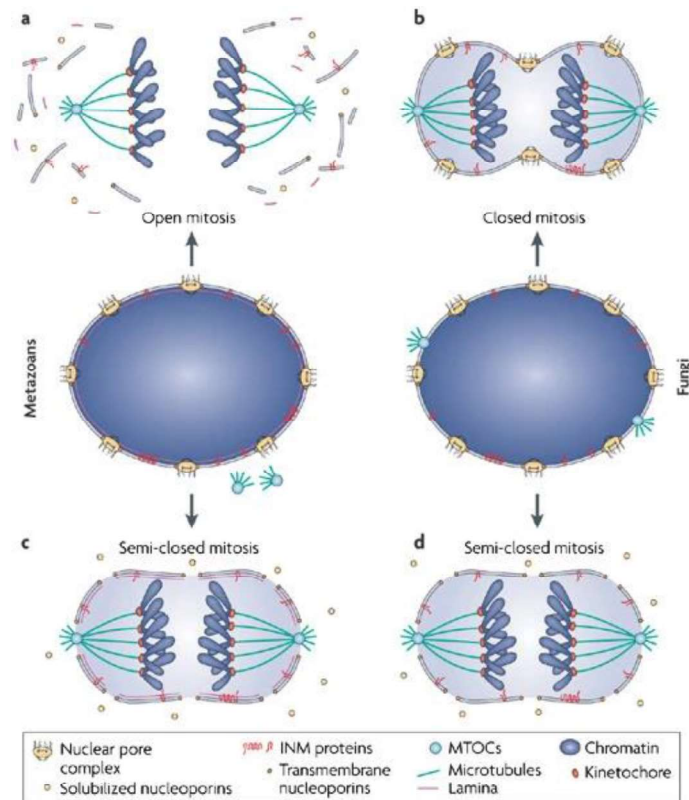
Figure 9. Schematic representation of the different types of mitosis. a: Open mitosis that involves total breakdown of the NE early in mitosis. **b:** Closed mitosis where the NE remains intact through mitosis. **c and d:** Semi-closed mitoses, in which the NEBD is only partial. Taken from [6].

2.2.1 NEBD

Mitotic entry involves a cascade of phosphorylation events that drive dramatic architectural changes such as chromatin condensation, spindle assembly and disassembly of the NE (fig 10). NEBD is triggered by the activation of mitotic kinases that phosphorylate various substrates including nucleoporins (NUP), lamins and histones. NUPs are hyper-phosphorylated by CDK1 and PLK kinases causing NPCs disassembly and release from the NE. CDK1 also phosphorylates lamins triggering nuclear lamina disassembly, while VRK1 phosphorylates BAF and disrupts the interaction of LEM-d proteins with chromatin and lamins. Altogether, these phosphorylation events results in increased NE permeability[97–99]. Microtubules also play an important role in NEBD by mechanically pulling the NE and creating and extending holes. Ultimately, all this processes lead to full disruption of the NE. Microtubules are also involved in clearing up remains of the NE from the chromatin (fig 10)[100]. The resulting disassembled nuclear envelope membranes retract into the mitotic ER that is excluded from the area occupied by the spindle and the mitotic chromosomes to allow pulling of the mitotic chromosomes by the spindle (fig 10)[101].
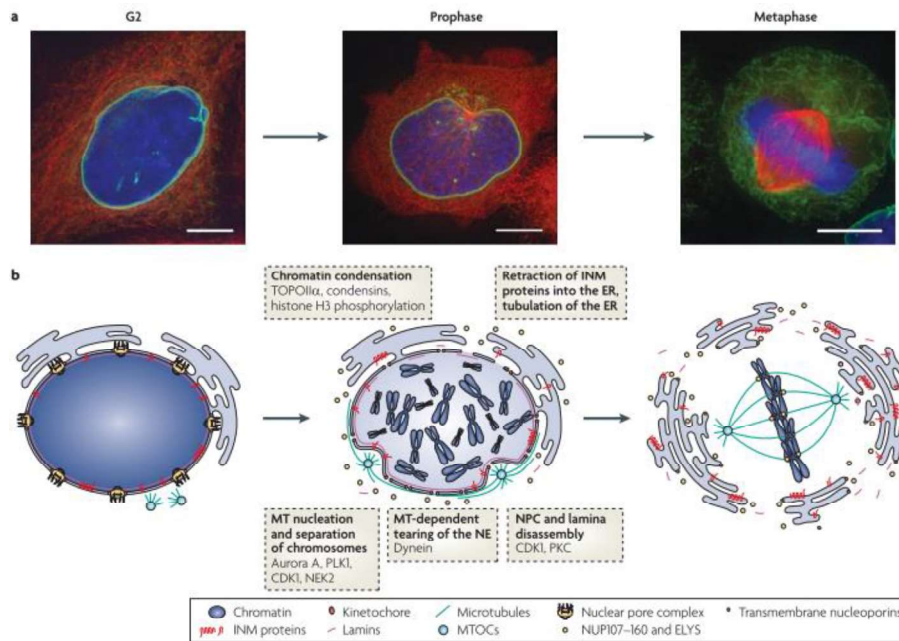
Figure 10. NEB. a: Immunostaining of HeLa cells with αTubulin antibodies (red). The green signal corresponds to GFP-LAP2β. DNA is stained with Hoechst (blue). Scale bars correspond to 10μm. **b:** Schematic representation of the events that trigger NEBD at the entry of mitosis. Taken from[6].

2.2.2 NER

In late anaphase, when kinetochores are properly attached to the mitotic spindle and SAC is satisfied, NER begins around the two masses of decondensing chromosomes. NER involves the activity of various phosphatases, which reverse the mitotic phosphorylations that initiate NEBD, and requires coordination of membrane recruitment, NPC insertion and lamina reformation (fig 11).
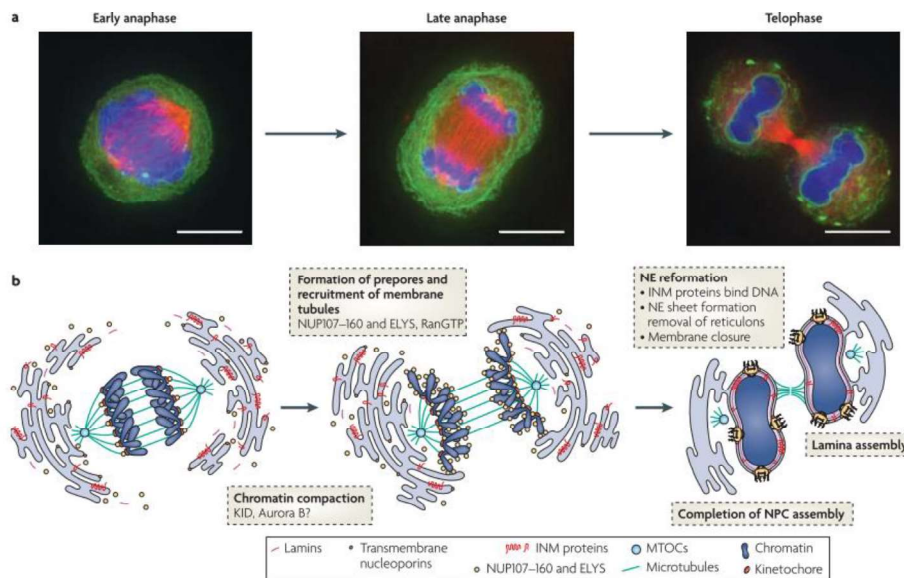
Figure 11. NER. a: Immunostaining of HeLa cells with αTubulin antibodies (red). The green signal corresponds to GFP-LAP2β. DNA is stained with Hoechst (blue). Scale bars correspond to 10μm. **b:** Schematic representation of the events that lead to NER. Taken from[6].

NE membranes emerge from the mitotic ER to reach chromatin. There are different models regarding the morphology of the emerging membranes and the way they wrap around chromatin, either in the form of tubules or sheets. INM proteins anchor chromatin to the reassembling NE. For instance, the INM protein laminB receptor (LBR) interacts with histones H3/H4 and heterochromatin 1 protein (HP1), while LEM-d proteins bind to chromatin and lamins either directly or indirectly, through the interaction with BAF[102]. Membrane recruitment is coordinated with NPCs assembly. Upon NEBD, NUPs are phosphorylated and associate with importin-β, a chaperone that inhibits NUPs binding to the membrane and keeps them free in the cytoplasm. In NER, high RanGTP levels generated in the proximity of chromatin induces importin-β disassociation and NUPs are dephosphorylated by yet uncharacterized protein phosphatases[103]. At this stage, two regions can be identified in the reassembling NE that

differ in the type of INM proteins and abundance of NPCs. The "core" regions are adjacent to the spindle and contain BAF, LAP2α, Emerin and A-type lamins, but they are poor on NPCs. Instead, peripheral "non-core" regions contain high levels of NPCs and are enriched in B-type lamins and LBR proteins. Regions with low NPCs levels are refilled during interphase by a *de novo* NPCs assembly mechanism (fig 12)[56,58]. Finally, the patches of reassembling NE membranes that wrap chromatin are fused to form a continuous NE in a process involving the activity of various GTPases such as SNAREs and atlastins. Additionally, the ESCRT-machinery seals the sites of microtubule insertion in a process known as annular fission[104].
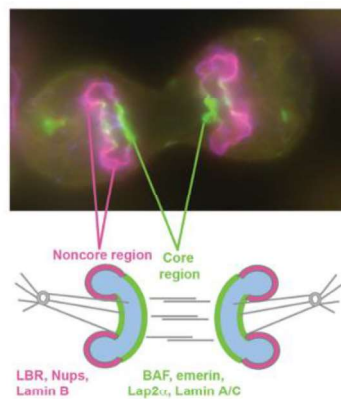
Figure 12. "Core" and "non-core" regions formed during NER. Immunostaining of a HeLa mitosis in late anaphase with αEmerin (green) and αLBR (purple) that mark the "core" and "non-core" regions, respectively. The lower panel shows a schematic representation of the "core" and "non-core" regions indicating their main components. Taken from[103].

2.2.3   The contribution of BAF to NEBD and NER

Cycles of phosphorylation and dephosphorylation events regulate the interaction of BAF with chromatin and NE components during mitosis. At the entry of mitosis, the conserved Ser/Thr Vaccinia-related kinase 1 (VRK1) phosphorylates human BAF at S3 and T4 residues located in

the N-terminal domain (fig 7)[73]. The *Drosophila* VRK1 homologue is Nucleosomal histone kinase 1 (NHK1). This phosphorylation impairs binding of BAF to chromatin, as well as the interaction with LEM-d proteins and lamins. BAF phosphorylation by VRK1 is an early event in mitosis that triggers its release from chromatin and nuclear membrane proteins and facilitates NEBD (fig 13). Depletion of VRK1 prevents disassociation of BAF from NE elements and chromatin causing delayed mitosis and NE morphology defects[42,73–75,105].
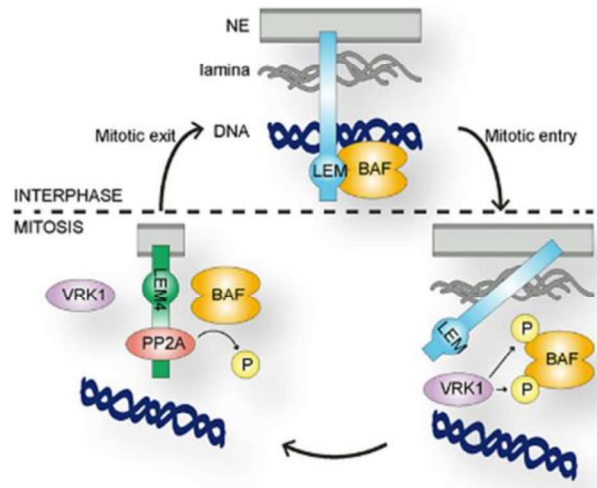
Figure 13. Cycles of phosphorylation and dephosphorylation regulate BAF binding to chromatin and the NE during mitosis. At the entry of mitosis, BAF is phosphorylated by VRK1/NHK1 kinase and loses its affinity for the NE and chromatin, facilitating NEBD. At the end of mitosis, PP2A dephosphorylates BAF and restores its binding to the NE and chromatin, playing a crucial role in NER. Taken from[106].

At the end of mitosis, BAF is dephosphorylated and recovers its ability to bind chromatin and the NE proteins (fig 13). BAF is amongst the first proteins detected at the "core" regions of the reassembling NE and it has been proposed to nucleate the recruitment of LEM-d proteins and A-type lamins (fig 14)[46,56,107]. In *C. elegans* and mammals, BAF dephosphorylation at mitosis exit has been shown to be mediated by PP2A protein phosphatase. PP2A-mediated BAF dephosphorylation

requires Lem4 that promotes PP2A phosphatase activity and binds and inhibits VRK1 (fig 13)[65,108]. Along the same lines, in *Drosophila* cells, PP2A/B55 also mediates dephosphorylation of BAF and lamins and its depletion delays NER[109]. PP4 protein phosphatase has also been shown to be capable of dephosphorylating BAF in mammalian cells and PP4 knock-down leads to BAF hyperphosphorylation and causes NE defects[76].
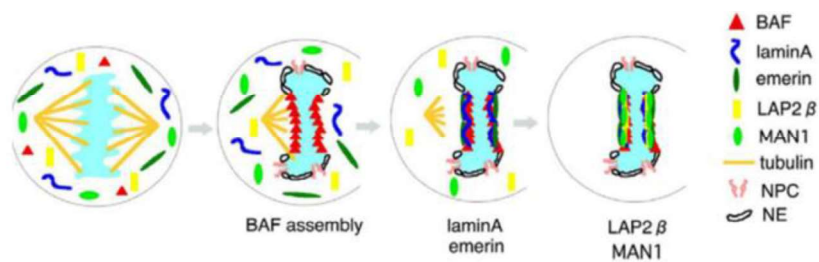
Figure 14. The contribution of BAF to NER. At the end of mitosis, BAF is dephosphorylated and is amongst the first proteins recruited to the "core" regions during NER. Taken from[56].

The ability of BAF to cross-bridge distant sites is also important to maintain the bulk of decondensing chromosomes as a single entity during NER. In the absence of BAF, the NE reassembles around individual chromosomes leading to chromatin fragmentation and the formation of micronuclei (fig 15)[82].
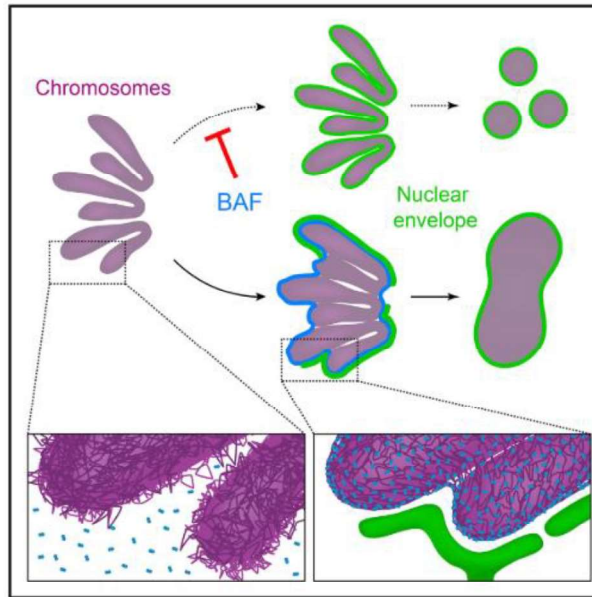
Figure 15. BAF prevents nuclear fragmentation at NER. The lack of BAF leads to the formation of micronuclei due to the impossibility of keeping the chromatin all together as a single mass. Taken from[82].

BAF also plays a role in keeping the integrity of the NE by repairing NE fractures. BAF localizes at the sites of rupture and recruits LEM-d proteins and associated membranes to repair the rupture (fig16)[110].
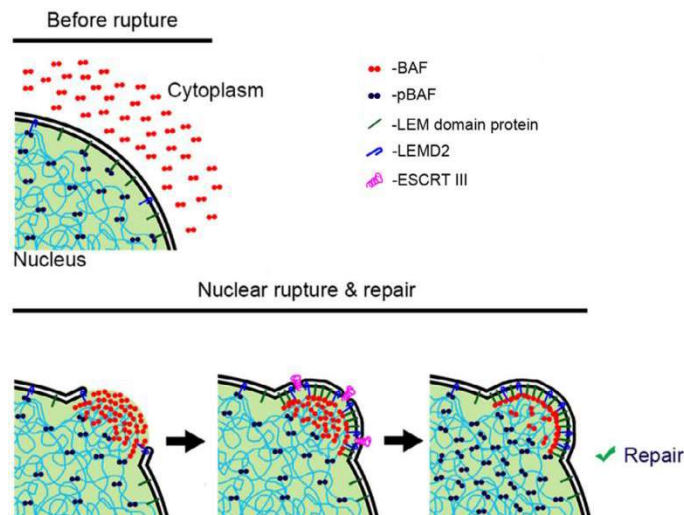
Figure 16. BAF is required for repairing NE ruptures. Cytosolic BAF is **mobilized** to the sites of NE ruptures and recruits LEM-d proteins, ESCRT-III, and membranes to the rupture to heal it. Adapted from[110].

2.2.4 Micronuclei

Micronuclei (MN) are small nucleus-like structures (1-5µm in diameter) found in the cytoplasm separated from the primary nucleus.

MN form when the NE assembles on individual chromosomes or fragments of chromosomes. Different mechanisms can give rise to the formation of MN. During chromosome segregation, lagging chromosomes are highly prone to MN formation. The SAC is the main mechanism preventing MN formation and its malfunctioning is a major cause of MN formation. In particular, the SAC is not efficient in sensing merotelic attachments, in which one sister chromatid is attached to microtubules from opposite poles, and, although in most cases, they reincorporate to the main mass of chromatin, failure to do so give rise to MN. Merotelic attachments are commonly seen in cells with extra copies of centrosomes or when centrosomes are not properly distributed in the spindle poles. Centromere inactivation or instability, as well as defective cohesion cleavage, also cause lagging/broken chromosomes and, thus, MN formation (fig 17 upper panel). NER defects and NE ruptures in interphase can also give rise to MN (fig 17 lower panel)[111,112].
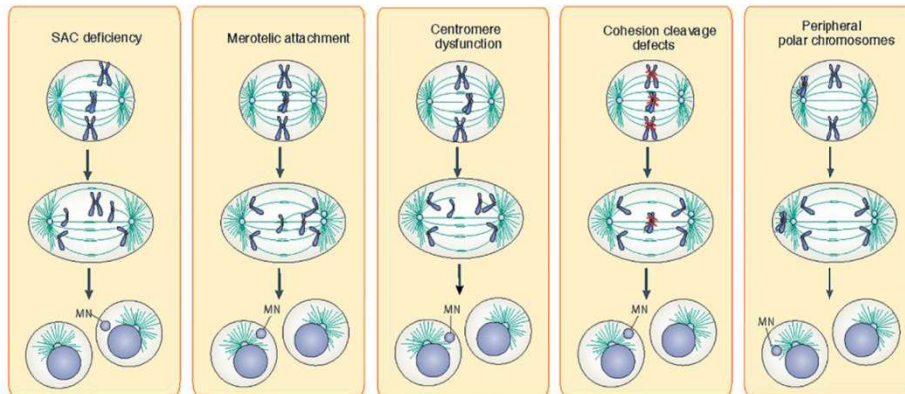
Figure 17. Causes of MN formation. The upper panel shows MN origins caused during mitosis such as SAC deficiency, merotelic attachment, centromere dysfunction, cohesion cleavage defects and peripheral polar chromosomes. The lower panel shows MN origins outside mitosis such as defects in NE reassembly at the end of mitosis or rupture of the NE during interphase. Adapted from[111].

Not much is known about the fate of MN. In most cases, they persist for one or more cell cycles, but they can also be extruded out of the cell, fused back to the nucleus or disrupted and degraded[111]. MN are unstable since their NE usually misses NPCs and "non-core" NE proteins and, as such, they are deficient in DNA replication and repair, and accumulate DNA damage. As a result, MN are prone to chromotripsis[113], a catastrophic event in which fragmented chromosomes are randomly reassembled *via* double-stranded break repair (DBR). This produces important chromosomal rearrangements

and is a source of aneuploidy and chromosome instability (CIN), which are hallmarks of cancer and other pathological conditions[114–116].

3. MITOTIC PROTEIN PHOSPHATASES

Balance between the activity of different kinases and phosphatases plays a crucial role orchestrating mitosis progression. Table 4 summarizes the main mitotic kinases and phosphatases, and their known functions in mitosis.

KINASES	FUNCTION
WEE	CDK1 inhibition Regulation of entry to mitosis
CDK1	Disassembly of the NE Chromatin condensation Assembly of the mitotic spindle Assembly of the kinetochore Golgi fragmentation Positive regulator of the APC/C^{cdc20} complex Involved in localization of Aurora B and PLK to the mitotic spindle Main inhibitor of PP1 and PP2A/B55
Aurora A type	Assembly of the mitotic spindle
Aurora B type	Chromatin condensation Regulator of the kinetochore function Regulator of the spindle dynamics Positive regulator of the APC/C^{cdc20} complex Control of chromosome segregation Cytokinesis
Polo like kinase (PLK)	Centrosome activation Chromatin condensation Positive regulator of the APC/C complex Cytokinesis
BubR1	Positive regulator of the APC/C complex
MPS1	Main positive regulator of the APC/C complex
VRK1/NHK1	BAF phosphorylation

PHOSPHATASES	FUNCTION
PP1	Main CDK1 antagonizing phosphatase Stabilization of the microtubule-kinetochore attachments
PP2A/B55	Main CDK1 antagonizing phosphatase
PP2A/B56	Maintenance of centromeric cohesion Counteracting Aurora B kinase at the kinetochore
PP4	Centrosome function Centromeric integrity
PP6	Temporal regulation of the spindle formation

Table 4. Main mitotic kinases and phosphatases and their function in mitosis.

In eukaryotes entry to mitosis is triggered by an abrupt activation of key kinases, the most important of which is the CDK1/cyclin B complex also known as maturation-promoting factor (MPF). In addition to MPF, PLK or Aurora kinases play also important roles in the spatiotemporal regulation of multiple mitotic events (Table 4). In order to exit mitosis, this hyper-phosphorylated state must be reversed. This is achieved by the inhibition and/or degradation of mitotic kinases and other key mitotic factors, and the activation of mitotic phosphatases. In budding yeast, Cdc14 is the main phosphatase driving mitotic exit. However, in Metazoan, depletion of the Cdc14 homologues, hCdc14A and hCdc14B phosphatases in the case of human, has no significant phenotype. Instead, multiple members of the main protein phosphatases families (PP1, PP2A, PP4, and PP6) are key players in regulating mitotic exit.

There are three groups of phosphatases based on their sequence, structure and catalytic mechanism. The first group is the protein

serine/threonine-specific phosphatases (PSTPs). This group is subdivided into two families: the metallodependent phosphatases (PPM) family (PP2C) and the phosphoprotein phosphatases (PPP) family (PP1, PP2A, PP2B, PP4, PP5, PP6 and PP7). Both groups are dependent on metal ions for catalysis but they have different mechanisms of dephosphorylation. A second group is formed by the protein tyrosine phosphatases (PTP) and finally a third group consists of the Asp-based protein phosphatases. PPPs are the main phosphatases acting during mitosis and, in particular, PP1, PP2A, PP4 and PP6 have been most studied (Table 4 and figure 18)[117].
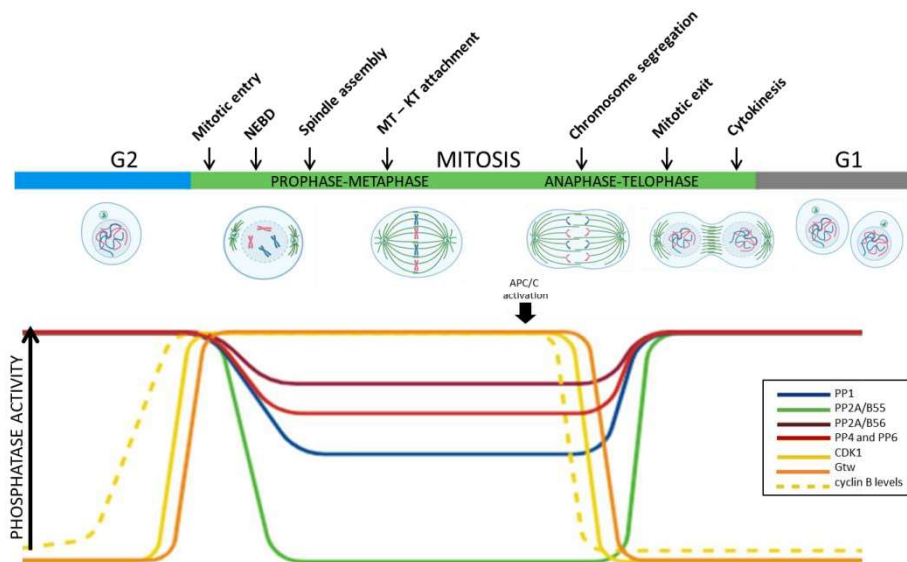
Figure 18. Schematic representation of the activity of the main mitotic phosphatases and kinases. At the entry of mitosis kinases predominate and this situation is reversed once the SAC is satisfied. Upon APC/C activation, cyclin B is degraded causing the inactivation of CDK1 and the activation of the phosphatases. Adapted from [118].

In general, phosphatases are multisubunit complexes in which a catalytic subunit associates with additional regulatory subunits that provide substrate specificity, act as scaffolds, target an active complex to specific subcellular locations and/or regulate phosphatase activity. Generally, substrate specificity of PPPs depends on the recognition of

35

short linear motifs (SLiMs) that are degenerated and bind to a conserved pocket on the phosphatase. The activity of phosphatases is usually controlled by phosphorylation and their activation depends on a coordinated crosstalk between different phosphatases and/or kinases[106]. Overall, mitotic exit involves a sophisticated molecular mechanism that regulates the correct timing of activation of each phosphatase and the sequential dephosphorylation of specific substrates in the right order and at the right place[106,119,120]. Table 5 summarizes the main mitotic phosphatases in *Drosophila*.

Gene name	Gene family and subunit type	Human orthologues	Defects observed in mitosis when performing a knockdown or in Drosophila mutants
Pp1-87B	PP1 catalytic	PP1CA	Cells accumulating at prometaphase and failure in chromosome segregation
flw (flag wing)	PP1 catalytic	PP1CB	Chromosome segregation defects
mts (microtubule star)	PP2A catalytic	PP2CB	Cells are arrested at prometaphase and a small number of cells making it to telophase contain aberrant phosphorylated H3 levels on decondensed chromosomes
PP2A-29B	PP2A regulatory	PP2A/A	Instability of the catalytic subunit
wdb (widerborst)	PP2A regulatory	PP2A/B56	Cells with abnormal chromatin dispersion throughout the spindle and alterations in sister

			chromatid cohesion
tws/aar (twins/abnormal anaphase resolution)	PP2A regulatory	PP2A/B55	Cells arrested at anaphase showing high amounts of lagging chromosomes and chromosome bridges
Pp4-19C	PP4 catalytic	PP4C	Aberrant centrosome maturation
PP4R2r	PP4 regulatory	PP4R2	Aberrant centrosome maturation
Flfl (falafel)	PP4 regulatory	PP4R3B	Problems with the centromere assembly
PPV	PP6	PP6C	Cells accumulating at prometaphase
PpD3	PP5	PP5C	Increased frequency of cells with aberrant number of centrosomes

Table 5. Main phosphatases involved in mitosis exit in *Drosophila Melanogaster*. Taken from[121].

3.1 PP1

PP1 is one of the most abundant phosphatases in the cell and regulates a variety of processes including glycogen metabolism, transcription, cell polarity, response to DNA damage, trafficking of vesicles and cell cycle progression. PP1 is one of the main phosphatases antagonizing CDK1 phosphorylation at the end of mitosis and it also counteracts other kinases such Aurora B or PLK. PP1 is involved in the regulation of kinetochore-microtubule attachment, chromosome segregation, chromatin decondensation and cytokinesis[122–125].

PP1 is a heterodimer of one catalytic subunit and one of many possible regulatory subunits that targets the active complex to specific substrates and localizations. For PP1, the vast majority of substrates contain the RVxF SLiM[126]. In addition, the activity of PP1 is regulated by mitotic kinases such as CDK1 and Aurora that directly regulate activity of the phosphatase or modify the PP1-SLiM interaction[127]. In this regard, at the entry of mitosis, CDK1 phosphorylation inhibits PP1 activity. Upon CDK1 inactivation at mitosis exit, PP1 auto-dephosphorylation reverts this phosphorylation and restores full PP1 activity[128].

3.2 PP2A

PP2A phosphatases are abundant and are involved in several functions such as cell growth, cell motility, apoptosis, differentiation, DNA damage response and progression through cell cycle. PP2A usually functions as a heterotrimeric complex consisting of one catalytic C-type subunit, one scaffold A-type subunit and one regulatory B-type subunit. The human genome encodes for two catalytic isoforms (PP2Aα and PP2Aβ), two A-type subunits (PR65α and PR65β) and at least 15 different B-type subunits, of which B55 and B56 are the B-subunits of the two main mitotic PP2A complexes[129].

In *Drosophila* PP2A catalytic subunit is known as Microtubule Star (MTS), PP2A regulatory subunits involved in mitosis are a B55 type Twins (TWS) and a B56 type Widerbroast (WDB) and their functions seem to be evolutionary conserved (Table 5)[121,130].

3.2.1 PP2A/B55

PP2A/B55 activity is tightly regulated during cell cycle progression. At mitosis entry, PP2A/B55 is repressed and is maintained inactivate until

late in mitosis when, together with PP1, acts as a major CDK1-antagonizing phosphatase and induces mitosis exit. In *Drosophila*, PP2A/B55 inactivation at mitosis entry depends on phosphorylation by the mitotic kinase Greatwall (Gtw)[131] (MASTL in humans) that, in its turn, is activated by CDK1 phosphorylation. Active Gtw phosphorylates Endos (ENSA/Arpp19 in humans), which are competitive inhibitors of PP2A/B55. At mitosis exit, CDK1 inactivation prevents Gtw activation and, in addition, activates PP1 that dephosphorylates Gtw, reinforcing its inactivation. As a consequence, Endos are no longer activated and PP2A/B55 activity resumes. On the other hand, PP2A/B55 dephosphorylates Endos and reinforces Endos inactivation[120,132–137]. It has also been proposed that PP1 may directly activate PP2A/B55 (fig 19)[138]. The molecular basis of substrate recognition by B55 is not well understood since no SLiM has yet been identified. However, it is known that PP2A/B55 has a strong preference for phosphor-threonines and it has been proposed to have higher affinity for substrates in which the phospho-residue is flanked by basic residues with a nonpolar aminoacid in position +2 favouring dephosphorylation[119,139].
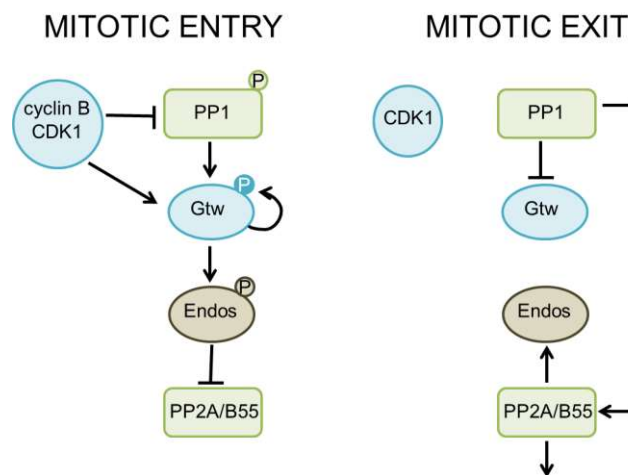
Figure 19. PP2A/B55 regulation during mitosis. At mitotic entry (left panel) PP2A/B55 is repressed by a mechanism that involves active CDK1 and Gtw. At the end of mitosis (right panel) CDK1 and Gtw kinases are inactivated and no

longer repress PP2A/B55. Adapted from [140].

3.2.2 PP2A/B56

One of the main functions of PP2A/B56 is to maintain CDC25 inactive until mitosis entry. CDC25 activation counteracts MPF inhibition by WEE kinases and promotes mitosis progression. PP2A/B56 activity is maintained to a moderate level during mitosis. In fact, PP2A/B56 localizes to the centromere and kinetochore during mitosis through the interaction with the SAC component BubR1 and shugoshin[141]. The interaction with BubR1 is mediated by a LxxIxE motif that has been identified as SLiM for B56[142] (fig 20) and places the phosphatase at the kinetochore where stabilizes kinetochore-microtubule attachments[143,144]. On the other hand, shugoshin does not have this motif. Specific B56 isoforms that bind shugoshin localize at the centromere and prevent cleavage of centromeric cohesins[141,145]. PP2A/B56 acts by counteracting various kinases such as CDK1, PLK1 and Aurora B.
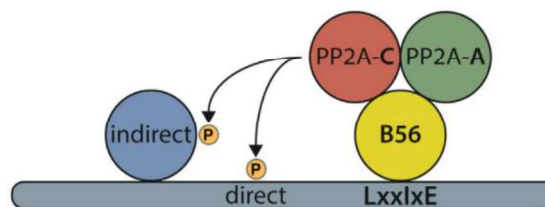
Figure 20. Substrate recognition by PP2A/B56. The regulatory B56 subunit recognises the SLiM motif LxxIxE and dephosphorylates residues located upstream. Taken from[142].

3.3 PP4

The major form of PP4 functions as heterotrimeric complex consisting of an evolutionary conserved catalytic subunit and two types of regulatory subunits, a structural protein (R2) and a regulatory one (R3). The regulatory subunit R3 contains a well conserved

Enabled/VASP homology 1 (EVH1) domain at its N-terminal that confers specificity to different substrates and subcellular localizations. Typical EVH1 domains bind proline rich sequence[146] but several studies propose EVH1 domain of PP4 to represent a new class of the EVH1 family that directly bind FxxP and MxPP motifs (fig 21)[147,148]. The exitance of SMK-1, a second target-binding domain that binds its substrates in an FxxP, MxPP independent manner, has recently been proposed[148].
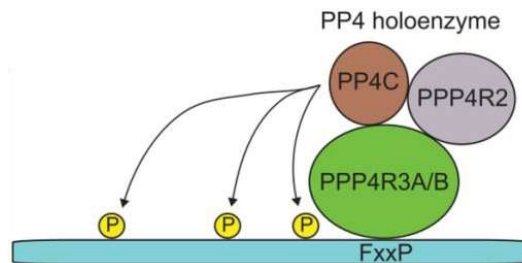
Figure 21. Substrate recognition by PP4. The regulatory R3 subunit recognises FxxP motif and dephosphorylates residues located upstream. Taken from[147].

Importantly for mitosis, PP4 has been described to regulate microtubule organization at centrosomes during mitosis and to dephosphorylate BAF in human cells[76,149,150]. Moreover, work in *Drosophila* has shown that PP4 localizes at the centromere and regulates centromere integrity. PP4 is recruited to the centromere by direct binding of the EVH1 domain of Flfl, to the Falafel- Interacting Motif (FIM) present in the C-terminal part of CenpC (fig 22). The expression of a mutant form of CenpC lacking the FIM domain impairs the centromeric localization of PP4 complex and induces CenpC re-localization to the spindle poles during mitosis[148,151].
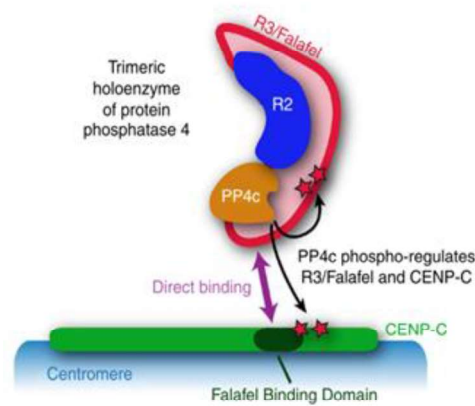
Figure 22. Recruitment of PP4 to centromeres. In *Drosophila,* CenpC recruit PP4 to the centromere through the direct interaction of Flfl with the FIM of CenpC. At the centromere PP4 regulates CenpC phosphorylation. Taken from [151].

3.4 PP6

PP6 works as a trimeric complex composed of a catalytic subunit, a Sit4-associated protein domain containing subunit and an Ankyrin repeat domain subunit. PP6 inhibits Aurora A activity at centrosomes by dephosphorylating its T-loop. It has been recently described that CDK1 phosphorylation of the PP6 regulatory subunit creates a docking site for PLK1 kinase. PLK1 phosphorylation negatively regulates PP6 ensuring high levels of Aurora A activity at the correct timing during mitosis. This complex regulation between Aurora A, PLK1 and PP6 has an impact in chromosome alignment and spindle formation temporal regulation[152,153].

4. THE CENTROMERE

The centromere is the region of the chromosomes where the kinetochore assembles during cell division creating a platform for the correct attachment of the spindle microtubules (fig 23). This mechanism is essential for ensuring accurate sister chromatid segregation to the daughter cells. Defective attachment of spindle microtubules causes segregation defects and aneuploidy, which is a common characteristic of tumour cells[154,155].
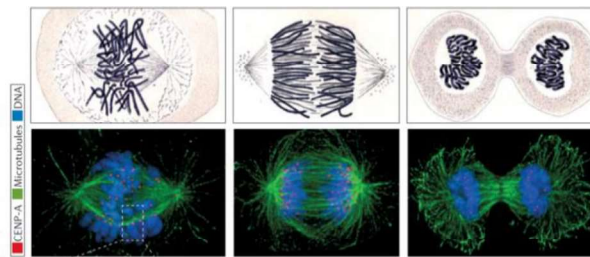
Figure 23. Visualization of the centromere at different mitosis stages. Mitotic Salamander cells drawn by Walther Fleming (top panel) are compared to immunofluorescence images of human cells (bottom panel) stained for microtubules (green), CenpA (red) and DNA (blue). Left images are cells at prometaphase-metaphase, middle images are cells at anaphase and right images are cells at telophase. Taken from[156].

4.1 Centromere identity: CenpA

Despite centromere function is evolutionarily conserved, the molecular organization of centromeres shows important differences across eukaryotes (fig. 24). Some plants and nematodes like *C. elegans* contain holocentric chromosomes, in which the centromere assembles along the entire length of the chromosome. However, most eukaryotes have monocentric chromosomes, in which the centromere assembles at a single chromosomal *locus,* whose size ranges from few basepairs (point centromeres) to megabases (regional centromeres). Point centromeres are best studied in budding yeast, in which all chromosomes contain a short conserved 125bp long DNA sequence

that is sufficient for kinetochore assembly. Instead, regional centromeres are longer and more complex. In the regional centromeres of *S. pombe* and *C.albicans*, a central AT-rich core region is flanked by repetitive heterochromatic DNA elements, while the regional centromeres of higher eukaryotes are largely composed by highly repetitive heterochromatic DNA elements. In these case, the actual primary sequence of centromeric DNA is neither necessary not sufficient for centromere function, as shown by the formation of neocentromeres at ectopic non-repetitive DNA sites and the random inactivation of one centromere in dicentric chromosomes. Instead, regional centromeres are epigenetically specified by the presence of a specialized chromatin organization in which the canonical histone H3 is replaced by a centromere-specific H3 variant, CenpA (also known as CenH3)[156]. CenpA is required for proper centromere/kinetochore assembly, being essential for viability in all eukaryotic species studied to date[157,158].
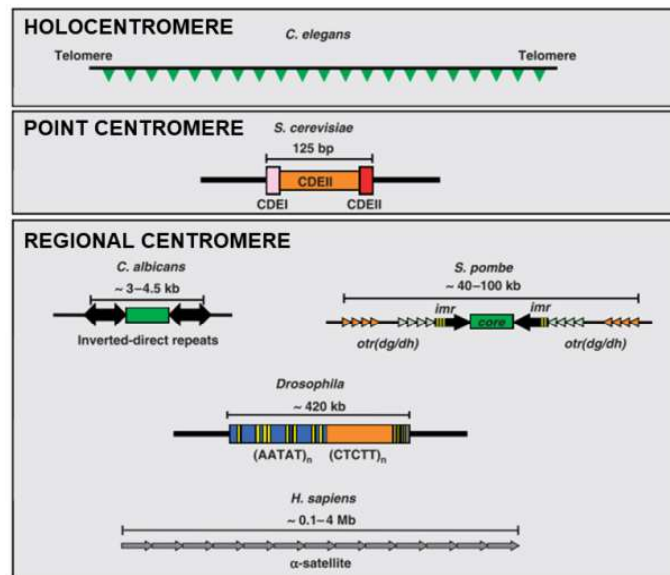
Figure 24. Schematic representation of the different types of centromeres. In the holocentric chromosomes of *C. elegans* centromeres, the centromere assembles along the entire chromosome (upper panel). Instead, *S. cerevisiae* has point centromeres, in which centromere function resides in a short 125bp long DNA sequence composed by a central AT-rich CDEII region flanked by conserved

CDEI and CDEIII elements (middle panel). However, most other eukaryotes (i.e. *C. albicans, S. pombe, Drosophila* and *H. sapiens*) have large regional centromeres enriched in repetitive heterochromatic DNA elements (lower panel). Taken from[159].

CenpA was first identified in humans and, with some remarkable exceptions, is present in all eukaryotes regardless of whether they have holocentromeres, point centromeres or regional centromeres[158]. CenpA contains a characteristic central histone fold domain (HFD), which shares significant homology with that of canonical H3, flanked by unstructured N- and C-terminal domains, which are only weakly conserved with respect to canonical H3, as well as in CenpA of different species (fig 25)[160]. The central HFD mediates centromere targeting of CenpA, which depends of the L1α2 region (CenpA targeting domain (CATD)). CATD is crucial for the interaction with specific CenpA chaperones that mediate CenpA deposition. CATD also mediates interaction with specific E3 ligases, which regulate CenpA expression and prevent miss-incorporation at non-centromeric sites, and with CenpN[161] and CenpC[162] centromeric proteins. The C-terminal domain is also essential for CenpC binding. On the other hand, the N-terminal domain is involved in recruitment of kinetochore proteins, such as BubR1 and the COMA complex[160].
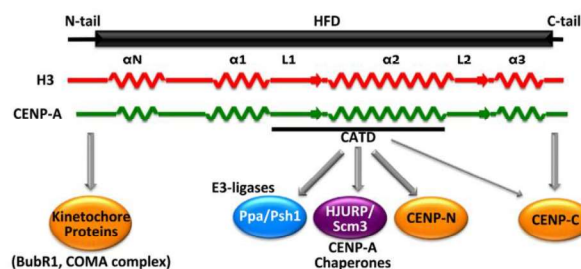
Figure 25. Schematic representation of the main features of canonical histone 3 and CenH3. The CATD domain is critical for targeting CenpA to the centromere, while the N-terminal domain is involved in recruiting kinetochore proteins and the C-terminal domain is recruiting CenpC. Taken from[160].

45

Centromeric CenpA deposition is replication independent and, in most species, occurs in late telophase-early G1, though deposition in metaphase has also been observed in *Drosophila*[163,164]. CenpA deposition requires specific chaperones, such as HJURP in humans and Scm3 in *S. pombe*. HJURP interacts with CenpA through the CATD and prevents CenpA degradation. In *Drosophila*, CenpA deposition depends on the unrelated chaperone chromosome alignment defect 1 (CAL-1)[165,166].

In centromeric chromatin, CenpA containing nucleosomes are interspersed with H3 containing nucleosomes and, in mitotic chromosomes, are positioned outwards in the surface of the centromere facing to the kinetochore, while H3 containing face inwards. This structural organization is proposed to mediate recruitment of kinetochore proteins and facilitate its assembly. In addition, centromeric chromatin is flanked by pericentromeric heterochromatin that has high density of cohesins, being critical to maintain sister chromatid cohesion up until the metaphase to anaphase transition (fig 26)[167].
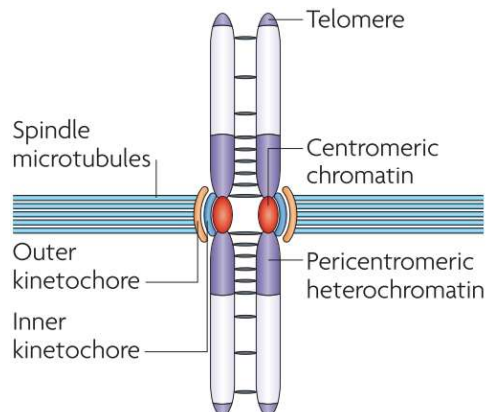
Figure 26. Schematic representation of 3D organization of centromeric chromatin in mitosis. CenpA nucleosomes face outwards in the surface of the centromere, recruit kinetochore proteins to properly assemble the kinetochore and attach spindle microtubules. Pericentromeric chromatin provides cohesion of the

sister chromatids. Taken from[168].

Centromeric chromatin is characterized by a specific pattern of post-translational modifications. In particular, centromeric H3 containing nucleosomes carry epigenetic modifications of transcriptionally active chromatin, such H3K4me2 and H3K36me, and, indeed, centromeric regions are actively transcribed by RNA polymerase II (RNAPII). This more open conformation of the centromeric chromatin facilitates CenpA deposition. CenpA containing nucleosomes are also decorated with a number of modifications, which are only poorly understood. On the other hand, pericentromeric chromatin contains typical heterochromatic marks, such H3K9me2,3 (fig 27)[156].
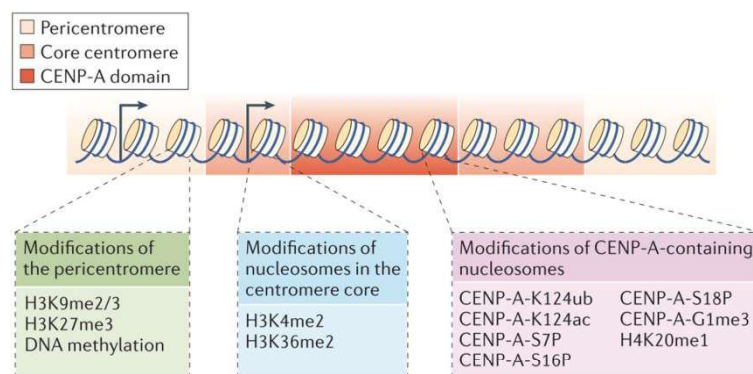
Figure 27. The centromeric chromatin. Graphic representation of the post-translational modification of the pericentromeric and core centromere chromatin. Taken from[156].

Moreover, non-coding transcripts originated from both centromeric chromatin and pericentromeric heterochromatin play functional roles at the centromere (fig 28). Centromeric transcripts have been proposed to mediate recruitment of centromeric proteins, such as CenpC, and to maintain higher order chromatin structures, while pericentromeric transcripts are involved in heterochromatinization and act as boundary between these two chromatin types[169,170].
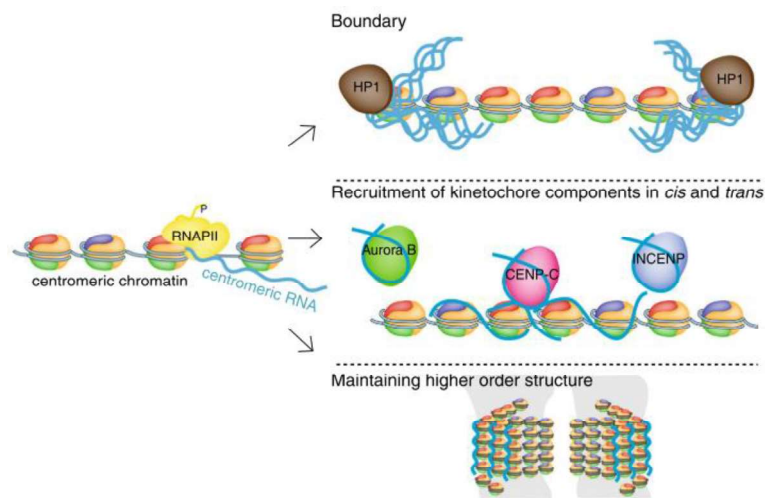
Figure 28. Schematic representation of centromeric RNAs and their functions. Centromeric RNAs act as a boundary between centromeric chromatin and pericentromeric heterochromatin, recruit and stabilize centromeric proteins, and contribute to higher order chromatin organization . Taken from[169].

4.2 The constitutive centromere associated network (CCAN): CenpC

The CCAN is an interface of proteins that constitutively binds the centromere during the whole cell cycle and links centromeric chromatin to the outer kinetochore in mitosis (fig 29). In vertebrates, the CCAN is composed by 16 proteins grouped in 7 functional groups based on genetic and biochemical analysis[156]:

- CenpB
- CenpC
- CenpH/CenpI/CenpK
- CenpL/CenpM/CenpN
- CenpO/CenpP/CenpQ/CenpR/CenpU
- CenpT/CenpW
- CenpS/CenpX

Although the CCAN is evolutionary conserved between yeast and vertebrates, in *Drosophila* and *C. elegans* is composed by only the CenpC (fig 29)[171].
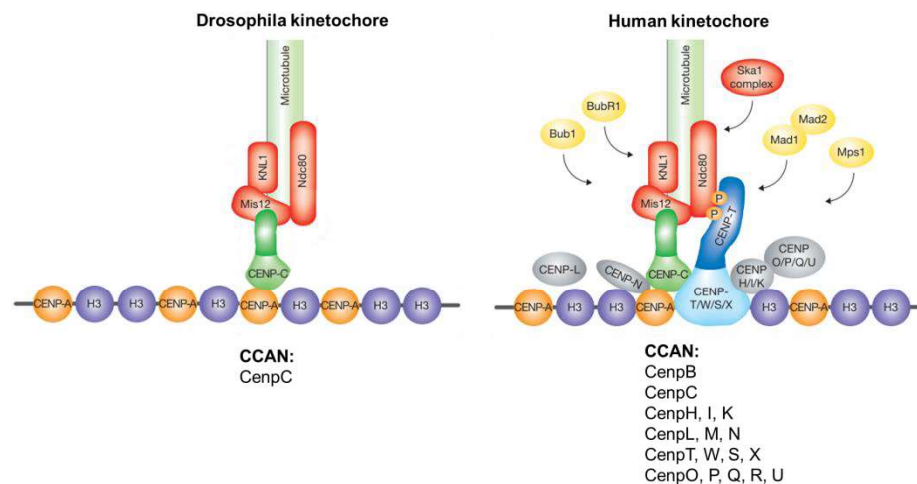
Figure 29. The CCAN of *Drosophila* and human kinetochores. In the *Drosophila* kinetochore, CCAN is composed only by CenpC (left), whereas in the human kinetochore (right) the CCAN is composed by 16 Cenp proteins. Adapted from[171].

CenpC is an essential centromere component that links CenpA containing nucleosomes to the outer kinetochore protein Mis12 and plays a crucial role in kinetochore assembly. CenpC depletion interferes with kinetochore assembly causing chromosome segregation defects and mitotic delays[172,173]. In vertebrates, CenpC acts upstream of other CCAN components since its N-terminal domain has been described to be responsible for recruiting other CCAN components, outer kinetochore proteins and checkpoint elements during mitosis[173,174]. In *Drosophila*, CenpC deposition at centromeres occurs in interphase, at the late S and G2, and during metaphase[163]. Centromeric localization of CenpC depends on CenpA and, in *Drosophila*, centromeric localization of CenpC, CenpA and CAL-1 is interdependent[163]. CenpC dimerizes and is capable of binding DNA and RNA. In this regard, it has been shown that specific non-coding

RNAs mediate centromeric CenpC localization in *Drosophila*[170,175,176].

CenpC is regulated by phosphorylation. In yeast, Aurora B has been proposed to phosphorylate CenpC at the Mis12 binding site in erroneous kinetochore-microtubule attachments. This phosphorylation weakens microtubule attachment and prevents chromosome missegregation[177]. In chicken and human cells, it has been described that CenpC phosphorylation by CDK1 at the C-terminal region favours CenpA-CenpC interaction[178]. On the other hand, in *Drosophila,* the FIM domain of CenpC directly interacts with the PP4 regulatory subunit Flfl and mediates centromeric localization of PP4. This interaction is crucial for stabilizing CenpC at the centromere during mitosis[151].

4.3 Centromeric BAF (cenBAF)

Previous work in our group showed that, in *Drosophila,* a fraction of BAF (cenBAF) associates with the centromere throughout the cell cycle (fig. 30) and co-immunoprecipitates with CenpC [92]. In interphase, BAF also localizes to heterochromatin. At mitosis entry, phosphorylation by VRK1/NHK1 weakens BAF binding to chromatin and the bulk of BAF is released from heterochromatin, while cenBAF remains bound to the centromere (fig 30a). In addition, while a phospho-mimetic BAF mutant form is not capable of binding chromatin, a phospho-dead BAF mutant localizes at centromeres in metaphase chromosomes, (fig 30b). These results suggest that the fraction of cenBAF that remains at the centromere during mitosis is not phosphorylated. How cenBAF is kept not phosphorylated during mitosis was not known.
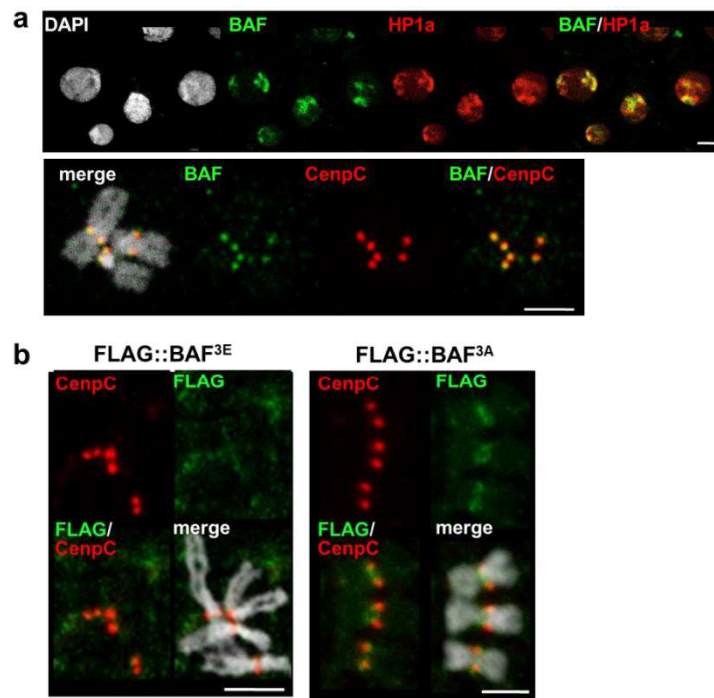
Figure 30. Centromeric BAF localization. a: The patterns of immunolocalization with αBAF antibodies (green), and αHP1a (red, upper panel) or αCenpC (red, lower panel). DNA is stained with DAPI. The upper panel shows interphase S2 cells where BAF co-localizes at the heterochromatic regions marked by HP1a. Scale bars correspond to 5μm. The lower panel presents metaphase chromosomes from S2 cells showing co-localization between BAF and CenpC at the centromeric localization. Scale bars correspond to 2,5μm. **b:** Immunostaining with αFLAG antibodies (green) in metaphase chromosomes from cells transiently expressing a phosphormimic form of BAF (FLAG::BAF^{3E} (left panel)) or a phosphodead form of BAF (FLAG::BAF^{3A} (right panel)). Immunostaining with αCenpC antibodies (red) is also presented. DNA is stained with DAPI. Scale bar is 5μm. Adapted from [92].

cenBAF is important for centromere assembly and function since BAF depletion leads to decreases centromeric CenpA and CenpC levels, and increases the percentage of mitoses with chromosome segregation defects (fig 31)[92].
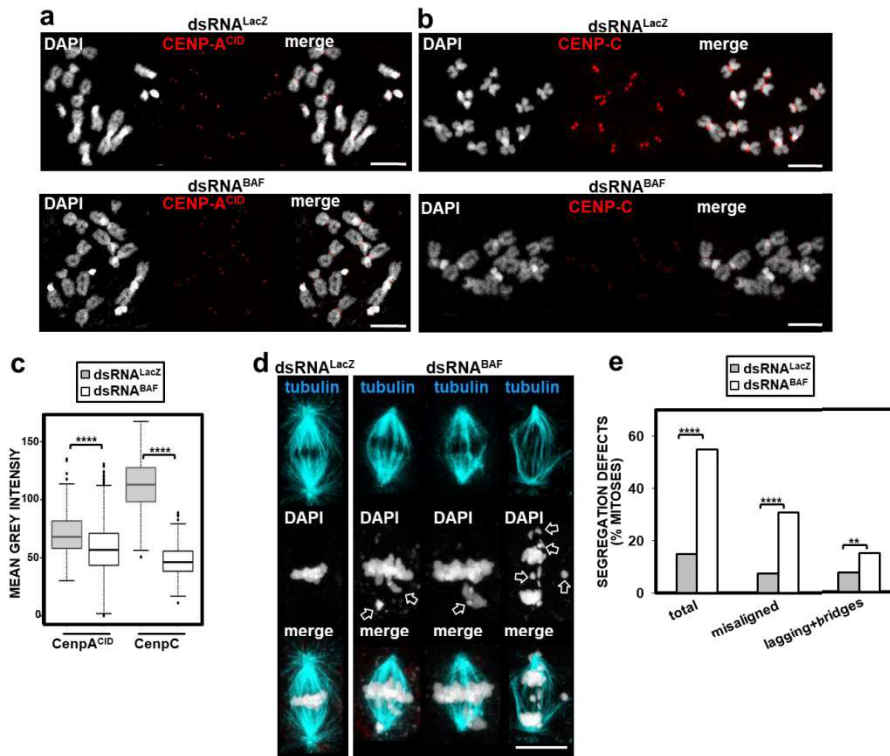
Figure 31. cenBAF is required for centromere assembly and function. Taken from[92]. **a** and **b** Centromeric immunolocalization with αCenpA^{CID} and αCenpC antibodies (red) in metaphase chromosomes from control (dsRNA^{LacZ}) and BAF depleted (dsRNA^{BAF}) S2 cells. DNA is stained with DAPI. Scale bars correspond to 5 µm. **c:** Mean grey values per centromere of αCenpA^{CID} and αCenpC fluorescence presented in a and b. Values correspond to a representative experiment out of five independent experiments showing equivalent results (N > 382; Kruskal–Wallis test, ****p-value < 0.0001. **d:** Metaphase figures from dsRNA^{BAF} and control dsRNA^{LacZ} cells. αTubulin immunostaining (blue) marks the mitotic spindle and DNA is stained with DAPI. Arrows indicate chromosome segregation defects. Scale bar corresponds to 5 µm. **e**: Percentages of mitoses showing segregation defects for dsRNA^{BAF} and control dsRNA^{LacZ} cells. Values are the sum of two independent experiments showing equivalent results (N > 104; two-tailed Fisher's test, **p < 0.01, ****p < 0.0001).

4.4 The outer kinetochore: SAC

CCAN recruits the components of the outer kinetochore which are known as the KMN network and is integrated by KNL1 protein, the Mis12 complex and the Ndc80 complex. These proteins begin to be detectable at the kinetochores at G2 and are dissociated at the end of

mitosis. Interaction between the kinetochore and microtubules is the main task of the KMN network (fig 32)[179,180].
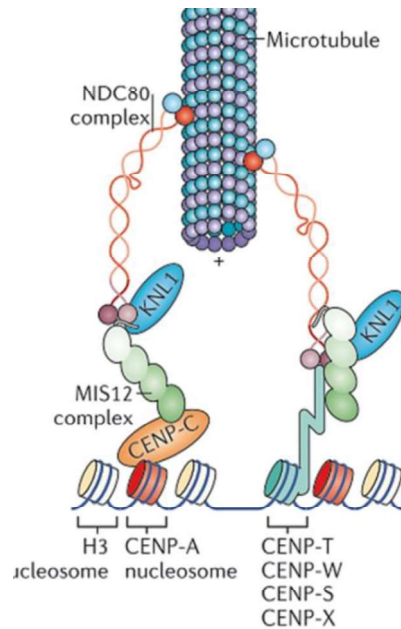
Figure 32. Schematic representation of the main outer kinetochore components. The outer kinetochore is composed by Mis12 complex, KNL1 and Ndc80 complex. They bind to the centromere during mitosis and mediate spindle microtubule attachment. Taken from[156].

The outer kinetochore also contains activities that sense proper spindle attachment and regulate metaphase to anaphase progression. APC/C activation is key to promote transition to anaphase (fig 33)[181,182]. APC/C is an E3 ubiquitin ligase that targets several proteins for proteolytic degradation. One of its substrates is securin, a protein that inhibits separase. When APC/C is activated, securin is degraded by the proteasome allowing separase to be active and cleave centromeric cohesins releasing sister chromatids cohesion. Another important APC/C target is cyclin B that when degraded leads to CDK1 inactivation. As a consequence, APC/C regulates metaphase to anaphase transition and mitosis exit. APC/C activity is inhibited until kinetochores are properly attached to the mitotic spindle and the SAC is satisfied. Unattached kinetochores are marked by MPS1, a kinase

that drives a signalling cascade leading to the recruitment of the mitotic checkpoint effector complex (MCC) components Mad2, BubR1, Cdc20 and Bub3 to the kinetochores. Importantly, MPS1 signalling induces a closed configuration of Mad2 that binds and sequesters the APC/C coactivator Cdc20 (fig 33)[183]. Once sister chromatids are properly attached to opposite poles of the mitotic spindle, tension is generated that releases MCC components, inducing a conformational change in Mad2 to an open conformation that no longer binds Cdc20. As a consequence, free Cdc20 activates APC/C[181,182].
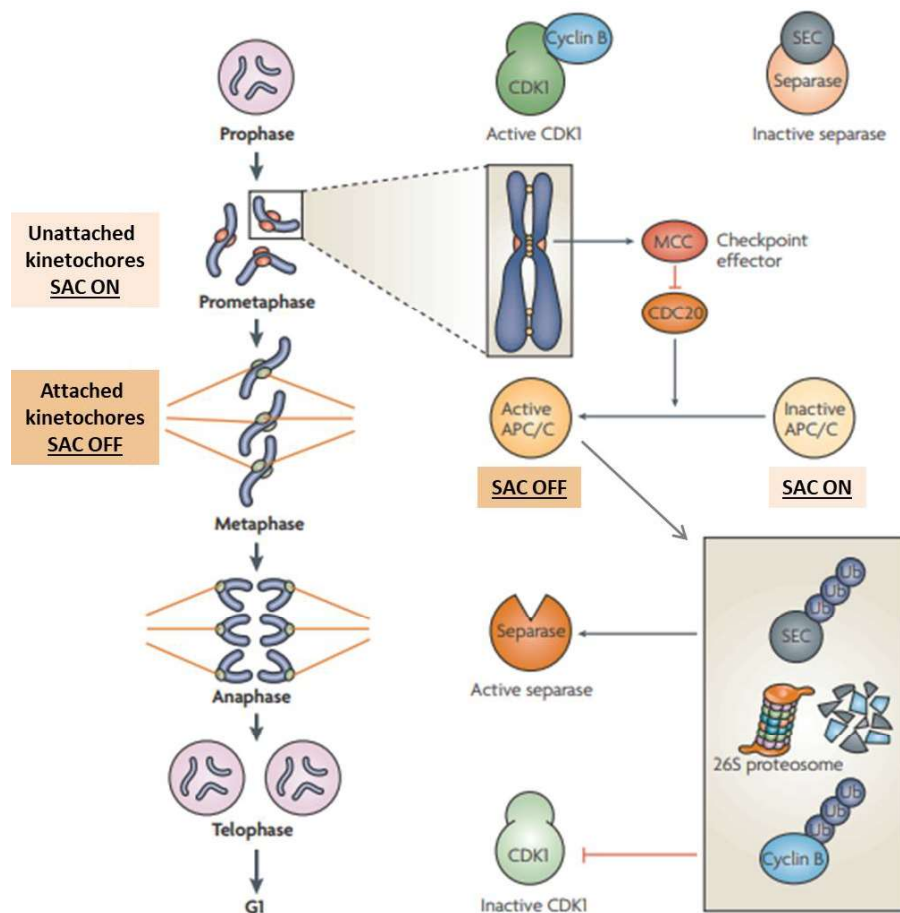
Figure 33. Schematic representation of SAC. When kinetochores are properly attached to microtubules the SAC is satisfied and Cdc20 is able to interact and activate the APC/C complex. APC/C targets securin and cyclinB to degradation, promoting metaphase to anaphase transition and mitosis exit. Adapted from[184].

Besides MPS1, there are several other kinases involved in SAC regulation. CDK1 phosphorylates kinetochore components favouring the stabilization of proteins that inhibit the progression of SAC. Aurora B phosphorylates the outer kinetochore protein Ndc80 at kinetochores that are not properly attached to microtubules, leading to its de-attachment and indirectly promoting MPS1 recruitment. As soon as correct attachments are formed, several phosphatases are involved in dephosphorylating kinetochore proteins to stabilize microtubule attachment and to favour SAC progression. In this regard, PP2A/B56, which is recruited to the kinetochore *via* its interaction with BubR1, opposes MPS1 and Aurora B stabilizing microtubule-kinetochore attachments (fig 34)[6,185].
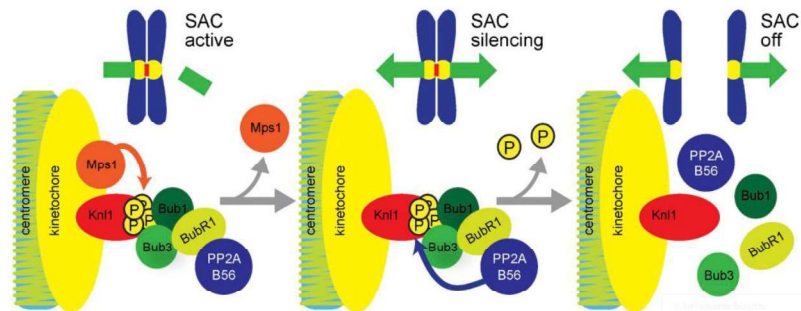
Figure 34. Schematic representation of the role of PP2A/B56 at the kinetochore. PP2A/B56 is recruited to the kinetochore by its interaction with BubR1 and antagonises MPS1 and Aurora B phoshorylations to stabilize microtubule-kinetochore attachment and promote SAC silencing. Taken from[186].

The SAC ensures fidelity of chromosome segregation during mitosis. However, some chromosome segregation aberrations, such as merotelic attachments and acentric chromosome fragments caused by DNA breaks are not well sensed by the SAC. These defects can lead to the generation chromatin bridges and lagging chromosomes that are left behind from the bulk of segregating chromosomes (fig 35)[187].
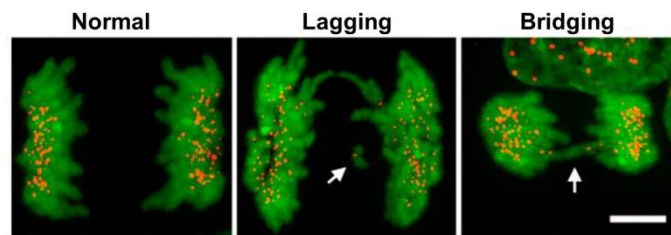
Figure 35. Chromosome segregation defects. Immunostainings of retinal pigment epithelium cells in mitosis in which the red signal corresponds to kinetochores stained with PICH and the green signal to DNA stained with Hoechst. Scale bars correspond to 10µm. A normal mitosis is shown in the left. Arrows indicate lagging chromosomes (centre) and chromatin bridges (right).

It has been proposed that a chromosome segregation checkpoint senses these problems and delays anaphase progression (fig 36)[188]. This checkpoint consists of an Aurora B phosphorylation gradient, in which high Aurora B concentration in the midzone prevents decondensation of the lagging chromosomes and delays NER to favour their incorporation to the bulk of segregating chromosomes. This Aurora B gradient may act by stabilizing cyclin B therefore converting the Aurora B gradient into a CDK1 activity gradient. Overall, this checkpoint co-ordinately regulates chromosome segregation, chromatin decondensation and NER to boost the correction of segregation defects left undetectable by the SAC[189–192]. In addition, Aurora B is also involved in the NoCut pathway, also known as abscission checkpoint. Aurora B locally senses the presence of chromatin bridges and inhibits abscission[193,194].

Aurora B gradient

Aurora B < PP	Aurora B > PP	Aurora B < PP
Dephosphorylated substrates	Phosphorylated substrates	Dephosphorylated substrates
Decondensed chromsomes	Condensed chromsomes	Decondensed chromsomes
NER	No NER	NER

The lagging chromosomes keeps decondensed and no NE is assembled around it.

The NE is not fully assembled where the main nucleus faces the midzone area (higher Aurora B) allowing the lagging chromosome to be reincorporated.

Figure 36. The Aurora B gradient favours the reincorporation of lagging chromosomes into the main mass of chromatin. High levels of Aurora B at the midzone area of the cell cause phosphorylation of substrates delaying decondensation of the chromatin and NER to happen around the lagging chromosome. This facilitates its reincorporation to the main mass of chromatin. Adapted from[190].

5. THE PERICHROMOSOMAL COMPARTMENT

Mitotic chromosomes are surrounded by a perichromosomal comparted composed by proteins and RNA molecules, many of them derived from the nucleoli, that coat the mitotic chromosomes (fig 37)[195]. This perichromosomal layer plays a protective role by creating a physical barrier that insulates chromosomes from cytoplasmic elements and maintains chromosome structure upon NEB[196,197]. However, its actual composition and functions are not fully understood yet. The list of components of the chromosome periphery compartment keeps growing, but little is known about the specific contribution of each of them. The best characterized component of the perichromosomal layer is the nucleolar protein Ki-67[197]. Although Ki-67 is found only in vertebrates, αKi-67 antibodies recognizes an antigen found in the NE of the early *Drosophila* embryo[198].
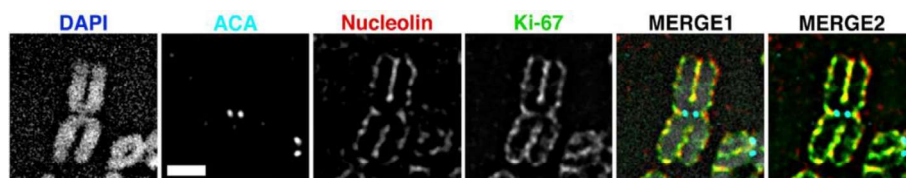
Figure 37. The perichromosomal layer. Immunostainings of mitotic chromosomes from retinal pigment epithelial cells with αACA (light blue), which marks the centromere, αNucleolin (red) and αKi-67 (green), which are two components of the perichromosomal periphery of nucleolar origin. DNA is stained with DAPI (grey). Scale bar corresponds to 1μm. Taken from[199].

Ki-67 is a well-known proliferation marker used to determine the prognostic of tumour progression[200]. Structurally, it is composed by a C-terminal domain with chromatin binding properties and a N-terminal domain that extends out from chromatin and contains a PP1 binding site and a forkhead-associated (FHA) domain[201]. The chromatin assembly factor 1 (CAF-1) has been proposed to work as the Ki-67

chaperon[202]. Ki-67 binds chromatin and interacts with components of the perichromosomal, such as pescadillo ribosomal biogenesis factor 1 (PES1), nucleolin, nucleolar protein interacting with the FHA domain of Ki-67 (NIFK) or B23, being required for their localization[201,203]. Ki-67 is regulated by CDK1 phosphorylation during mitosis and cooperates with Repo-man to recruit PP1 to the perichromosomal layer at the end of the mitosis, where dephosphorylates Ki-67 itself and other nucleolar proteins[203].

Ki-67 is required for establishment and maintenance of the rod shaped structure of mitotic chromosomes, prevents fusion of chromosomes that are in close proximity and, at the end of mitosis, contributes to create a boundary that insulates mitotic chromatin from cytoplasmic components[204,205]. At early mitosis, Ki-67 forms repulsive molecular brushes that maintain chromosomes as individual entities. These brushes collapse at the end of mitosis, favouring the clustering of chromosomes at NER (fig 38)[206,207].
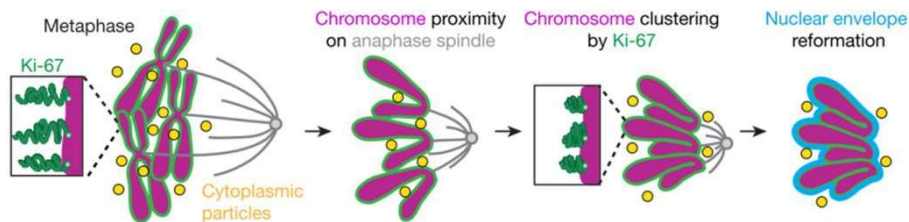
Figure 38. The role of the perichromosomal component Ki-67 in nucleo-cytoplasmic compartmentalization during mitosis. Ki-67 (green) keeps chromosomes (purple) as individual structures but, at the end of the mitosis, it helps clustering of chromosomes and insulates them from cytoplasmic elements (yellow). Taken from**[132]**.

OBJECTIVES

Barrier-to-Autointegration Factor (BAF) binds chromatin and interacts with NE LEM-d proteins, helping to anchor chromatin to the NE. Phosphorylation regulates BAF function. At mitosis entry, VRK1/NHK1-dependent phosphorylation releases BAF from chromatin and weakens the interaction with LEM-d proteins, contributing to NEBD. Later, at mitosis exit, dephosphorylation of BAF restores binding to both chromatin and LEM-d proteins, being crucial for NER.

Work in our group showed that a fraction of BAF (cenBAF) associates with the centromere through mitosis and, most likely, stays non-phosphorylated during mitosis. However, the mechanisms and factors that regulate cenBAF localization and prevent its phosphorylation are not known. This work addresses these questions. In particular, the specific objectives of this thesis are:

1. Analysis of the role of protein phosphate PP4 in determining cenBAF localization and the consequences of its disruption.

2. Analysis of the pattern of BAF phosphorylation and its regulation by protein phosphatases PP2A and PP4.

RESULTS

1. THE REGULATION OF cenBAF LOCALIZATION

1.1 cenBAF localization depends on PP4

Previous work in our group suggested that, in contrast to the bulk of BAF that is phosphorylated by VRK1/NHK1 and released from chromatin at mitosis entry, the fraction of BAF that remains associated to the centromere during mitosis (cenBAF) was not phosphorylated[92]. However, the factors and mechanisms regulating centromeric cenBAF localization were unknown. In this regard, it was shown that, in *Drosophila,* PP4 localizes at the centromere during mitosis through the direct interaction of the regulatory Flfl subunit with CenpC[151]. Moreover, it was shown that PP4 dephosphorylates BAF in mammalian cells[76]. All these observations, led us to hypothesize that PP4 may be involved in regulating cenBAF localization during mitosis.

To test this possibility, we used an experimental approach in which centromeric localization of PP4 is impaired. The FIM domain of CenpC mediates direct interaction with Flfl and, thus, PP4 recruitment. In order to impair centromeric PP4 localization, we took advantage of *Drosophila* S2 cell lines stably expressing an RNAi-resistant GFP::CenpCΔFIM^R form that lacks the FIM domain (fig 39a) and, as control, a cell line expressing full length RNAi-resistant GFP::CenpC^R. We expected that RNAi depletion of endogenous CenpC would affect Flfl recruitment to the centromere in GFP::CenpCΔFIM^R-expressing cells, but not in control GFP::CenpC^R-expressing cells. Indeed, immunostaining experiments showed that, upon CenpC depletion, αFlfl signal was reduced to undetectable levels in a large proportion of mitosis in GFP::CenpCΔFIM^R-expressing cells in comparison to control GFP::CenpC^R-expressing cells (fig 39b and c).
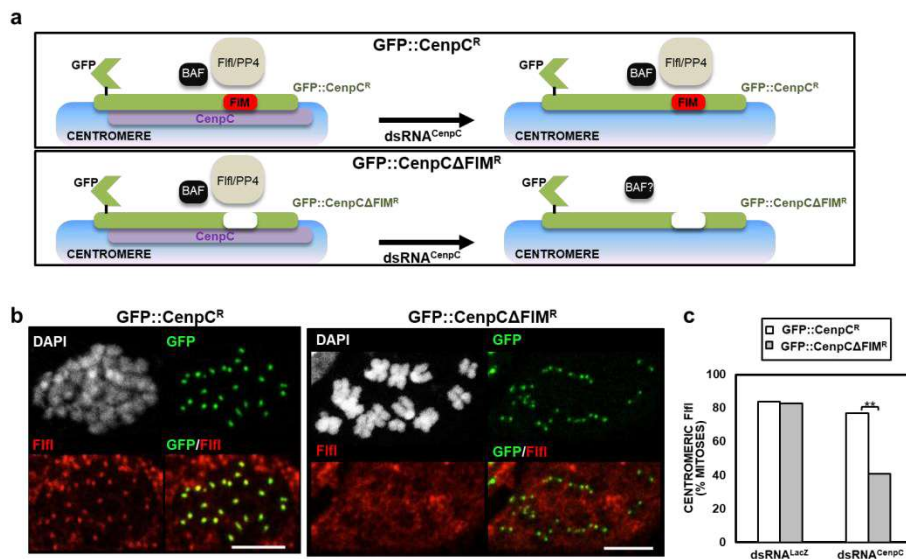
Figure 39. Centromeric Flfl localization is impaired in cells expressing a CenpCΔFIM^R form missing the FIM domain. a: Schematic representation of the experimental approach used in this work. We hypothesized that depletion of endogenous CenpC in cells expressing an RNAi-resistant GFP::CenpCΔFIM^R construct would impair centromeric Flfl localization and, thus, PP4 recruitment. The FIM domain is indicated in red and endogenous CenpC is indicated in magenta. **b:** Immunostainings with αFlfl antibodies (red) are presented for CenpC depleted cells expressing the indicated constructs. GFP signals (green) are direct fluorescence. DNA is stained with DAPI (white). Scale bars correspond to 5µm. **c:** Quantitative analysis of the results shown in c: The proportion of mitoses where Flfl is detected at the centromeres is presented for control dsRNA^{LacZ} and dsRNA^{CenpC} cells expressing the indicated constructs. Values are the sum of 3-5 independent experiments showing equivalent results (N> 45; two-tailed Fisher's test, p-value **<0.01).

Next, we analysed the effects of impairing centromeric PP4 recruitment on cenBAF localization. We observed that, while depletion of endogenous CenpC in control GFP::CenpC^R-expressing cells did not affect cenBAF levels, depletion in cells expressing GFP::CenpCΔFIM^R strongly reduced cenBAF (fig 40a). In addition, we observed that immunoprecipitation with αBAF antibodies pulled-down full length GFP::CenpC^R, but not GFP::CenpCΔFIM^R (fig 40b).
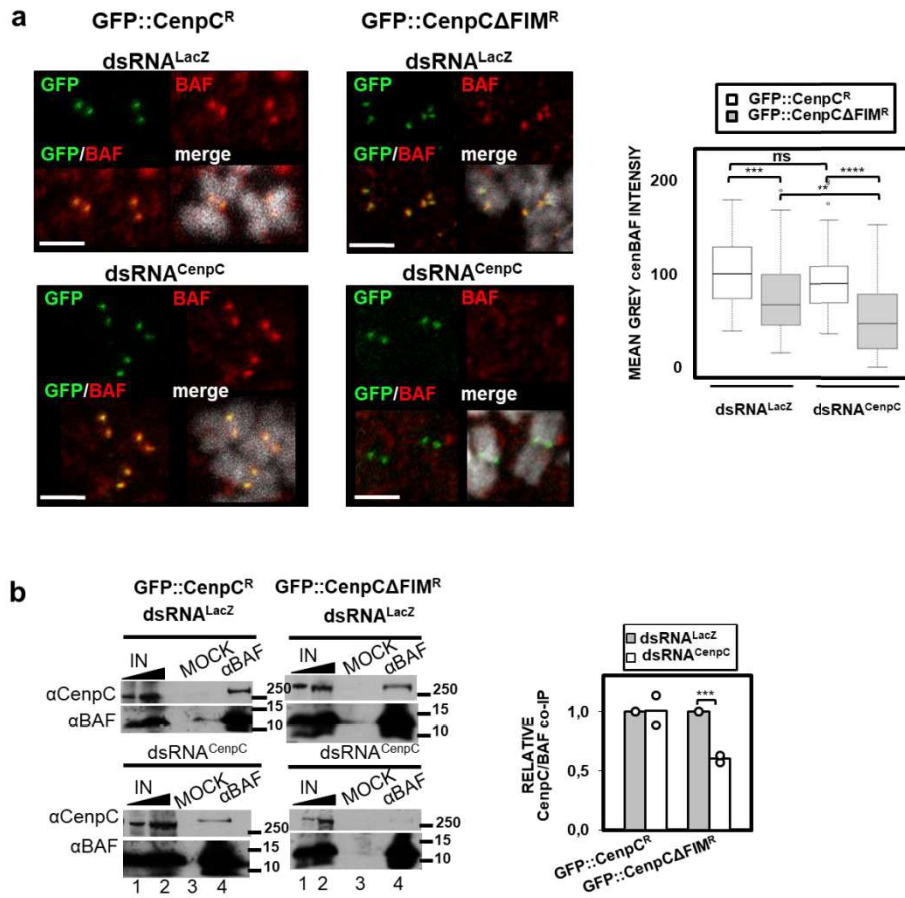
Figure 40. cenBAF localization is impaired in CenpCΔFIM^R-expressing cells.
a: In the left, αBAF staining (red) presented in cells expressing GFP::CenpC^R (left) or GFP-CenpCΔFIM^R (right) upon CenpC depletion (dsRNA^{CenpC}) and in control (dsRNA^{LacZ}) cells. GFP (green) is direct fluorescence. DNA is stained with DAPI (white). Scale bars are 2.5µm. In the right, quantification of the mean grey value of αBAF signal per centromere is shown for control dsRNA^{LacZ} and dsRNA^{CenpC} cells expressing the indicated construct. Values correspond to a representative experiment out of five independent experiments showing equivalent results (N > 48; Kruskal–Wallis test, p-value: ns > 0.05, **p < 0.01, ***p < 0.001, ****p < 0.0001). **b:** In the left, co-IP experiments performed with αBAF antibodies using extracts prepared from control dsRNA^{LacZ} and dsRNA^{CenpC} cells expressing GFP::CenpC^R (left) and GFP::CenpCΔFIM^R (right) (lanes 4). Lanes 3 correspond to mock IPs performed with preimmune serum. Lanes 1 and 2 correspond to 2% and 5% of the input material, respectively. IP-materials are analysed by WB using αCenpC and αBAF antibodies. In the right, quantitative analysis of the co-IPs is presented. The CenpC/BAF ratio normalized with respect to the corresponding control dsRNA^{LacZ} is presented for cells expressing the indicated constructs. Results are the average of 2 independent experiments (two-tailed t-test, p-value: *** <0.001).

69

Similar results were observed upon Flfl depletion (fig. 41). Flfl-depleted cells showed normal total BAF levels, as judged by WB analysis (fig. 41a). However, similar to what was observed in CenpC-depleted CenpCΔFIM-expressing cells, Flfl-depleted cells showed reduced cenBAF levels (fig 41b) and impaired CenpC co-immunoprecipitation with αBAF antibodies (fig 41c).
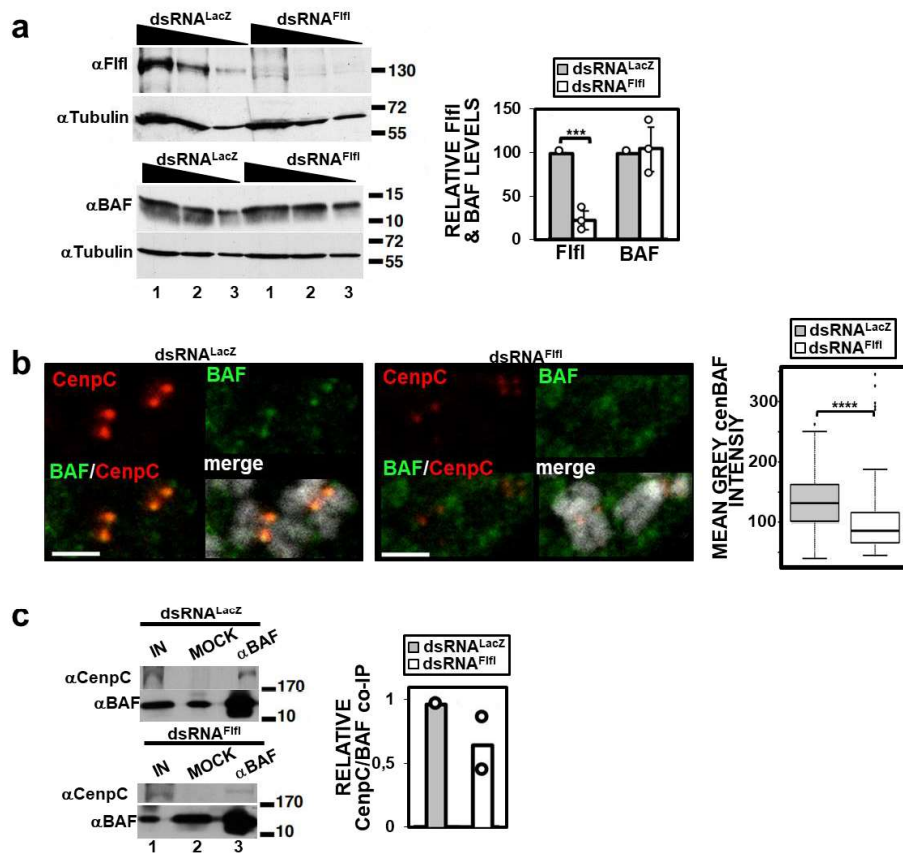
Figure 41. Flfl depletion disrupts cenBAF localization. a: In the left, the levels of Flfl (top) and BAF (bottom) are determined by WB in total cell extracts prepared from cells treated with dsRNA against Flfl (dsRNA[Flfl]) (right) or against LacZ (dsRNA[LacZ]) (left). Increasing amounts of extract are analysed (lanes 1-3). αTubulin antibodies are used for normalization. The position of MW markers (in kDa) is indicated. In the right, quantitative analyses. The relative Flfl and BAF levels are presented for dsRNA[Flfl] and control dsRNA[LacZ] cells. Results are the average of 3 independent experiments (error bars are SD; two-tailed t-test, p-value ***< 0.001). **b:** In the left, immunostainings with αBAF (green) and αCenpC antibodies (red) are presented for mitotic chromosomes from dsRNA[Flfl] (right) and control dsRNA[LacZ] (left) cells. DNA was stained with DAPI. Scale bars correspond

to 2.5µm. In the right, quantitative analysis. The mean grey values per centromere of αBAF fluorescence are shown for dsRNA^{Flfl} and control dsRNA^{LacZ} cells. Values correspond to a representative experiment out of 3 independent experiment showing equivalent results (N= 67; Kruskal-Wallis test, p-value ****< 0.0001). **c:** In the left, coIP experiments performed with αBAF antibodies using extracts prepared from dsRNA^{Flfl} (bottom) and control dsRNA^{LacZ} (top) cells (lanes 3). Lanes 2 correspond to mock IPs performed with preimmune serum. Lanes 1 correspond to 3% of the input material. IP-materials are analysed by WB using αCenpC and αBAF antibodies. The position of MW markers (in kDa) is indicated. In the right, quantitative analysis. The relative ratio of αCenpC and αBAF signals is presented for dsRNA^{Flfl} and control dsRNA^{LacZ} cells. Results are the average of 2 independent experiments (two-tailed t-test, p-value > 0.05).

Altogether these results suggest that centromeric localization of cenBAF depends on PP4/Flfl.

1.2 Impaired centromeric localization of PP4 and cenBAF induces the accumulation of perichromosomal BAF during mitosis

We observed that, concomitant to decreased cenBAF, CenpC depletion in GFP::CenpCΔFIM^R-expressing cells induced intense αBAF immunostaining at the perichromosomal compartment in ~50% of the mitosis, which is infrequent when CenpC depletion is performed in control GFP::CenpC^R-expressing cells (fig 42a). However, WB analysis shows that total BAF levels do not significantly change upon CenpC depletion in both GFP::CenpCΔFIM^R-expressing cells and control GFP::CenpC^R-expressing cells (fig 42b). Similarly, Flfl depletion also increased the percentage of mitosis with perichromosomal BAF (fig 43). We noticed that GFP::CenpCΔFIM^R-expressing cells also showed increased perichromosomal BAF in control cells treated with dsRNA^{Lacz}, though to a much lower frequency than when endogenous CenpC is depleted (fig. 42a, graph in the right).

71
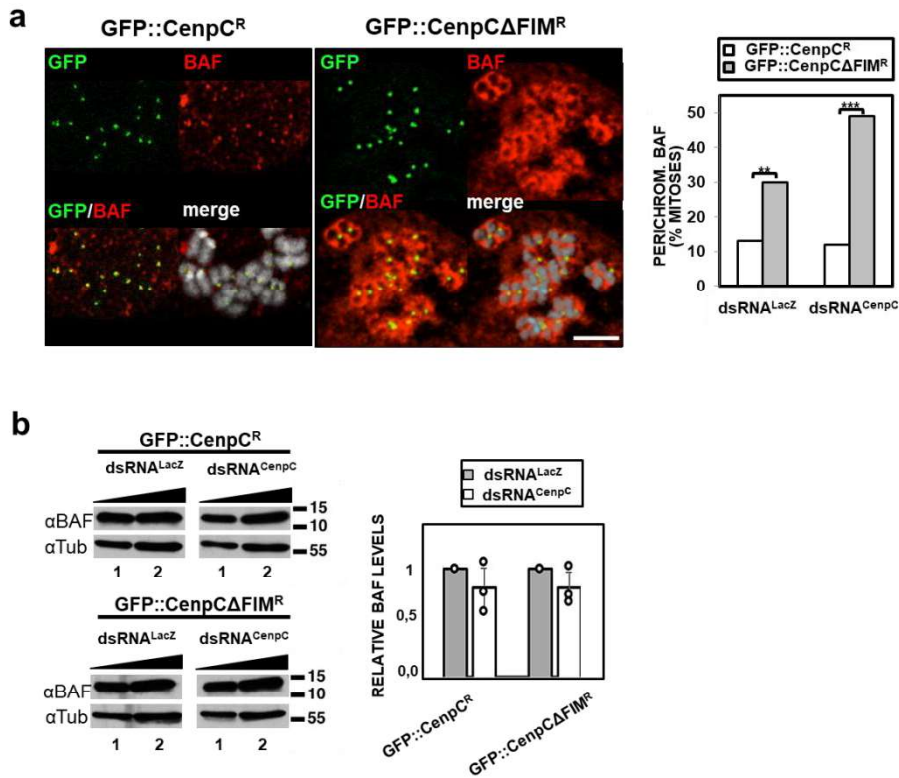
Figure 42. GFP::CenpCΔFIM^R expressing cells show aberrant accumulation of perichromosomal BAF during mitosis. a: In the left, immunostainings with αBAF antibodies (red) are presented in dsRNA^CenpC cells expressing the indicated constructs. GFP signals are direct fluorescence (green). DNA is stained with DAPI (white). Scale bars correspond to 5µm. In the right, the percentages of mitoses showing perichromosomal BAF are presented for control dsRNA^LacZ and dsRNA^CenpC cells expressing the indicated constructs. Values correspond to the sum of 3-4 independent experiments showing equivalent results (N > 73; two-tailed Fisher's test, **p-value < 0.01, ***p-value < 0.001). **b:** In the left, the levels of BAF are determined by WB with αBAF antibodies in total extracts prepared from cells expressing GFP::CenpC^R (top) and GFP::CenpCΔFIM^R (bottom) treated with dsRNA^LacZ (left) and dsRNA^CenpC (right). Increasing amounts of extract are analysed (lanes 1 and 2). αTubulin antibodies are used for normalization. The position of MW markers (in kDa) is indicated. In the right, quantitative analysis is shown. The relative levels of BAF in cells expressing GFP::CenpC^R and GFP::CenpCΔFIM^R after treatment with dsRNA^LacZ and dsRNA^CenpC are presented. Results are the average of 3 independent experiments (error bars are SD; two-tailed t-test, p-value > 0.05).
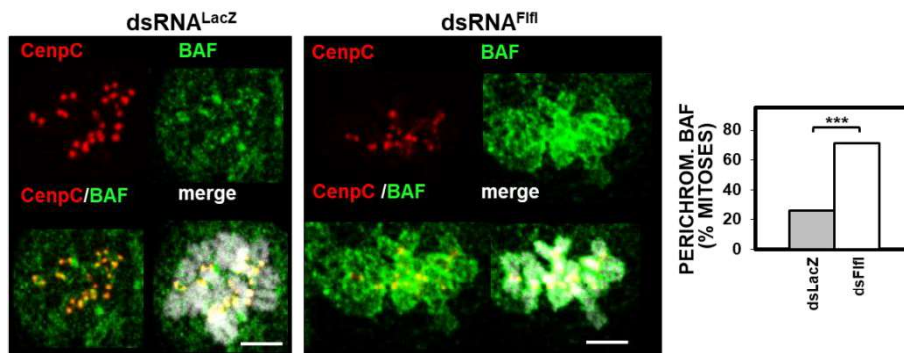
Figure 43. FLFL depletion leads to aberrant accumulation of perichromosomal BAF during mitosis. The left panel shows patterns of immunolocalization with αBAF (green) and αCenpC (red) antibodies for control dsRNA^{LacZ} cells and cells treated with dsRNA against Flfl (dsRNA^{Flfl}). DNA is stained with DAP (white). Scale bars correspond to 5µm. The right panel shows the percentage of mitosis with perichromosomal BAF for the indicated RNAi-treated cells. Values are the sum of 7 independent experiments showing equivalent results (N>300; two-tailed Fisher's test, ***p < 0.001).

As shown above, impairing centromeric PP4 localization in CenpC depleted GFP::CenpCΔFIM^R-expressing cells, as well as in Flfl-depleted cells, reduces centromeric cenBAF levels (figs. 40 and 41). In this regard, in CenpC-depleted GFP::CenpCΔFIM^R-expressing cells, we observed a positive correlation between the presence of perichromosomal BAF and reduced cenBAF levels at the centromere since, mitoses showing perichromosomal αBAF immunostaining have lower cenBAF levels than mitoses without perichromosomal BAF (fig 44).
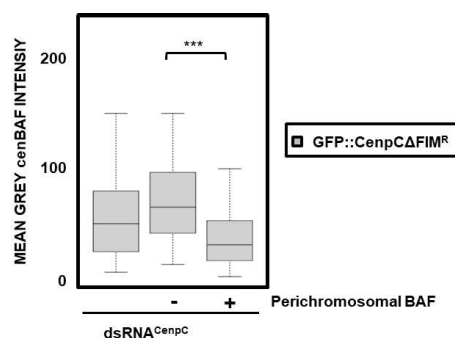
Figure 44. Perichromosomal BAF accumulation correlates with reduced cenBAF levels. The mean grey intensity per centromere of αBAF fluorescence for CenpC-depleted cells expressing GFP::CenpCΔFIM^R showing or not showing perichromosomal BAF accumulation. Values correspond to a representative

experiment out of five independent experiments showing equivalent results (N > 38; Kruskal–Wallis test, ***p-value < 0.001,).

Altogether these results suggest that disturbing centromeric localization of PP4 and cenBAF induces aberrant accumulation of BAF in the perichromosomal compartment.

1.3 The accumulation of perichromosomal BAF depends on PP2A

Normally, in mitosis, the bulk of BAF stays phosphorylated and free in the mitotic cell. Phosphorylated BAF (pBAF) re-associates with chromatin only after chromosomes start to decondense in late anaphase/telophase, an event that marks the formation of the "core region" and the initiation of NER. The association of BAF with chromatin is regulated by PP2A phosphatase that, at mitotic exit, dephosphorylates free pBAF and restores its binding to chromatin[65,109]. In this regard, we hypothesized the accumulation of perichromosomal BAF depends on PP2A function. To analyse this possibility, we used Flfl-depleted cells that, as shown above, accumulate BAF in the perichromosomal compartment (fig 43). We observed that co-depletion of the Drosophila PP2A catalytic subunit Microtubule star (MTS) in Flfl-depleted cells strongly reduces perichromosomal BAF, while, on the other hand, MTS depletion alone does not induce perichromosomal BAF accumulation (fig 45a). The efficiency of the knockdowns was confirmed by WB (fig 45b). Altogether, these results suggest that the accumulation of perichromosomal BAF observed when centromeric PP4/cenBAF localization is impaired involves premature dephosphorylation of free pBAF by PP2A earlier than expected in mitosis. In this regard, we observed that perichromosomal BAF was not recognize by a αpBAF[92].

74
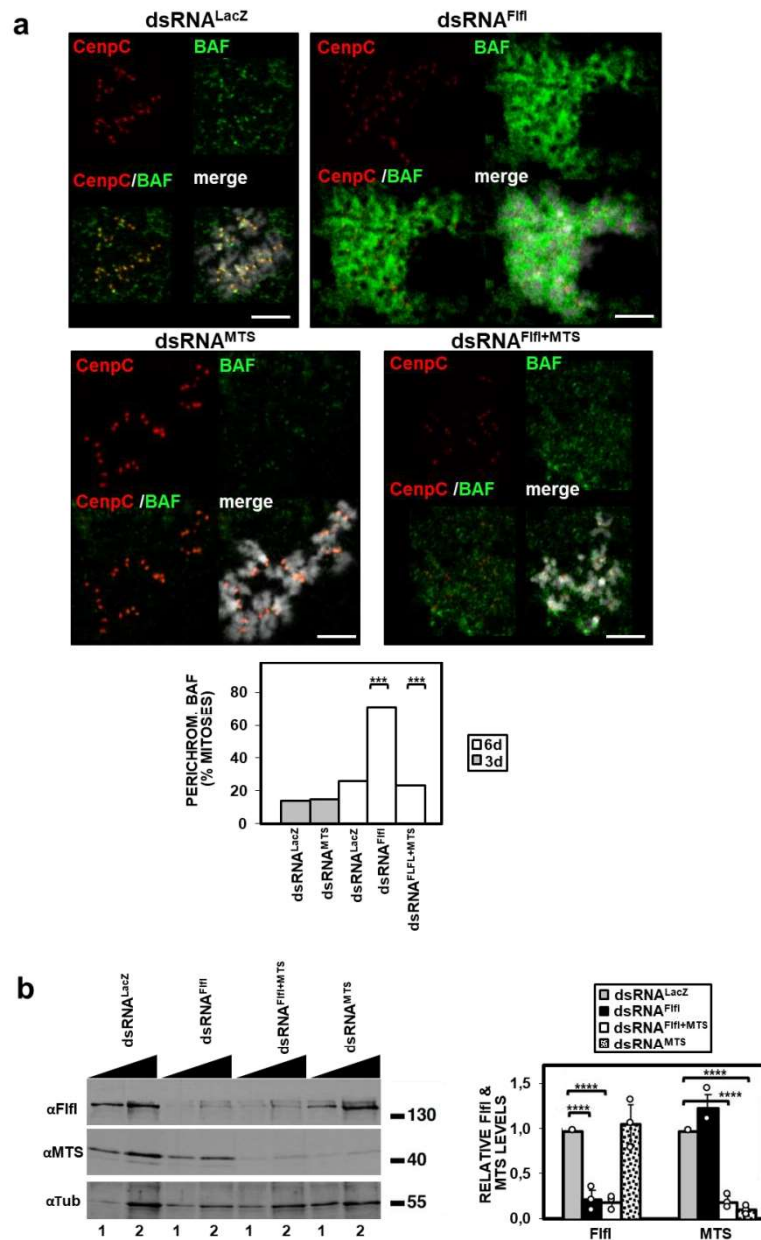
Figure 45. Perichromosomal BAF accumulation depends on PP2A: a: In the left, increasing amounts of extracts (lanes 1 and 2) prepared from control dsRNA^{LacZ} cells and from cells treated with dsRNA against Flfl (dsRNA^{Flfl}), MTS (dsRNA^{MTS}), and both Flfl and MTS (dsRNA$^{Flfl+MTS}$) are analysed by WB using αFlfl and αMTS antibodies. αTubulin antibodies were used for loading control. The position of MW markers (in kDa) is indicated. In the right, quantitative analysis of the results. The relative Flfl and MTS levels are presented for the indicated RNAi-treated cells. Results are the average of 3 independent experiments (error bars are SD; two-tailed t-test,**** p-value < 0.0001). **b:** In the top, the patterns of

immunolocalization with αBAF (green) and αCenpC (red) antibodies are presented for control dsRNA^{LacZ} cells and cells treated with dsRNA against Flfl (dsRNA^{Flfl}), MTS (dsRNA^{MTS}), and both Flfl and MTS (dsRNA$^{Flfl+MTS}$). DNA is stained with DAPI. Scale bars correspond to 5µm. In the bottom, the percentages of mitoses showing perichromosomal BAF are presented for the indicated RNAi-treated cells. Depletion is carried out for 3 or 6 days as indicated. Values are the sum of 5–9 independent experiments showing equivalent results (N > 165; two-tailed Fisher's test, ****p-value < 0.0001).

1.4 Constitutive targeting of BAF to centromeres stabilizes PP4 at centromeres and prevents perichromosomal BAF accumulation

Next, we analysed the effect of constitutive targeting of BAF to the centromere. For this purpose, we obtained cell lines expressing a GBP::FLAG::BAF construct together with GFP::CenpCΔFIM^R truncated form. We hypothesized that GBP::FLAG::BAF would be tethered to centromeres by specifically recognizing the GFP-moiety of GFP::CenpCΔFIM^R construct via the GFP-binding protein (GBP) (fig 46a). Immunostaining with αFLAG antibodies confirmed targeting of GBP::FLAG::BAF to the centromere in both control GFP::CenpCΔFIM^R-expressing cells treated with dsRNA^{LacZ} and upon depletion of endogenous CenpC (fig 46b).
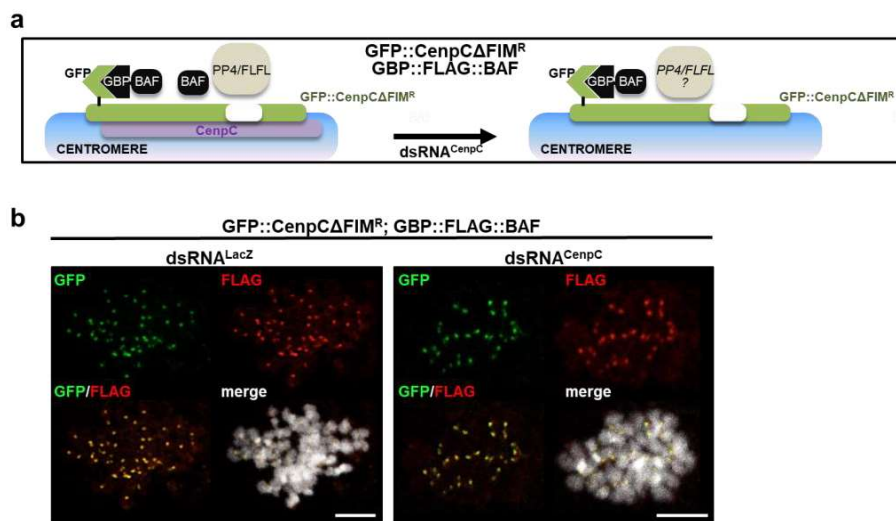
Figure 46. Constitutive targeting of BAF to centromeres. a: Schematic representation of the experimental approach used. Expression of GBP::FLAG::BAF in GFP::CenpCΔFIM^R-expressing cells will constitutively target BAF to centromeres *via* the recognition of the GFP moiety of GFP::CenpCΔFIM^R by the GBP domain of GBP::FLAG::BAF. The absence of the FIM domain is indicated in white. Endogenous CenpC is also indicated in magenta. **b:** Immunostainings with αFLAG antibodies (red) are presented for mitotic chromosomes from dsRNA^{CenpC} (right) and control dsRNA^{LacZ} (left) cells expressing GFP::CenpCΔFIM^R and GBP::FLAG::BAF. GFP signals are direct fluorescence (green). DNA is stained with DAPI (white). Scale bars correspond to 5μm.

To assess possible side effects of the expression of GBP::FLAG::BAF, we analysed its expression in control GFP::CenpC^R-expressing cells. We observed that expression of GBP::FLAG::BAF in GFP::CenpC^R-expressing cells did not significantly affect centromeric CenpA^{CID} levels (fig. 47a) or increase the frequency of segregation defects (fig. 47b), suggesting that centromere integrity and function was not affected. Similarly, expression of GBP:FLAG::BAF in GFP::CenpC^R-expressing cells did not affect NE morphology, as determined by immunostaining with αLaminB antibodies (fig 47c).
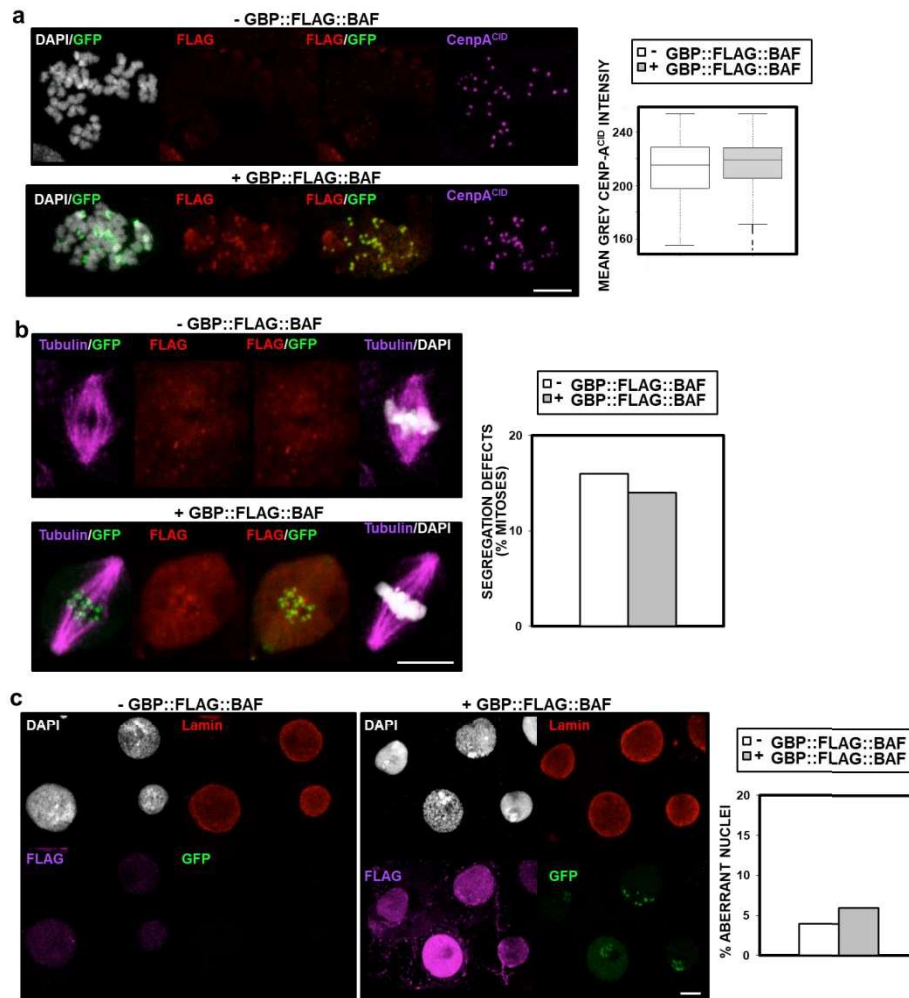
Figure 47. Expression of GBP::FLAG::BAF in control GFP::CenpC^R-expressing cells. a: In the left, immunostainings with αFLAG (red) and αCenpA^CID (magenta) antibodies are presented for mitotic chromosomes from GFP::CenpC^R cells expressing GBP::FLAG::BAF (bottom) or not (top). GFP signal is direct fluorescence (green). DNA was stained with DAPI (white). Scale bar corresponds to 5μm. In the right, quantitative analysis of the results. The mean grey values per centromere of αCenpA^CID fluorescence are shown for GFP::CenpC^R cells expressing GBP::FLAG::BAF or not (N>451). **b:** In the left, metaphase figures from GFP::CenpC^R cells expressing GBP::FLAG::BAF (bottom) or not (top). Immunostainings with αFLAG (green) and αTubulin (magenta) antibodies are shown. GFP signal is direct fluorescence (green). DNA is stained with DAPI (white). Scale bar corresponds to 5μm. In the right, quantitative analysis of the results. The percentage of segregation defects are presented for GFP::CenpC^R cells expressing GBP::FLAG::BAF or not (N>18). **c:** In the left, immunostainings with αLaminB antibodies (red) and αFLAG (magenta) antibodies are presented for GFP::CenpC^R cells expressing GBP::FLAG::BAF (right) or not (left). GFP signal (green) is direct fluorescence. DNA is stained with

DAPI (white). Scale bar corresponds to 5μm. In the right, quantitative analysis of the results. The percentage of cells showing altered NE morphology is presented for GFP::CenpC[R] cells expressing GBP::FLAG::BAF or not (N>111).

Interestingly, we observed that targeting GBP::FLAG::BAF to centromeres in CenpC-depleted GFP::CenpCΔFIM[R]-expressing cells rescued centromeric localization of Flfl (figs. 48a and 48b) without affecting the efficiency of depletion of endogenous CenpC (fig 48c). These results suggest that constitutive targeting of BAF to centromeres stabilizes centromeric PP4 independently of the interaction with CenpC.
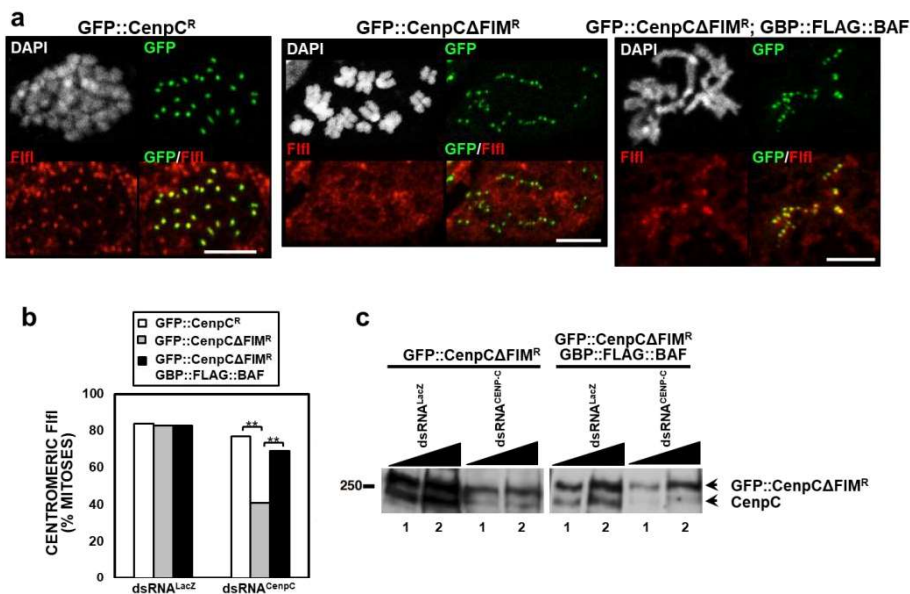
Figure 48. Constitutive targeting of GBP:FLAG::BAF to centromeres in CenpC-depleted GFP::CenpCΔFIM[R]-expressing cells rescues centromeric Flfl localization. a: Immunostainings with αFlfl antibodies (red) are presented for CenpC-depleted cells expressing the indicated constructs. GFP signals (green) are direct fluorescence. DNA was stained with DAPI (white). Scale bars correspond to 5μm. **b:** Quantitative analysis of the results shown in **a.** The proportion of mitoses where Flfl is detected at the centromeres is presented for control dsRNA[LacZ] and dsRNA[CenpC] cells expressing the indicated constructs. Values are the sum of 3-5 independent experiments showing equivalent results (N> 45; two-tailed Fisher's test, p-value **<0.01). **c:** WB analysis with αCenpC antibodies of increasing amounts of extracts (lanes 1 and 2) prepared from control dsRNA[LacZ] and dsRNA[CenpC] cells expressing the indicated constructs. The positions of endogenous CenpC and the GFP::CenpCΔFIM[R] form are indicated. The position of MW markers (in kDa) is indicated.

Importantly, we observed that expression of GBP::FLAG::BAF in GFP::CenpCΔFIM[R]-expressing rescued the accumulation of perichromosomal BAF observed upon CenpC depletion (fig. 49). We noticed that expression of GBP::FLAG::BAF also reduced the accumulation of perichromosomal BAF observed in control cells treated with dsRNA[LacZ] (fig 49).
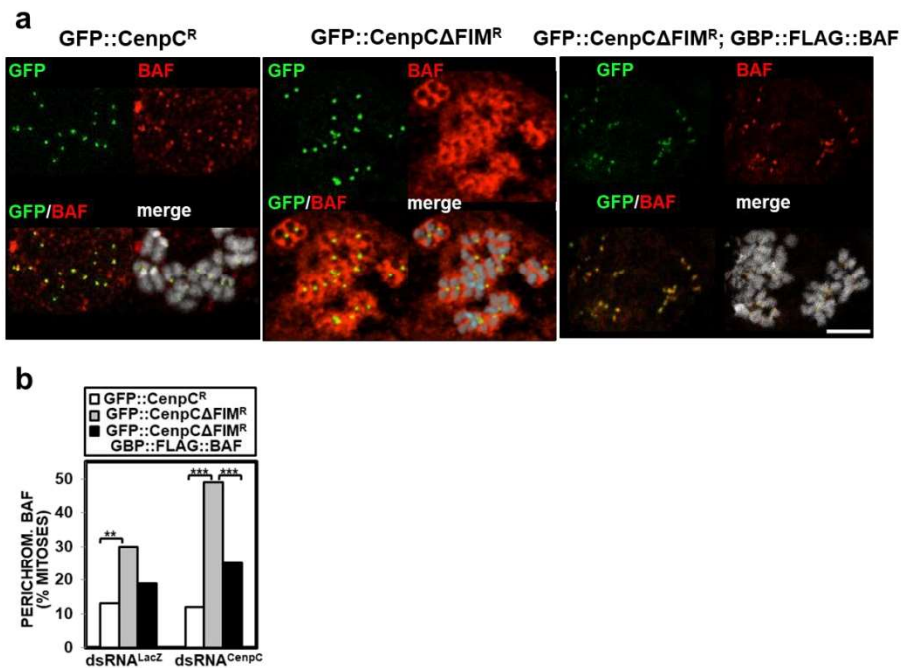
Figure 49. cenBAF prevents the accumulation of perichromosomal BAF in mitosis. a: Immunostainings with αFlfl antibodies (red) are presented for CenpC-depleted cells expressing the indicated constructs. GFP signals (green) are direct fluorescence. DNA was stained with DAPI (white). Scale bars correspond to 5μm. **b:** Quantitative analysis of the results shown in **a.** Percentages of mitoses showing perichromosomal BAF are presented for control dsRNA[LacZ] and dsRNA[CenpC] cells expressing the indicated constructs. Values correspond to the sum of 3-4 independent experiments showing equivalent results (N > 73; two-tailed Fisher's test, **p < 0.01, ***p < 0.001).

1.5 Disrupting centromeric cenBAF/PP4 localization alters NE morphology

We observed that impairing centromeric cenBAF/PP4 localization alters nuclear morphology since, in comparison to control GFP::CenpC^R-expressing cells, CenpC-depleted GFP::CenpCΔFIM^R-expressing cells showed an increased frequency of NE morphology defects, as determined by immunostaining with αLaminB antibodies (figs 50a and b). These defects ranged from nuclear budding and the formation of micronuclei, to multinucleated cells and cells with enlarged nucleus of irregular NE (fig 50c). Notably, these defects were significantly rescued when BAF was constitutively targeted to centromeres in cells expressing GBP::FLAG::BAF (figs 51a and 51b), suggesting that they are a direct consequence of the disruption of cenBAF/PP4 localization at the centromere.
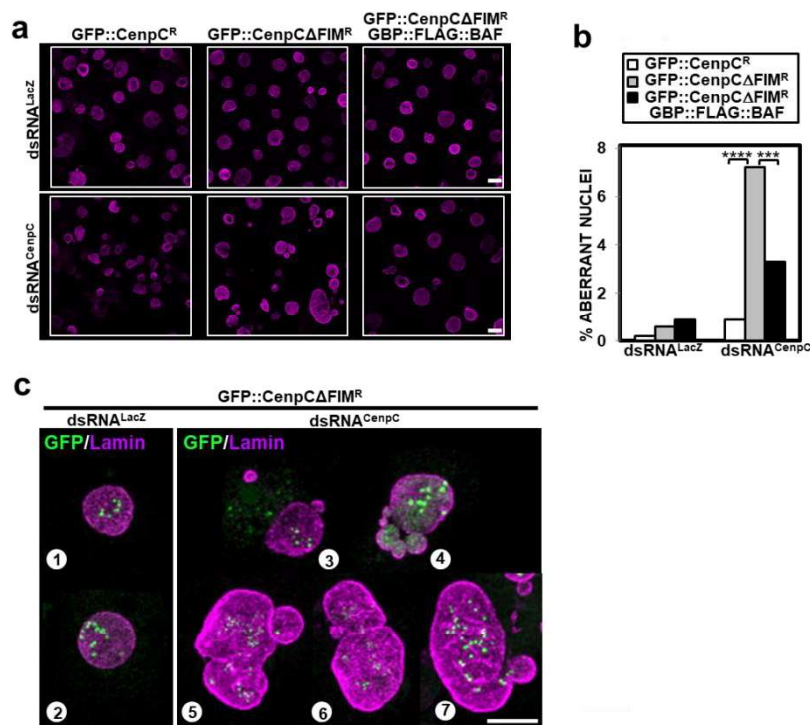
Figure 50. GFP::CenpCΔFIM^R expressing cells show altered nuclear morphology. a: Immunostainings with αLaminB antibodies (magenta) of control

dsRNA^{LacZ} and CenpC-depleted dsRNA^{CenpC} cells expressing the indicated constructs. Scale bars correspond to 10 µm. **b:** Quantitative analysis of the results shown in **a.** The percentage of cells showing altered nuclear morphology is presented for control dsRNA^{LacZ} and dsRNA^{CenpC} cells expressing the indicated constructs. Values are the sum of 3–4 independent experiments showing equivalent results (N > 334; two-tailed Fisher's test, ***p-value < 0.001, ****p-value < 0.0001). **c:** Enlarged images of immunostainings with αLaminB antibodies (magenta) of dsRNA^{CenpC} cells (images 3–7) and control dsRNA^{LacZ} cells (images 1 and 2) expressing GFP::CenpCΔFIM^R. GFP signals are direct fluorescence. Scale bar corresponds to 5µm.

In this regard, live cell imaging experiments performed in our group show that depletion of endogenous CenpC in GFP::CenpCΔFIM^R-expressing cells increased the overall duration of mitosis in comparison to control dsRNA^{LacZ} cells[92]. In particular, the time from NEBD to anaphase onset was significantly increased. These defects were not observed in GFP::CenpC^R-expressing cells[92]. These results suggest that disruption of the centromeric localization of cenBAF/PP4 affects mitosis progression.

Next, we analysed NE status during mitosis. For this purpose, we performed IF experiments using αH3PSer10, to mark mitotic cells, and αLaminB antibodies to monitor NE status. In control dsRNA^{LacZ} cells, αLaminB immunostaining marks the NE in interphase, becomes diffuse through the cytoplasm after NEBD start in late prophase and it relocates to the NE during NER in telophase (fig 51a left panel). However, in CenpC-depleted GFP::CenpCΔFIM^R-expressing cells, we often detect less diffuse αLaminB immunostaining in late prophase (fig 50a right panel). Moreover, the proportion of αPS10-positive cells showing NE-assembled αLaminB immunostaining increases upon CenpC depletion in GFP::CenpCΔFIM^R-expressing cells in comparison with control GFP::CenpC^R-expressing cells (fig 50b). Altogether these results suggest that, upon disruption of cenBAF/PP4 localization, the NE remains partially assembled during mitosis.
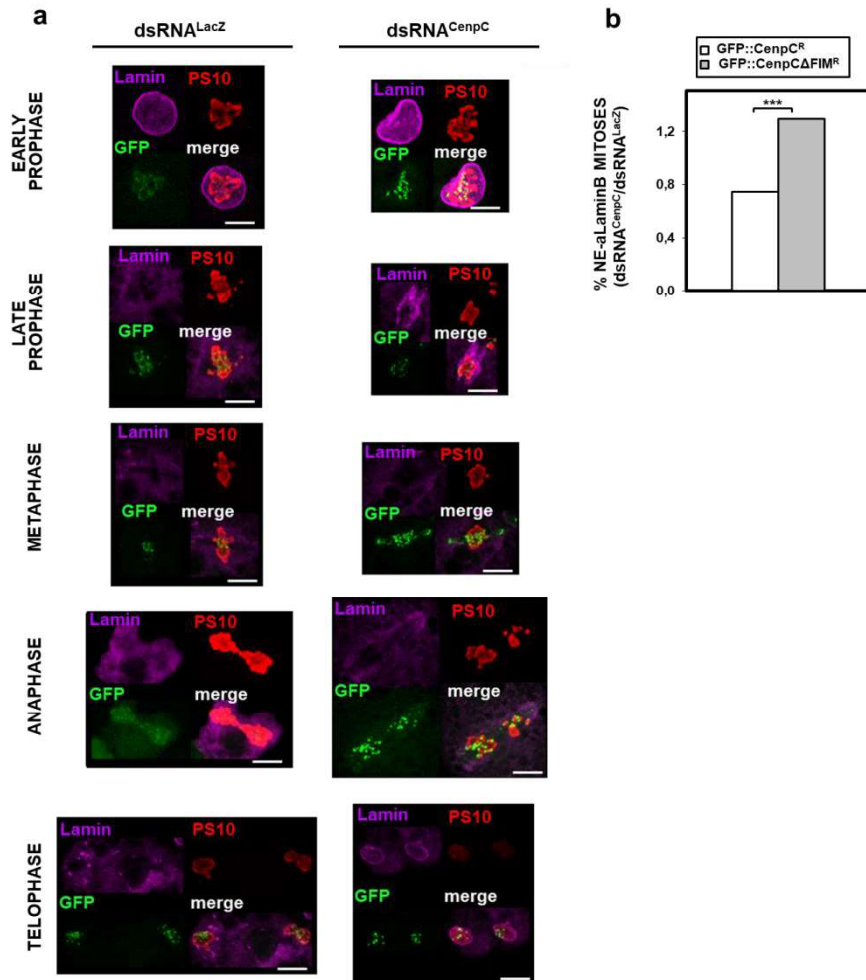
Figure 51. GFP::CenpCΔFIM^R expressing cells show NE defects during mitosis. a: Immunostainings with αLaminB antibodies (magenta) and αPS10 (red) of control dsRNA^{LacZ} and CenpC-depleted dsRNA^{CenpC} cells expressing GFP::CenpCΔFIM^R. Mitotic phases are indicated. GFP (green) is direct fluorescence. Scale bars correspond to 5µm. **b**: The relative proportion of mitoses showing NE-assembled αLaminB immunostaining upon CenpC depletion with respect to control dsRNA^{LacZ} cells is shown for GFP::CenpC^R and GFP::CenpCΔFIM^R-expressing cells. Values are the sum of 5–8 independent experiments showing equivalent results (N > 92; Chi-square test, ***p < 0.001).

2. BAF PHOSPHORYLATION

2.1 T4 and S5 are the main phosphosites of *Drosophila* BAF

Phos-tag gel electrohoresis analyses performed in our group identified mono- (1pBAF) and diphosphorylated (2pBAF) BAF species[92] (see also fig 54) and three residues in the N-terminal region (S2, T4 and S5) have been proposed as putative phosphosites[90]. In this regard, work in our group showed that replacement of these three residues by A or E abolishes BAF phosphorylation[92]. However, no detailed analysis of the specific contribution of each residue was carried out. For this purpose, we determined the pattern of phosphorylation of mutant forms in which one, two or all three residues are mutated to A (fig. 52a). Stable S2 lines expressing FLAG-tagged constructs from the endogenous BAF promoter could be derived for all the mutants except for the double T4AS5A and the triple S2AT4AS5A forms. Phos-tag gel electrophoretic analysis showed that, while both 1pBAF and 2pBAF species were detected in the S2A mutant, only 1pBAF species could be detected in the single T4A and S5A mutant forms (fig 52b, left), suggesting that T4 and S5, but not S2, are phosphorylated. In good agreement, the double S2AT4A and S2AT5A lack 2pBAF species (fig 52b, right). To determine the pattern of phosphorylation of the double T4AS5A mutant, we performed transient expression experiments since the corresponding stable S2 lines could not be obtained. In transient expression experiments, after transfection, cells were treated for 3 hours with the phosphatase inhibitor okadaic acid (OA) to increase phosphorylation. These transient expression experiments recapitulate the results obtained with the stable S2 lines and, in addition, showed that the double T4AS5A mutant was not phosphorylated (fig. 52c). Similarly, the triple S2AT4AS5A mutant form was not phosphorylated

either (fig 52c). Altogether these results suggest that T4 and S5 are the main phosphosites of BAF in *Drosophila* and that they can be independently phosphorylated.
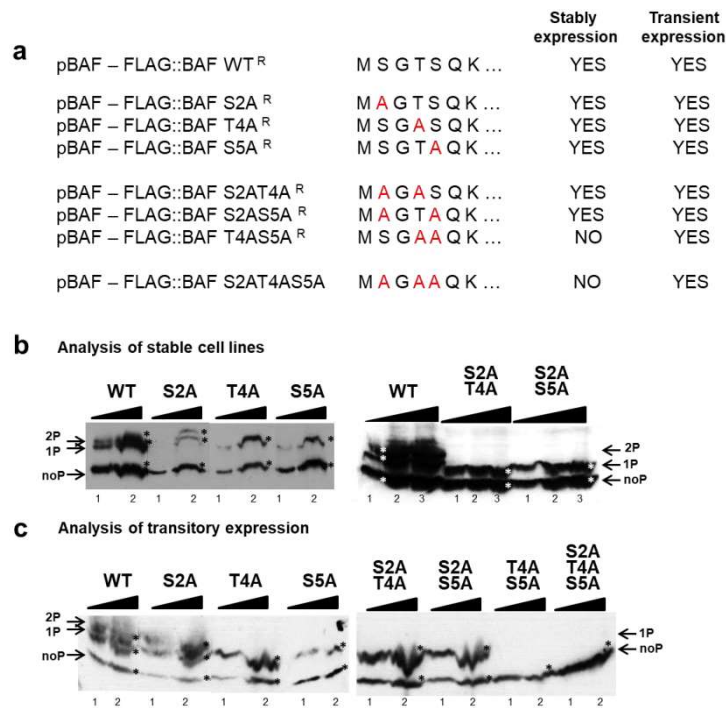
Figure 52. T4 and S5 are the main residues involved in BAF phosphorylation. a: Sequence of BAF N-terminus (aa1-7). For each mutant, phosphorylable residues that are replaced to A are marked in red. All the mutants were stable expressed in S2 cells except for the double T4AS5A and triple S2AT4AS5A which were only analysed by transient expression. **b:** Analysis by phostag gels of the phosphorylation pattern of the indicated phosphomutant forms of BAF stably expressed in S2 cells. Increasing amounts of total extracts (lines 1-2 or 1-3) are analysed by WB using αFLAG antibodies. The positions corresponding to non-phosphorylated (noP), and mono- (1P) and di-phosphorylated (2P) BAF species are indicated and highlighted by *. **c:** Analysis by phostag gels of the phosphorylation pattern of the indicated phosphomutant forms of BAF transiently expressed in S2 cells. Cells were treated for 3hours with OA prior to the preparation of the extract. Increasing amounts of total extracts (lines 1-2) are analysed by WB using αFLAG antibodies. The positions corresponding to non-phosphorylated (noP), and mono- (1P) and di-phosphorylated (2P) BAF species are indicated and highlighted by *.

The inability to derived stable cell lines with the double T4AS5A and triple S2AT4AS5A mutants may reflect a deleterious effect of their expression in S2 cells. In this regard, work in our group showed that a C-terminal BAF::YFP form acts as a dominant negative mutant, while a N-terminal YFP::BAF form is functional[92]. Interestingly, while the N-terminal YPF::BAF construct showed a normal phosphorylation pattern, phosphorylation of the C-terminal BAF::YFP was strongly impaired (fig 53a). Replacing the YFP-tag by an smaller HA-tag did not recover phosphorylation of the C-terminal BAF::HA form (fig 53b). These results confirm that phosphorylation is essential for normal BAF function and that forms that cannot be phosphorylated might act as dominant negative mutations. Furthermore, coIP experiments showed that, while the N-terminal YFP::BAF form interacted with endogenous BAF, the C-terminal BAF::YFP construct did not (fig 53c), suggesting that BAF::YFP is not able to dimerized. In fact, the structure of BAF dimers suggest that a C-terminal tag interferes with dimerization (fig. 8). On the other hand, dimerization is essential for the interaction of BAF with other factors, such as emerin that binds to the dimer interface (fig. 8). These observations suggest that dimerization is required for BAF phosphorylation by VRK1/NHK1.
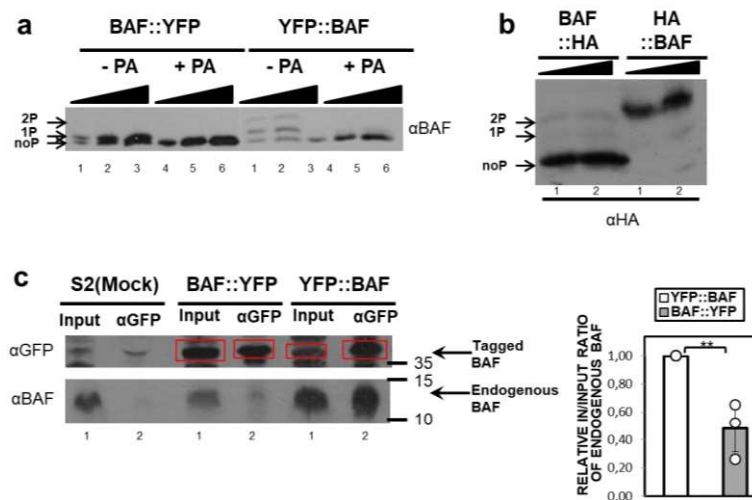
Figure 53. Tagging BAF at its C-terminal impairs its proper phosphorylation.
a: The patter of phosphorylation of BAF::YFP and YFP::BAF is analysed by
phostag gel electrophoresis. Extracts were prepared from cells transiently
expressing BAF::YFP or YFP::BAF treated with alkaline phosphatases (lines 4-6)
or not (lanes 1-3). Increasing amounts of extracts are analysed by WB using
αBAF antibodies. The positions corresponding to non-phosphorylated (noP), and
mono- (1P) and di-phosphorylated (2P) BAF species are indicated. **b:** The patter
of phosphorylation of BAF::HA and HA::BAF is analysed by phostag gel
electrophoresis. Total extracts were prepared from cells transiently expressing
BAF::HA treated for 3hours with OA. Increasing amounts of extracts (lines 1 and
2) are analysed by WB using αHA antibodies as indicated. The positions
corresponding to non-phosphorylated (noP), and mono- (1P) and di-
phosphorylated (2P) BAF species are indicated and highlighted by *. **c:** co-IP
experiments with αGFP antibodies in extracts from control S2 cells (left), and cells
stably expressing BAF::YFP (central) or YFP::BAF (right) (lanes 2). Lanes 1
correspond to 5% of the input. IPs were analysed by WB using αGFP and αBAF
antibodies. The position of MW markers (in kDa) is indicated. Quantitative
analysis of the results of the IP is shown in the right panel. The ratio of the input of
the endogenous BAF and IP endogenous BAF signals normalized respect to
YFP::BAF is presented for cells expressing BAF::YFP. Results are the average of
three independent experiments (error bars are SD, two-tailed t-test, **p-value =
0.01).

2.2 PP2A is the main BAF phosphatase

Both PP2A and PP4 phosphatases have been postulated to dephosphorylate BAF[65,76,108,109]. To determine their specific contribution to BAF dephosphorylation, we have performed knock-down experiments in S2 cells. In these experiments, we treated cells for 3 hours with OA to induce BAF phosphorylation and, then, after removing OA, we followed recovery of non-phosphorylated BAF. Cells treated with DMSO were taken as control. A time course experiment performed in control dsRNA[LacZ] cells showed increased phosphorylation upon OA treatment and full recovery 3h after OA removal (fig 54).
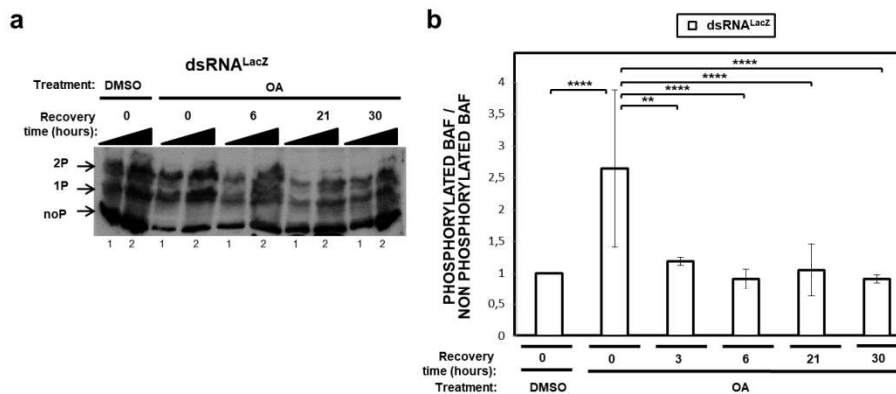
Figure 54. OA treatment and recovery in for control dsRNA[LacZ] S2 cells. a: The pattern of BAF phosphorylation is analysed by phostag gel electrophoresis. Cells are treated for 3 hours with either DMSO (control) or OA. After OA treatment, cells are recovered for 3, 6, 21 and 30 hours. Increasing amounts of total cells extracts (lines 1-2) are prepared from each condition and analysed by WB using αBAF antibodies. The positions corresponding to mono- (1P) di- (2P) and non-phosphorylated (noP) BAF species are indicated. **b:** Relative levels of total phosphorylated BAF, including mono- and di-phosphorylated forms, to non-phosphorylated BAF are presented for control dsRNA[LacZ] treated with DMSO or OA and at increasing times after OA treatment. Values are normalised to the DMSO condition and correspond to the average of 5 independent experiments (errors bars are SD, two-tailed t-test, **p<0.01, ****p<0.0001).

Next, we analyzed recovery after OA treatment in cells depleted for the PP2A catalytic subunit (MTS in *Drosophila*) and the PP4 catalytic subunit (PP4c). The extent of MTS and PP4c depletion was determined by WB analysis (fig. 55a). We observed that, in comparison to control dsRNA[lacZ] cells, MTS- and PP4c-depleted showed increased BAF phosphorylation after OA treatment. However, while BAF phosphorylation is recovered to control levels in PP4c-depleted cells, it remains high in MTS-depleted cells even 30h after recovery (fig 55b). These results indicate that BAF dephosphorylation is impaired in MTS-depleted cells, but not in PP4c-depleted cells, suggesting that BAF is mainly dephosphorylated by PP2A.

Interestingly, we observed that, while the ratio of 2pBAF/1pBAF remains constant during recovery in control and PP4c-depleted cells, it decreased in MTs-depleted cells (fig 55c), indicating that 1pBAF accumulates during recovery. These results suggest that MTS depletion strongly impairs dephosphorylation of 1pBAF species.

Altogether these results suggest that PP2A is the main BAF phosphatase that preferentially dephosphorylates mono-phosphorylated BAF species.
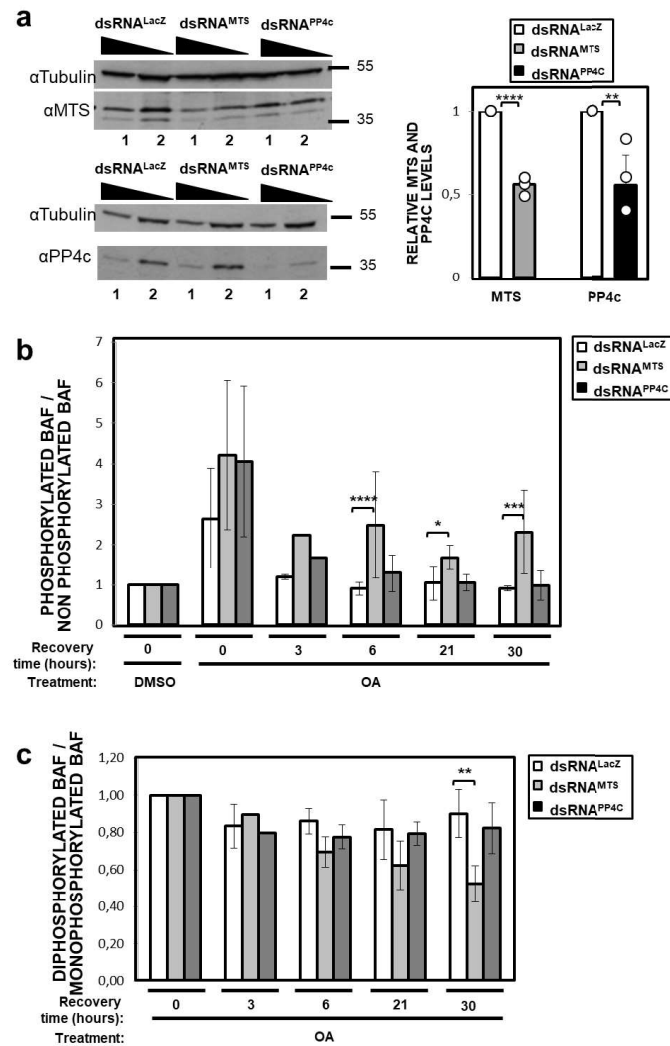
Figure 55. PP2A is the main BAF phosphatase. a: The efficiency of the MTS and PP4c depletion is determined by a WB analysis. The levels of MTS (top) and PP4c (bottom) are determined by WB in total cell extracts prepared from S2 cells treated with the indicated dsRNA. Increasing amounts of extracts are analysed (1-2). αTubulin antibodies are used for normalization. The position of MW markers (in KDa) is indicated. Quantitative analysis of the results is shown in the right, where the relative MTS and PP4c levels are presented for dsRNA^{LacZ}, dsRNA^{MTS} and dsRNA^{PP4c} treated cells. Results are the average of 3 independent experiments (error bars are SD, two tailed t-test, p-value**<0.01, p-value****<0.0001). **b:** Time course of recovery after OA treatment of BAF phosphorylation is presented for control dsRNA^{LacZ} cells, and MTS-depleted (dsRNA^{MTS}) and PP4c-depleted (dsRNA^{PP4c}) cells. The ratio of total phosphorylated BAF (including mono- and diphosphorylated) to nonphosphorylated BAF is shown. Values correspond to the average of 3 or more

independent experiments and are normalized to the control DMSO condition (errors bars are SD, mixed linear model, p-values adjusted for multiple testing using Benjamin-Hochberg,, *p<0.05, ***p<0.001, ****p<0.0001). **c:** The ratio of diphosphorylated BAF versus monophosphorylated BAF during recovery after OA treatment is presented for control dsRNA[LacZ] cells, and MTS-depleted (dsRNA[MTS]) and PP4c-depletec (dsRNA[PP4c]) cells. Values are the average of 3 or more independent experiments and are normalized to 0h recovery condition (error bars are SD, mixed linear model, p-values adjusted for multiple testing using Benjamin-Hochberg, **p<0.01).

Next, we analysed which PP2A isoform is involved in BAF dephosphorylation. For this purpose, we performed similar experiments in cells depleted for the PP2A regulatory subunits B56 (WDB in *Drosophila*) and B55 (TWS in *Drosophila*) (fig. 56). The extent of WDB and TWS depletion was determined by WB analysis (fig. 56a). We observed that, in both cases, recovery of BAF dephosphorylation after OA treatment was compromised (fig 56b), suggesting that PP2A/WDB and PP2A/TWS are both involved in BAF dephosphorylation. In this regard, work performed in our laboratory showed, similar to depletion of the catalytic MTS subunit, depletion of WDB and, though to a lesser extent of TWS, rescue the accumulation of perichromosomal BAF observed in Flfl-depleted cells.
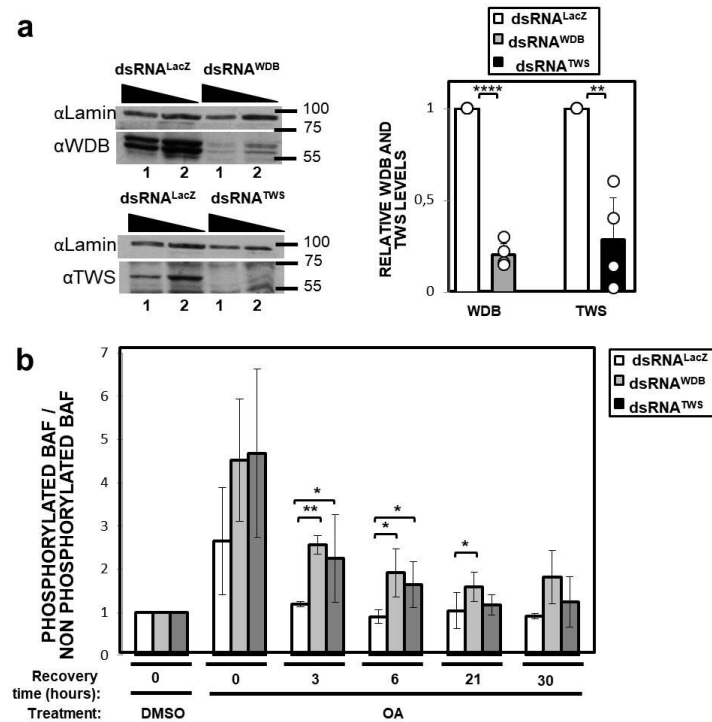
Figure 56. WDB and TWS are both involved in BAF dephosphorylation. a: The efficiency of WDB and TWS knockdowns is determined by a WB analysis. The levels of WDB (top) and TWS (bottom) are determined by WB in total cell extracts prepared from S2 cells treated with the indicated dsRNA. Increasing amounts of extracts are analysed (1-2). αLamin antibodies are used for normalization. The position of MW markers (in KDa) is indicated. Quantitative analysis of the results is shown in the right, where the relative WDB and TWS levels are presented for dsRNA[LacZ], dsRNA[WDB] and dsRNA[TWS] treated cells. Results are the average of 4 independent experiments (error bars are SD, two-tailed t-test, p-value**<0.01, p-value****<0.0001). **b:** Time course of recovery after OA treatment of BAF phosphorylation is presented for control dsRNA[LacZ] cells, and WDB-depleted (dsRNA[WDB]) and TWS-depleted (dsRNA[TWS]) cells. The ratio of total phosphorylated BAF (including mono- and diphosphorylated) to nonphosphorylated BAF is presented for control dsRNA[LacZ], dsRNA[WDB] and dsRNA[TWS]. Values correspond to the average of 3 or more independent experiments and are normalized to the control DMSO condition (errors bars are SD, mixed linear model, p-values adjusted for multiple testing using Benjamin-Hochberg,, *p<0.05, **p<0.01).

DISCUSSION

1. cenBAF FORMS A CENTROMERIC NETWORK WITH PP4 AND CenpC

Work in our lab showed that a fraction of BAF (cenBAF) localizes at the centromere[92]. At mitosis, while the bulk of BAF is phosphorylated by VRK1/NHK1 and released for chromatin[73–75,105], cenBAF remains associated with centromeric chromatin and, most likely, stays not-phosphorylated[92]. Here, we have shown that the protein phosphate PP4, which is recruited to the centromere by the interaction of its regulatory Flfl subunit with CenpC[151], is required for centromeric cenBAF localization in mitosis. Our results show that deletion of the FIM domain of CenpC, which mediates interaction with Flfl/PP4[151] and its recruitment to the centromere (fig 39)[151], destabilizes centromeric cenBAF localization (fig 40). These results support the hypothesis that recruitment of PP4 by CenpC keeps cenBAF non-phosphorylated and bound to the centromere in mitosis. However, the situation is more complex since work in our lab showed that depletion of BAF, which strongly reduces cenBAF, destabilizes CenpC at the centromere[92] (see also fig 31 in section 4.3 of the Introduction) and, thus, reduces centromeric localization of PP4[92]. The mechanisms by which cenBAF stabilizes CenpC at the centromere are not well understood. It is possible that, either directly or indirectly, cenBAF interacts with CenpC since BAF and CenpC co-immunoprecipitate[92]. Alternatively, given that BAF has been shown to affect histone modifications and higher-order chromatin organization[49,50], it is also possible that cenBAF modifies centromeric chromatin in a way that stabilizes CenpC. Altogether, these results suggest a model by which CenpC mediates recruitment of PP4 to centromeres, PP4 retains cenBAF at centromeres in mitosis, which in turn stabilizes CenpC (fig 57). Consistent with this hypothesis, decreased centromeric PP4 in Flfl-depleted cells reduces centromeric CenpC levels[92]. Interestingly, results reported here suggest that

cenBAF also stabilize PP4 at centromeres independently of CenpC, since constitutive targeting BAF to the centromere rescues centromeric PP4 localization in cells expressing a CenpCΔFIM truncated form, which lacks the FIM domain and fails to recruit PP4 (figs 48).
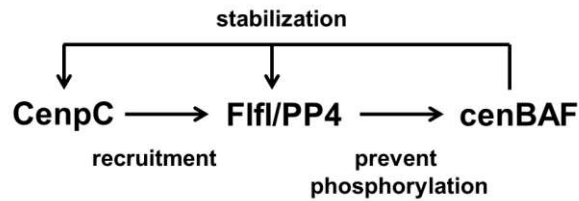
Figure 57. Interdependence of cenBAF, Flfl/PP4 and CenpC for their centromeric localization. CenpC directly interacts with Flfl/PP4 and recruits it to the centromere localization. Flfl/PP4 is required for the proper positioning of CenpC and cenBAF . cenBAF stabilizes CenpC and centromeric Flfl/PP4.

On the light of the interdependent centromeric localization of CenpC, PP4, and BAF, we would like to propose that these three factors form a novel network of centromeric interactions. Whether they physically interact to form a centromeric complex remains to be determined. This network forms a positive feedback loop that reinforces assembly of centromeric chromatin and kinetochore formation and, hence, ensures faithful chromosome segregation, explaining why BAF-depleted cells show strong chromosome segregation defects[92] (see also fig 31 in section 4.3 of the Introduction).

2. THE CENTROMERIC cenBAF/PP4 NETWORK REGULATES PP2A-DEPENDENT BAF DEPHOSPHORYLATION

The present work shows that disruption of the centromeric cenBAF/PP4 leads to an abnormal accumulation of BAF at the perichromosomal compartment in mitosis (fig 42 and 43). Our results also show that depletion of MTS, the catalytic subunit of PP2A, significantly reduces the accumulation of perichromosomal BAF (fig 45), suggesting that perichromosomal BAF is nonphosphorylated and that PP2A is required for its accumulation upon disruption of the centromeric cenBAF/PP4 network. Consistent with this possibility, results from our group showed that perichromosomal BAF is not recognized by an antibody that specifically recognises phosphorylated BAF[92].

The observation that the accumulation of perichromosomal BAF in mitosis depends on PP2A was somehow unexpected since, under normal conditions, PP2A is silenced at the entry of mitosis[120,132–138] and remains inactivate until late anaphase-telophase, when its reactivation induces dephosphorylation of multiple substrates, including BAF. Thus, our results suggest that the centromeric cenBAF/PP4 network regulates PP2A silencing in mitosis. Our model proposes that ectopic PP2A activation in mitosis counteracts VRK1/NHK1-dependent phosphorylation of BAF, which stays largely non-phosphorylated and, thus, associates with chromatin, accumulating at the perichromosomal compartment (fig. 58).
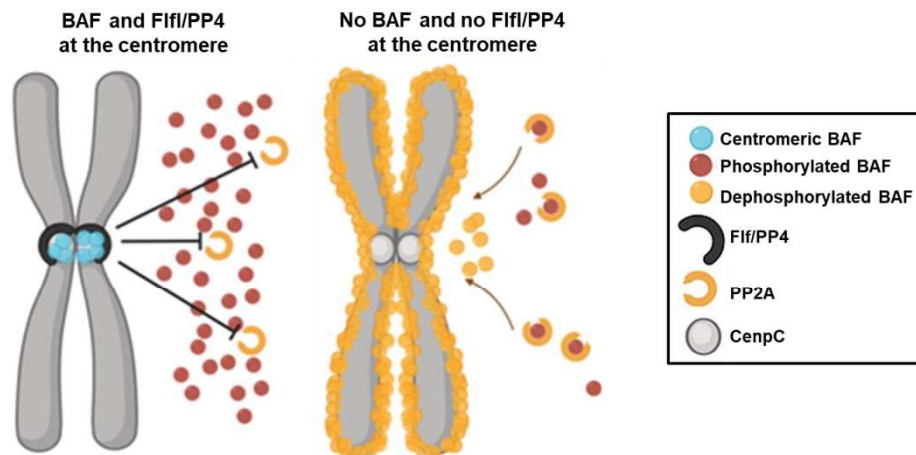
Figure 58. The centromeric cenBAF/PP4 network regulates PP2A inactivation and BAF phosphorylation in mitosis. Left: Under normal conditions, the centromeric cenBAF/PP4 network keeps PP2A silenced during mitosis. Right: Disruption of the centromeric cenBAF/PP4 network induces ectopic PP2A activation in mitosis, counteracting VRK1/NHK1-dependent phosphorylation of BAF that stays non-phosphorylated and associates with chromatin, accumulating at the perichromosomal compartment.

How does centromeric cenBAF/PP4 regulate PP2A silencing in mitosis is not known. In this regard, we have also shown here that constitutive targeting of cenBAF at centromeres in cells expressing CenpCΔFIM abolishes accumulation of perichromosomal BAF (fig 49). Importantly, under these conditions, centromeric PP4 localization is rescued (fig 48), suggesting that restricting PP4 localization at centromeres may play an important role in the regulation of mitotic PP2A inactivation. It is possible that, either directly or indirectly, free PP4 activates PP2A. For instance, PP4 could dephosphorylate Endos, or another yet unknown PP2A inhibitor, relieving PP2A silencing. Restricting PP4 localization to the centromere might prevent Endos inactivation. It is also possible that PP4 counteracts CDK1 phosphorylation of Gtw that, in its turn, activates Endos. Further work is required to clarify the mechanism by which the centromeric cenBAF/PP4 network regulates PP2A silencing during mitosis.

The model proposed above (fig 58) suggests that centromeric cenBAF/PP4 regulates BAF dephosphorylation at mitosis exit. Though highly speculative, the centromeric cenBAF/PP4 network might act like a checkpoint that signals PP2A activation at mitosis exit. It is possible that, at some point after transition to anaphase, centromeric cenBAF/PP4 localization could be released and PP2A inactivation could be alleviated, contributing to the cascade of events that drives mitosis exit and, in particular, inducing BAF dephosphorylation. From this point of view, disruption of the centromeric cenBAF/PP4 network would greatly impact mitosis progression. In fact, work in our group showed that impairing centromeric cenBAF/PP4 localization increases mitosis duration with a strong delay in anaphase onset[92]. At least in part, these defects could be due to altered BAF phosphorylation since it has been shown that VRK1 depletion, which impairs BAF phosphorylation, causes a similar delay in anaphase onset and increases mitosis duration in mammalian cells[75].

The regulation of BAF phosphorylation is important for both NEBD and NER. At mitosis entry, BAF phosphorylation weakens its binding to chromatin and NE LEM-d proteins, facilitating NEBD[42,73,75,89,105], while, at mitosis exit, BAF dephosphorylation restores its binding to chromatin and the NE LEM-d proteins, being essential for recruitment of BAF to the core regions and NER[46,56,65,107]. In this regard, upon disruption of the centromeric cenBAF/PP4 network, we observed mitoses with partially assembled NE (fig 51) and cells with strong NE morphology defects (fig 50). These observations suggest that the centromeric cenBAF/PP4 network regulates dynamics of NE disassembly/reassembly during mitosis.

As discussed above, the centromeric cenBAF/PP4 network stabilizes CenpC at centromeres and, thus, regulates centromere/kinetochore

assembly and chromosome segregation[92] (see also fig 31 in section 4.3 of the Introduction). cenBAF/PP4 ensures accurate chromosome segregation, while, on the other hand, it signals for mitotic NE disassembly/reassembly. This dual role of cenBAF/PP4, as a regulator of NE assembly and in the control of chromosome segregation, suggests a contribution to the co-ordination of these central mitotic events. Apart from BAF, several other NE components have been shown to play a role in kinetochore function. For instance, Mel-28/ELYS is required for NPC reassembly at the end of mitosis by recruiting the NUP107 subcomplex and associates with kinetochores during cell division being necessary for correct chromosome segregation[208–210].

To some extent, our observations reinforce the idea of a mitotic checkpoint that delays chromosome decondensation and NER until chromosome segregation is completed at the end of anaphase[188]. This likely involves cross-talk between different phosphatases that co-ordinately regulate the cascade of dephosphorylation events happening during mitotic exit. Centromeric PP4, but also PP2A/B56, which also localizes at the centromere[141], are potential candidates to be involved in this signalling pathway.

In summary, the results shown in this work led us to propose that cenBAF, together with PP4 and CenpC, forms a functional centromeric network that is required for faithful chromosome segregation and controls mitosis progression by regulating PP2A activity in mitosis. This network might participate in a mitotic exit checkpoint, co-ordinating chromosome segregation and NER.

3. BAF PHOSPHOREGULATION AND THE ROLE OF PP2A AND PP4

Phosphorylation is known to regulate BAF function. Here, we have determined that T4 and S5 are the main phosphosites of BAF in *Drosophila* (fig 52). Recent *in-vitro* studies showed that the equivalent T3 and S4 residues of human BAF (fig 7) are the main sites of phosphorylation by VRK1, with S4 being phosphorylated first and T3 accounting for BAF diphosphorylation[44]. However, our results show that, in *Drosophila*, both T4 and S5 can be monophosphorylated independently *in-vivo*. In *Drosophila*, S2 was also proposed to be a potential site for VRK1/NHK1 phosphorylation[91,92]. Instead, our results show that this residue, which is not conserved in human BAF, is not a main phosphosite in *Drosophila*. The identification of the main BAF phosphosites opens the door to the analysis of the specific contribution of each phosphorylation to BAF localization and function. From this point of view, phosphorylation mutants generated in the course of this work are going to be a very useful tool.

Phosphorylation is proposed to impair binding of BAF to DNA and the interaction with NE LEM-d proteins and lamins[42,73–75,105]. However, recent results by Marcelot *et al.*[44]*,* showed that, *in-vitro,* BAF phosphorylation abolishes binding to DNA, but does not impair binding to Emerin and lamin A/C. BAF dimerization appears essential for binding to LEM-d proteins since they interact through a central hydrophobic pocket in the BAF dimer interface (fig 8)[45,53,79]. In this regard, BAF dimerization involves extensive interactions between the C-terminal regions of each monomer (fig 8)[78,79], which are not likely perturbed by phosphorylation since it occurs at the N-terminal region[42,44,73,105]. On the other hand, the N-terminal HhH domain and K6 are involved in DNA binding (fig 8)[78,80,81]. Thus, it is likely that phosphorylation of the nearby T4 and S5 residues would strongly

impair binding to DNA. Our results show that a C-terminal BAF::YFP tagged form shows impaired dimerization, likely due to distortion of the dimer interface by the C-terminal tag, and phosphorylation (fig 53). This suggests that dimerization also may mediate phosphorylation. It is feasible that the hydrophobic pocket at the dimer interface also mediates interaction with VRK1/NHK1.

These observations suggest that a main effect of BAF phosphorylation is to regulate binding to DNA and release from chromatin. In this regard, work in our group showed that, likely due to impaired phosphorylation, the C-terminal BAF::YFP form is not fully released from chromatin in mitosis and, concomitantly, its expression is deleterious, showing a strong dominant negative effect[92]. It is possible that, if at some point in anaphase cenBAF is released from the centromere, the BAF::YFP form might not, which could be the cause of its deleterious effect.

At the end of mitosis, BAF dephosphorylation is essential for its function. PP2A and PP4 have been proposed to be involved in BAF dephosphorylation[65,76,108,109]. Here, we have analysed their specific contribution to BAF dephosphorylation after OA treatment. Our results show that depletion of the catalytic PP2A subunit MTS strongly impairs BAF dephosphorylation and recovery after OA treatment (fig 55), which is in agreement with previous results in our group[92] and confirms PP2A as a main BAF phosphatase. In addition, our results show an accumulation of monophosphorylated BAF during OA recovery in MTS-depleted cells (fig 55), suggesting that PP2A preferentially acts on monophosphorylated BAF, as previously proposed[92]. We also show that depletion of the regulatory subunits TWS (B55) and WDB (B56) induce similar defects on recovery after OA treatment (fig 56), suggesting that the both PP2A/TWS and PP2A/WDB phosphatases

isoforms regulate BAF phosphorylation. It was previously shown that PP2A/TWS dephosphorylates BAF at mitosis exit[109]. However, TWS depletion was shown to delay, but not abolish, BAF dephosphorylation and recruitment to the core regions[109], suggesting that additional phosphatases regulate BAF phosphorylation. From this point of view, the involvement of PP2A/WDB is particularly interesting since in *Drosophila* it localizes at the centromere in mitosis[211] and, unlikely PP2A/TWS, its activity is not fully silenced after mitosis entry (fig 18)[118,212,213]. WDB/B56 recognizes a short LxxIxE docking motif (SLiM) in their substrates[142]. BAF contains such motif (residues 24 to 32), which is well conserved among species (fig 59). Interestingly, a G25E mutation in human BAF has been reported to impair BAF dimerization and recruitment to the "core regions" at the end of mitosis[46,50,78], suggesting that PP2A/WDB might be involved in BAF dephosphorylation and chromatin binding at mitosis exit.
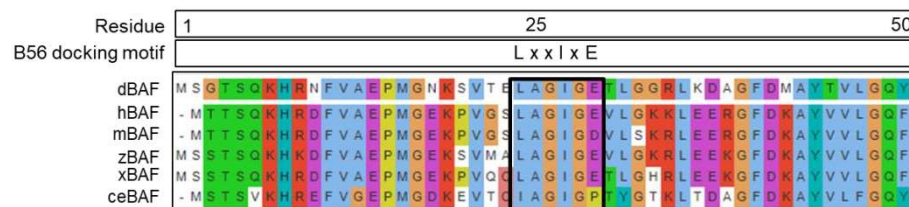
Figure 59. BAF from different species contains a conserved WDB/B56 binding motif. The amino acid sequence of BAF from human (hBAF), mouse (mBAF), zebrafish (zBAF), Xenopus (xBAF), Drosophila (dBAF) and Caenorhabditis elegans (CeBAF) is presented. The conserved LxxIxE WDB/B56 binding motif is indicated (residues 24 to 32), as determined using the B56 binding motif resource tool (http://slim.icr.ac.uk/pp2a/). Amino acid colour is defined by clustal X colour criteria.

Our results also show that depletion of PP4 does not significantly impair BAF dephosphorylation and recovery after OA treatment (fig 55), suggesting that PP4 does not regulate phosphorylation of free BAF. In this regard, previous results from our group showed that, opposite to what would be expected, depletion of the PP4 regulatory

subunit Flfl decreased total BAF phosphorylation[92], which could reflect enhanced PP2A-mediated BAF dephosphorylation in the absence of PP4. Although recent results suggest high flexibility of substrate recognition by PP4[148], the lack of known PP4 SLiM binding motifs in BAF supports that PP4 is not directly interacting with BAF. Nevertheless, our results cannot exclude the possibility that direct PP4-mediated BAF dephosphorylation is restricted to centromeres, and/or to a specific moment during cell cycle progression, since cenBAF accounts for only a small fraction of total BAF. It is possible that, at the centromere, CenpC serves as a platform for PP4-BAF interaction.

Further work is required to clarify the actual contribution of PP4 to BAF dephosphorylation at centromeres, as well as to determine the possible differential roles of PP2A/WDB and PP2A/TWS in the regulation of BAF phosphorylation. Current studies in our group aim to further characterize the specific subcellular localizations where these phosphatases may act on BAF and the specific functional contribution of each BAF phosphosite.

CONCLUSIONS

1. Protein phosphatase PP4, which is recruited to centromeres by CenpC, is required for centromeric BAF localization. Disrupting centromeric localization of PP4 in cells expressing a truncated CenpCΔFIM form missing the PP4 binding domain (FIM), or upon depletion of the PP4 regulatory subunit Flfl, prevents cenBAF localization.

2. Disrupting centromeric localization of cenBAF and PP4 results in the accumulation of BAF at the perichromosomal compartment in mitosis.

3. The accumulation of perichromosomal BAF depends on PP2A, which is normally inactive in mitosis, suggesting that disrupting centromeric localization of cenBAF and PP4 results in ectopic activation of PP2A in mitosis.

4. Disrupting centromeric localization of cenBAF and PP4 results in mitoses with partially assembled NE in metaphase, cells with altered NE morphology and the formation of micronuclei.

5. Altogether these results suggest a model by which CenpC, PP4 and cenBAF form a centromeric network that signals BAF dephosphorylation at mitosis exit by regulating PP2A activity.

6. T4 and S5 are the main BAF phosphosites in *Drosophila* and they can be independently phosphorylated.

7. Impaired BAF dimerization disturbs BAF phosphorylation, suggesting that dimerization is required for phosphorylation by VRK1/NHK1.

8. Depletion of the PP2A catalytic subunit MTS, as well as of the

main mitotic PP2A B-regulatory subunits TWS(B55) and WDB(B56), impairs BAF dephosphorylation and recovery after treatment with okadaic acid (OA). These results suggest that PP2A/TWS and PP2A/WDB are both capable of dephosphorylating BAF. Instead, depletion of the catalytic PP4 subunit does not affect recovery of BAF phosphorylation after OA treatment, suggesting that the bulk of BAF is not targeted by PP4 and that its activity on BAF might be restricted to the centromere.

MATERIALS AND METHODS

1. Materials

1.1 Plasmids

1.1.1 Generated plasmids

List of plasmids generated during this thesis.

Name	Description	Cloning information
pBAF-FLAG::BAF WT^R	Plasmid used for the expression of a full length WT BAF^R fused to N-terminal FLAG under the control of BAF promoter. Kanamycin. ^{R}: dsRNA resistant.	Plasmid Backbone: pBAF-HA::BAF^R. HA-tag was replaced by Flag-tag by PCR with oligos PromBAF-NheI-FLAG rev and BAFWT^R fw. It contains a NheI restriction enzyme site between pBAF and FLAG.
pBAF-FLAG::BAF S2A^R	Plasmid used for the expression of a full length BAF^R with S2 mutated to A fused to N-terminal FLAG under the control of BAF promoter. Kanamycin. ^{R}: dsRNA resistant.	Plasmid Backbone: pBAF-HA::BAF^R. HA-tag was replaced by Flag-tag by PCR with oligos PromBAF-NheI-FLAG rev and BAFS2A^R fw. It contains a NheI restriction enzyme site between pBAF and FLAG.
pBAF-FLAG::BAF T4A^R	Plasmid used for the expression of a full length BAF^R with T4 mutated to A fused to N-terminal FLAG under the control of BAF promoter.	Plasmid Backbone: pBAF-HA::BAF^R. HA-tag was replaced by Flag-tag by PCR with oligos PromBAF-NheI-FLAG rev and BAFT4A^R fw.

	Kanamycin. ^{R}: dsRNA resistant.	It contains a NheI restriction enzyme site between pBAF and FLAG.
pBAF-FLAG::BAF S5A^R	Plasmid used for the expression of a full length BAF^R with S5 mutated to A fused to N-terminal FLAG under the control of BAF promoter. Kanamycin. ^{R}: dsRNA resistant.	Plasmid Backbone: pBAF-HA::BAF^R. HA-tag was replaced by Flag-tag by PCR with oligos PromBAF-NheI-FLAG rev and BAFS5A^R fw. It contains a NheI restriction enzyme site between pBAF and FLAG.
pBAF-FLAG::BAF S2AT4A^R	Plasmid used for the expression of a full length BAF^R with S2 and T4 mutated to A fused to N-terminal FLAG under the control of BAF promoter. Kanamycin. ^{R}: dsRNA resistant.	Plasmid Backbone: pBAF-HA::BAF^R. HA-tag was replaced by Flag-tag by PCR with oligos PromBAF-NheI-FLAG rev and BAFS2AT4A^R fw. It contains a NheI restriction enzyme site between pBAF and FLAG.
pBAF-FLAG::BAF S2AS5A^R	Plasmid used for the expression of a full length BAF^R with S2 and S5 mutated to A fused to N-terminal FLAG under the control of BAF promoter. Kanamycin. ^{R}: dsRNA resistant.	Plasmid Backbone: pBAF-HA::BAF^R. HA-tag was replaced by Flag-tag by PCR with oligos PromBAF-NheI-FLAG rev and BAFS2AS5A^R fw. It contains a SpeI restriction enzyme site between pBAF and FLAG.
pBAF-BAF WT^R::FLAG	Plasmid used for the expression of a full length	Plasmid Backbone: pBAF-HA::BAF^R.

112

	BAF^R fused to C-terminal FLAG under the control of BAF promoter. Kanamycin. R: dsRNA resistant.	FLAG-tag at the C-terminal of BAF was added by PCR with oligos BAF^R Ct FLAG NheI rev and BAF^R C3 Ct BAF fw. HA-tag at the N-terminal was removed by a second PCR with oligos pBAF Ct SpeI rev and BAF WT^R fw. It contains a SpeI restriction enzyme site between pBAF and BAF and a NheI at the C-terminal of FLAG.
pBAF-BAF WT^R::HA	Plasmid used for the expression of a full length BAF^R fused to C-terminal HA under the control of BAF promoter. Kanamycin. R: dsRNA resistant.	Plasmid Backbone: pBAF-HA::BAF^R. HA-tag at the C-terminal of BAF was added by PCR with oligos BAF^R Ct HA NheI rev and BAF^R C3 Ct BAF fw. HA-tag at the N-terminal was removed by a second PCR with oligos pBAF Ct SpeI rev and BAF WT^R fw. It contains a SpeI restriction enzyme site between pBAF and BAF and a NheI at the C-terminal of HA.

1.1.2   Template plasmids for generating double strand RNA

List of plasmids used as a template for generating double strand RNA used during this thesis. For each of them, information regarding how it is obtained is presented in the following table.

Name	Cloning information/Source
pMK33-TAP::CenpC	Contains CenpC cDNA. Previously generated in the lab.
Flfl template	Contains Flfl cDNA. DGRC reference: FMO 09514.
MTS-TOPO	MTS sequence was amplified by PCR using genomic material from S2 as a template and dsMTS fw and dsMTS rev primers and then it was introduced in the TOPO 2.1 vector.
PP4c-TOPO	PP4c sequence was amplified by PCR using genomic material from S2 as a template and dsPP4c fw and dsPP4c rev primers and then it was introduced in the TOPO 2.1 vector.
TWS-TOPO	TWS sequence was amplified by PCR using genomic material from S2 as a template and dsTWS fw and dsTWS rev primers and then it was introduced in the TOPO 2.1 vector.
pOT2-WDB	Contains WDB cDNA. Gift from Dr. Lipinszki.

1.1.3 Lab plasmids

List of plasmids, previously generated in the lab, used during this thesis.

Name	Description	Source
pBAF-BAF::YFP	Plasmid used for the expression of a full length BAF fused to C-terminal YFP under the control of BAF promoter.	Dr Sònia Medina

	Kanamycin	
pBAF-YFP::BAF	Plasmid used for the expression of a full length BAF fused to N-terminal YFP under the control of BAF promoter. Kanamycin	Dr Sònia Medina
pBAF-HA::BAF^R	Plasmid used for the expression of a full length BAF^R fused to C-terminal HA under the control of BAF promoter. Kanamycin. ^{R}: dsRNA resistant.	Dr. Mònica Torras
pBAF-FLAG::BAF S2AT4AS5A	Plasmid used for the expression of a full length BAF with S2, T4 and S5 mutated to A fused to N-terminal FLAG under the control of BAF promoter. Kanamycin.	Dr Mònica Torras

1.2 Oligonucleotides

The list of the oligonucleotides used during this thesis is presented in the following tables.

1.2.1   Nucleotides for directed mutagenesis

Name	Sequence (5'-3')
PromBAF-NheI-FLAG rev	CTTGTCGTCATCGTCTTTGTAGTCCATGGCTAGCGT TTGTAGTTTGCT
BAF WT^R fw	ATGAGCGGAACCAGCCAAAA

BAF S2A^R fw	ATGGCGGGAACGTCGCAAAAGCATC
BAF T4A^R fw	ATGTCGGGAGCGTCGCAAAAGCATC
BAF S5A^R fw	ATGTCGGGAACGGCGCAAAAGCATC
BAF S2AT4A^R fw	ATGGCCGGAGCCAGCCAAAAGCATCGC
BAF S2AS5A^R fw	ATGGCCGGAACCGCCCAAAAGCATCGC
BAF T4AS5A^R fw	ATGAGCGGAGCGGCGCAAAAGCATCG
BAF^R Ct FLAG NheI rev	GCTAGCTCACTTGTCATCGTCTTTGTAGTCCAGAAATTCTTCACACCAGTC
BAF^R Ct HA NheI rev	GCTAGCTCAGCGTAATCTGGAACATCGTATGGGTA
BAF^R C3 Ct BAF fw	GGATCCACCGGATCTAGATAACTG
pBAF Ct SpeI rev	GCTAGCGTTTGTAGTTTGCTTTGCTGC

1.2.2   Oligonucleotides for double strand DNA synthesis

The T7 RNA polymerase promoter is highlighted.

Name	Sequence (5'-3')
dsCenpC fw	**TAATACGACTCACTATAGGGAGA**GGTACCACCTCCTATCGAATA
dsCenpC rev	**TAATACGACTCACTATAGGGAGA**GAATTCCAATTTGGATCTGGA
dsFlfl fw	**TAATACGACTCACTATAGGGAGA**ATGACGACTGACACCCGC
dsFlfl rev	**TAATACGACTCACTATAGGGAGA**ACAACTTTTCCTTTCGCA
dsLacZ fw	**TAATACGACTCACTATAGGG**ATGACCATGATTACGCCAAGC
dsLacZ rev	**TAATACGACTCACTATAGGG**CAATTTCCATTCGCCATTCAG

dsMTS fw	**TAATACGACTCACTATAGGG**GCCAAGGAGATTCTCTCC
dsMTS rev	**TAATACGACTCACTATAGGG**CTGGCCAAAGGTGTAACC
dsPP4c fw	**TAATACGACTCACTATAGGGAGA**ATGTCCGACTACAGCGAC
dsPP4c rev	**TAATACGACTCACTATAGGGAGA**CCACACGGCCGTCGATCC
dsTWS fw	**TAATACGACTCACTATAGGGAGA**CTGATCCGGGATCCACAGAATGTAA
dsTWS rev	**TAATACGACTCACTATAGGGAGA**CACACTTTGATGCTCAAGTAATCCC
dsWDB1 fw	**TAATACGACTCACTATAGGGAGA**TCGATCCGCCGCAGTTTGTCAAGAT
dsWDB1 rev	**TAATACGACTCACTATAGGGAGA**TCGACTGCTGCTGATGAGAGTTCAG
dsWDB2 fw	**TAATACGACTCACTATAGGGAGA**GCTCAAGAAGAAGGGTAAAAAGAGT
dsWDB2 rev	**TAATACGACTCACTATAGGGAGA**CCATATATACGATGCAATACCGTCT

1.3 Stable cell lines

Stable cells lines used in this thesis are shown in the following table. The name of each of them, which correspond to the protein that is stably expressed, is presented in the first row. In the second row the construct transfected to create the cell line and the appropriate antibody selection are shown. Finally, in which cell original cell line, either S2 cells or DMel-II, has been used to produce the cell line and several comments about it is presented in the third row.

Expressed protein	Construct and Selection	Original cell line and Comments	Results chapter
GFP::CenpC[R]	pMT-GFP::CenpC[R] Blasticidin	DMel-II cells Generated by Dr. Lipinszki [R]esistant to RNAi Cooper induction: 0.5mM, 22-24 hours	3.1
GFP::CenpCΔFIM[R]	pMT-GFP::CenpCΔFIM[R] Blasticidin	DMel-II cells Generated by Dr. Lipinszki [R]: dsRNA resistant Cooper induction: 0.5mM, 22-24 hours	3.1
GFP::CenpC[R] + GBP::FLAG::BAF	pMT-GFP::CenpC[R] pMT-GBP::FLAG::BAF Blasticidin + Hygromycin	DMel-II cells Generated by Dr. Lipinszki [R]: dsRNA resistant GBP=GFPbinding protein Cooper induction: 0.5mM, 22 hours	3.1
GFP::CenpCΔFIM[R]+ GBP::FLAG::BAF	pMT-GFP::CenpCΔFIM[R] pMT-GBP::FLAG::BAF Blasticidin + Hygromycin	DMel-II cells Generated by Dr. Lipinszki	3.1

		[R]: dsRNA resistant GBP=GFPbinding protein Cooper induction: 0.5mM, 22 hours	
BAF::YFP	pBAF- BAF::YFP Neomycin	S2 cells Previously generated in the lab	3.2
YFP::BAF	pBAF- YFP::BAF Neomycin	S2 cells Previously generated in the lab	3.2
FLAG::BAF[R] WT	pBAF-FLAG::BAF WT[R] Neomycin	S2 cells [R]: dsRNA resistant	3.2
FLAG::BAF[R] S2A	pBAF-FLAG::BAF S2A[R] Neomycin	S2 cells [R]: dsRNA resistant	3.2
FLAG::BAF[R] T4A	pBAF-FLAG::BAF T4A[R] Neomycin	S2 cells [R]: dsRNA resistant	3.2
FLAG::BAF[R] S5A	pBAF-FLAG::BAF S5A[R] Neomycin	S2 cells [R]: dsRNA resistant	3.2
FLAG::BAF[R] S2AT4A	pBAF-FLAG::BAF S2AT4A[R] Neomycin	S2 cells [R]: dsRNA resistant	3.2
FLAG::BAF[R]	pBAF-FLAG::BAF	S2 cells	3.2

S2AS5A	S2AS5A[R] Neomycin	[R]: dsRNA resistant		

1.4 Antibodies

The primary and secondary antibodies used for western blot, immunostaining and immunoprecipitation experiments are presented in the following tables.

1.4.1   Primary antibodies

Name	Specie	Characteristics	Dilution	Source
αBAF	Rabbit	Rabbit polyclonal. It was raised against bacterially expressed full length *D. Melanogaster* BAF.	WB: 1/2500 IF: 1/300 IP 1/200	Dr Azorin Lab Described in[92]
αCenpC	Rabbit	Rat polyclonal purified. It was raised against bacterially expressed *D. melanogaster* CenpC fragment (AA 505-1227).	IF: 1/250	Dr Azorin Lab Described in[92]
αCenpC	Rat	Rat polyclonal. It was raised against bacterially expressed *D. melanogaster* CenpC fragment (AA 505-1227).	WB: 1/3000 IF: 1/300	Dr Azorin Lab Described in[92]
αCID	Chicken	Chicken polyclonal	IF: 1/2000	Dr Lipinszki Lab

		purified		Described in[151]
αFlfl	Rat	Rat polyclonal	WB: 1/10000 IF: 1/600	Dr Lipinszki Lab Described in[151]
αFlag	Mouse	Mouse monoclonal	IF: 1/2000	Sigma, F3165
αFlag	Rabbit	Rabbit purified	WB: 1/2500	Sigma, F7425
αGFP	Mouse	Mouse monoclonal	WB: 1/2500	Roche, 1181446001
αGFP	Rabbit	Rabbit polyclonal	IP: 1/55	TermoFisher Scientific, A-11122
αH3PSer10	Rabbit	Rabbit polyclonal	IF: 1/3000	Millipore, 06-570
αLaminB	Mouse	Mouse polyclonal	IF: 1/1000	DSHB, ADL67.10
αMTS	Mouse	Mouse monoclonal	WB: 1/1000	BD-Transduction Laboratories, 610555
αTubulin	Mouse	Mouse monoclonal	WB: 1/5000 IF: 1/5000	Millipore, MAB3408
αTWS	Rabbit	Rabbit polyclonal	WB: 1/2000	Dr Archambault Lab
αWDB	Rabbit	Rabbit polyclonal	WB: 1/2000	Dr Lipinszki Lab

1.4.2   Secondary antibodies

Name	Dilution	Source
Cyanine 2 AffiniPure Goat αRabbit IgG	IF: 1/400	Jackson, 111-225-144
Cyanine 3 AffiniPure Goat αRabbit IgG	IF: 1/400	Jackson, 111-165-144
Cyanine 3 AffiniPure Goat αMouse IgG	IF: 1/400	Jackson, 115-165-146
Cyanine 5 AffiniPure Donkey αChicken IgG	IF: 1/400	Jackson, 703-175-155
Cyanine 5 AffiniPure Goat αMouse IgG	IF: 1/400	Jackson, 115-175-146
Cyanine 5 AffiniPure Goat αRabbit IgG	IF: 1/400	Jackson, 115-175-144
Cyanine 5 AffiniPure Goat αRat IgG	IF: 1/400	Jackson, 112-175-143
Peroxidase AffiniPure Donkey αMouse IgG	WB: 1/10000	Jackson, 715-035-150
Peroxidase AffiniPure Goat αRabbit IgG	WB: 1/10000	Jackson, 111-035-144
Peroxidase AffiniPure Donkey αRat IgG	WB: 1/10000	Jackson, 712-035-150

2. Methods

2.1 Manipulation of cells

2.1.1 Culturing cells

Drosophila S2 cells (SL2, Schneider 2; ATCC CRL-1963): The S2 cell line is derived from a primary culture of late stage (20-24 hours old) *Drosophila Melanogaster* embryos[214].

Drosophila Mel-II: The DMel-II cell line is derived from a culture of S2 cells adapted to grow in a free-serum media.

Both, S2 and DMel-II cells, are cultured at 25ºC and they grow semi-adherent to the surface of the flask. Cells are collected by pipetting and $3,5 \cdot 10^6$ cells are seeded in T25 (Corning) every 3-4 days.

S2 cells are grown in Schneider's Insect Medium (L 0207-500, Biowest) supplemented with 10% heat-inactivated FBS (10270, Gibco) and 1% penicillin-streptomycin (15140-122, Gibco).

DMel-II cells are grown in Insectagro DS2 Medium (13-402-00, Corning) supplemented with 2mM L-Glutamine (25030-032, Gibco) and 1% penicillin-streptomycin (15140-122, Gibco).

D.Mel-II cells are the ones used for double strand RNA treatment since this treatment has higher efficiency due to the lack of serum in the medium they are grown in. On the other hand, S2 cells are used for the experiments involving recovery from OA treatment since they are capable of recovering better from it.

Drosophila S2 and Drosophila DMel-II cell lines are frozen in FBS/10% DMSO and Free Medium/10% DMSO respectively in liquid nitrogen.

2.1.2 Cell transfection

2.1.2.1 Transitory transfection

Plasmid DNA is transiently transfected in S2 cells by the calcium phosphate precipitation method. This method allows DNA entrance to the cell by creating DNA-phosphate precipitates.

Day one: Plate cells

1. Two 60 mm^2 culture plate (Corning) are plated with $3 \cdot 10^6$ cells/ml in a final volume of 5ml each of them and are incubated for 24 hours.

Day two: Transfection

2. Each plate is transfected with 20μg of DNA. Reagent mix is prepared for 2,5 transfections. Therefore, 50μg of DNA are added to a final volume of 125 μl that is completed by sterilized water. Then 1 ml of 0.25M CaCl$_2$ is included to the mix.

3. Separately, in a 15 ml falcon tube 1ml of HEBS 2X (250mM NaCl 250, 9mM KCl, 1,5mM Na$_2$HPO4, 10mM glucose, 50mM pH 7,1 HEPES) is added.

4. HEBS is softly vortexed while the CaCl$_2$-DNA mixture is added drop by drop in order to create visible white precipitates. These precipitates are incubated at room temperature for 30minutes.

5. After this 30minutes the precipitates are re-suspended and 850μl of this mixture is added to each plate. Plates are incubated at 25ºC for 48hours.

Day four: Experiment

6. Collect the cells and proceed with the downstream experiment.
    .

2.1.2.2 Stable cell lines

After day 2 of transient transfection protocol, proceed with the following methodology:

Day three: Change of medium

6. 24 hours post-transfection, calcium phosphate precipitates are removed by centrifugation at 1000rpm and complete fresh medium is added to the cells.

Day five: Drug selection

7. The actual medium is removed and complete medium supplemented with the appropriate selection agents is added in order to select cells that express the DNA plasmid.

8. Medium is refreshed by centrifugation every 4-5 days to remove death cells and cells are re-plated in the old flask until selected clones show up.

A list of the stable cell lines used during this thesis project is presented in the *Materials* section.

2.1.2.3 CuSO4 induction

The expression of some of the constructs used in this thesis is regulated by a metallothionein promoter (pMT) that is inducible by its exposure to metal. Therefore, $CuSO_4$ is added to the medium of cells to express the DNA.

A stock solution of 1M $CuSO_4$ (C8027, Sigma) is prepared and kept at 4ºC. A 1:10 dilution of the stock medium is freshly prepared right before using it by diluting it with complete growth medium and the appropriate amount is added to the cells.

The specificities of the cupper treatment for each cell line are presented in the *Materials* section.

2.1.2.4 Okadaic acid treatment

OA is a well-known phosphatase inhibitor and a powerful tool for studying the role of phosphatases during mitosis[215].

10µg of OA (39302, Sigma) is dissolved in DMSO to a final concentration of 11µM. Aliquots of 50µl are prepared and kept at -20ºC.

For the OA treatment, $3 \cdot 10^6$ cells/ml S2 cells are seeded 48 hours before treatment. OA diluted with Schneider medium is added to a final concentration of 20nm during three hours. Since OA is diluted in DMSO cells treated with the same amount of DMSO is always added as a control.

When performing recovery experiments, after three hours of OA treatment this medium is carefully removed from the plate and replaced by fresh Schneider complete medium. Cells are collected at different times for further analysis.

2.1.3 Double strand RNA treatment

2.1.3.1 S2 cells

Day one: First dose

1. On the first day, $3 \cdot 10^6$ S2 cells are re-suspended in 2ml of pre-warmed serum-free medium. The corresponding amount of dsRNA is added to this medium and incubated for 1hour at room temperature. The appropriate amount of dsRNA treatment is presented in the following table:

Gene depleted	dsRNA concentration
LacZ	70µg
MTS	70µg
PP4c	100µg
TWS	70µg
WDB1 + WDB2	35µg + 35µg

2. 3mL of 1,7X FBS-medium are added to the mixture of cells and placed in 5ml flasks.

Day four: Second dose

3. Cells are diluted to a final concentration of $0.5 \cdot 10^6$ cells/ml and a second dose of the same amount of dsRNA is added.

Day seven: Experiment day

4. Cells are collected to perform the appropriate experiment.

2.1.3.2 DMel-II cells

Since DMel-II cells are grown in free-serum medium there is no need to pre-incubate the cell with dsRNA in an independent medium for 1hour.

The following amounts of dsRNA are directly added to DMel-II cells that have been previously seeded at $0.7 \cdot 10^6$ cells/ml concentration.

Gene depleted	dsRNA concentration
LacZ	30-50µg
MTS	30µg (single dose)
Flfl	40µg
CenpC	50µg

Three days after the first dose of dsRNA, DMel-II cells are diluted to a final concentration of $0.5 \cdot 10^6$ cells/ml and a second dose of the same amount of dsRNA is added before starting the appropriate experiment.

For MTS knockdown in DMel-II a single dose of dsRNA for 3 days is carried out since longer depletion time results in high cell death. In Flfl-depleted cells, MTS co-depletion is carried out simultaneously to Flfl-depletion during the last 3 days of the 6 days of treatment with dsRNA^{Flfl}.

2.2 Molecular biology methods

2.2.1 dsRNA synthesis

2.2.1.1 MEGAscript reaction

dsRNA is produced using a MEGAscript T7 kit (AM1334, Thermo Fisher Scientific). To set up the MEGAscript reaction (total volume 40µl) the following components are mixed:

> 16µL NTP's (4µL of each)
>
> 4µL 10X Buffer
>
> 4µL Enzyme mix
>
> 16µL PCR product flanked with T7

The reaction is incubated at 37°C overnight.

2.2.1.2 dsRNA purification

The double strand RNA generated is purified with the RNeasy Mini Kit (74104, Qiagen).

1. First 2µL TURBO DNase are added and incubated for 15 minutes at 37°C in order to get rid of the non-translated DNA PCR product.

From here on, RNeasy Mini Kit is used according to the manufacturer's

recommended protocol.

2. The volume is increased to 100µL with RNase free H2O and 350µL Buffer RLT and 250 µL of 100% ethanol are added and mixed by pipetting.

3. The sample (700µL) is transferred to an RNeasy spin column and spun down for 15s at full-speed.

4. Then, it is washed with 500µL Buffer RPE, spun down twice for 15seconds at full-speed and centrifuged an extra minutes at full-speed without any buffer.

5. Finally, the column is placed into a fresh collection tube and 50µL RNase-free water are added to the column membrane to elute the RNA. The tube is spin down for 1minute at full-speed and it is repeated using 30µL of RNase-free water to increase the amount of eluted RNA.

The RNA concentration is measured using nanodrop and an aliquot is saved to be checked on an agarose gel before keeping the dsRNA at -20°C.

2.3 Analysis of BAF phosphorylation

2.3.1 Extract preparation

Total cell extract

Cells are collected and spun down 5minutes at 1000rpm. Medium is removed and the pellet is re-suspended with a solution containing ½ 5xPLB and ½ water. 2µl of βmercaptoethanol every 50µl of extract are added. This mixture is vortexed and boiled for 2minutes prior to analysis by phostag gel.

Extracts with and without alkaline phosphatase treatment.

Extracts with and without alkaline phosphatase (AP) inhibitors are prepared in parallel when analysing phospho-BAF. Then, the extract treated without AP inhibitors is treated with AP in order to dephosphorylate BAF. This serves as a control to evaluate if certain bands seen in the gel correspond to phosphorylated forms of BAF.

1. 10ml of cells at $3.5 \cdot 10^6$cells/ml concentration are collected and divided into three different tubes: two tubes of 4.5ml and one tube of 1ml. All of them are washed three times with PBS.

2. Total cell extract is prepared with the tub containing 1ml of cells by suspending it with PLB-βmercaptoethanol. Each one of the other two tubes is re-suspended with 200μl of lysis buffer. One of them containing AP inhibitors and the other one without and they are left on

Lysis buffer with AP inhibitors	Lysis buffer without AP inhibitors
1% NP40 (Igepal)	1% NP40 (Igepal)
0.1% SDS	0.1% SDS
10% Glycerol	10% Glycerol
150mM NaCl	150mM NaCl
50mM Tris ph8	50mM Tris ph8
1x Protease Inhibitor cocktail (Sigma)	1x Protease Inhibitor cocktail (04693159001, Roche)
1mM PMSF	1mM PMSF
50mM NaF	
50nM OA	

ice for 30minutes.

3. Cells are gently pipped up and down for 30 times and spun down for 15minutes full speed at 4ºC. The supernatant can be kept at -20ºC or the protocol is continued.

4. 50µl of the extract without inhibitors is mixed with 10µl of 10xAP buffer and 40µl of AP (40 units) and left for 1hour at 37ºC so the alkaline phosphatase can de-phosphorylate this sample. 30µl of 5xPLB and 15µl of β-mercaptoethanol are added and the sample can be stored. 50µl of the extract with inhibitors is mixed with 50µl of water, 30µl of PLB and 15µl of βHOH and can be stored at -20ºC.

5. The high salt content of these extracts can disturbed the following phostag gel electrophoresis. In order to avoid that, these extracts are diluted in half with ½ 5xPLB and ½ water before running them in the gel.

2.3.2   Phostag gel analysis

Phostag gels are polyacrylamide gels containing the Phostag[TM] ligand. This technic allows separating proteins depending not only on its molecular weight but also on its phosphorylated state.

The Phostag[TM] ligand acts as a phosphate-trapping molecule. Phosphorylated proteins reversible bind to the Phostag[TM] immobilized in the gel during electrophoresis and they migrate slower. That creates a mobility delayed for the phosphorylated proteins in comparison to the non-phosphorylated that is detectable when developing the WB (fig 60).
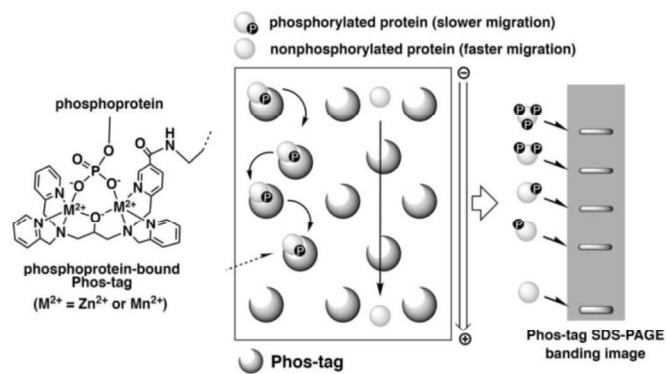
Figure 60. Phostag gel electrophoresis overview. Due to its reversible interaction with the Phostag[TM] ligand phosphorylated proteins run slower

during electrophoresis.

The protocol for analysing cell extracts by Phostag gels is the following.

     1. 50μM of acrylamide-pendant Phostag^{TM} ligand (AAL-107) and 100μM of MnCl$_2$ are added to 13% polyacrylamide resolving gel solution when detecting endogenous BAF or 12% when detecting tagged BAF before polymerization. The stacking gel is prepared as for a normal electrophoresis.

     2. After electrophoresis, gels are washed 10minutes in transfer buffer containing 1mM EDTA and 15 minutes in transfer buffer without EDTA. EDTA binds and gets ride of the manganese ion from the gel in order to preventing its interference with electroblotting.

After that, the protocol is followed as a typical western blotting.

2.4 Immunoprecipitation

2.4.1 Preparation of the cell extract:

     1. Approximately 200 · 10^6 cells are collected. Cells are pelleted and washed with PBS 3 times.

     2. The pellet is re-suspended in 3x volumes of IP lysis buffer and incubated on ice for 30minutes.

IP buffer
50mM Tris ph 8
150mM NaCl
10% Glycerol
5mM EDTA
0.5% NP40 (Igepal)
0.1mM PMSF
1x Protease Inhibitor Cocktail (04693159001, Roche)

3. 30x strokes using a Dounce homogenizer with clearance B/tight pestles are carried out in order to disrupt the cellular and nuclear membranes.

4. NaCl is added to a final concentration of 300mM and is incubated at 4°C for 30minutes with rotation.

5. The lysate is centrifuged at 14.000 rpm for 15minutes at 4°C and the supernatant is collected. 2-5%µl of protein extract is separated, mixed with PLB-βMercaptoethanol and kept at -20°C (input).

2.4.2   Immunoprecipitation:

1. For the pre-washing, 30µL of Protein A sepharose (170780, GE Healthcare) at a 50% suspension in IP Buffer are added to 500µl extract and incubated for 1h at 4°C with rotation.

2. The sample is centrifuged at 3,000 rpm for 2minutes and the supernatant is transferred to a new tube where the appropriate antibody is added (for amounts of antibodies see *Materials*). They are incubated overnight at 4°C with rotation.

3. Next day, 50µl of beads of Protein A Sepharose previously equilibrated with the appropriate buffer are used to bind BAF and GBP antibodies. It is incubated for 2hours at 4°C with rotation.

4. The beads are washed 5 times with IP buffer for 5minutes with rotation and then spun down at 2,000rpm for 2minutes at 4°C.

5. The beads are finally re-suspended in 60µL PLB-βHOH, vortexed and boiled for 2minutes at 95°C, and then spun down as only the supernatant is used.

It is important to always add a negative control (MOCK). When doing a αBAF IP, the extract is divided into two. In one tube, the BAF antibody is added, and in the other one a pre-immune rabbit antibody. When

doing a αGFP IP, S2 cells that do not express GFP protein are used as MOCK.

2.5 Directed mutagenesis

2.5.1 Primer phosphorylation

The appropriate primers were previously phosphorylated with the polynucleotide kinase (20350427, Roche). The following mix is prepared:

    1μl of the 100μM oligonucleotide

    1μl 10x of the polynucleotide buffer

    2μl 10mM of ATP

    10u (1μl) of polynucleotide kinase

    5μl of nuclease-free water

The reaction takes places for 2hours at 37ºC and then the enzyme is inactivated by incubating the mixture 10minutes at 70ºC

2.5.2 PCR

The full plasmid is amplified with primers containing the appropriate modifications (for primers used see *Materials section*) using the enzyme Phusion High Fidelity DNA polymerase (M0530, New England Biolab).

To set up the PCR reaction the following components are mixed:

    10ng of the template DNA

    2μl of the 10μM phosphorylated forward oligonucleotide

    2μl of the 10μM phosphorylated reverse oligonucleotide

    2μl of 10mM deoxynucleotides

    10μl of the 5X fusion HF buffer

Up to a final volume of 50µl with nuclease-free water

0,5µl of the DNA polymerase.

The amplification program is the following one:

Denaturation: 98°C – 15seconds

Annealing: 58°C – 30seconds

Extension: 72°C – 1:40minutes

2.5.3 Ligation and transformation

12µl of the PCR reaction are run in an agarose gel. The corresponding band is cut from the gel and eluted in 40µl by using the PCR DNA and gel band purification kit (28903470, Cytiva).

40µl of the eluted PCR product is ligated with the T4 DNA ligase (EL0016, Fermentas), overnight at 18ºC. The ligated product is transformed in bacteria and the subsequent colonies are validated by sequencing.

2.6 Cell immunostaining

2.6.1 Impacted cells

Day 1: Plate cells

1. One flask is plated by $3 \cdot 10^6$ cells in a final volume of 5ml medium.

Day 4: Colchicine treatment and first day of immunostaining

2. Cells are treated for 6h with 25µM colchicine (10295892001, Sigma). Colchicine is a drug that binds microtubules and prevents its assembly; as a consequence cells are arrested at mitosis.

3. 300µl of collected cells diluted at a concentration of $3 \cdot 10^6$ cells/ml are incubated for 5min with MAC buffer. MAC is a hypotonic buffer causing that the water gets into the cells pumping them up. It allows to properly visualizing the nuclear components when performing the subsequent immunostaining.

MAC hypotonic buffer
50mM Glycerol
5mM KCl
12mM NaCl
0,8mM CaCl
19mM Sucrose

4. 200µl of these cells are immobilized onto a slide by centrifugation for 10minutes at 500rpm with low acceleration in a ThermoShandon Cytospin using a single-chamber Cytofunnel.

5. Cells are fixed in 4% paraformaldehyde for 10minutes, washed with PBS and permeabilized by incubating 10minutes twice in 3%BSA, 0.5%TritonX-100 in PBS.

6. Cells are incubates with 20-30µl of the appropriate antibody dilution in 1%BSA and 0.1%TritonX-100 PBS solution (for antibodies used see *Materials*) and left 1hour at room temperature and then overnight at 4ºC in a humid chamber.

Day 5: Second day of immunostaining

7. Samples are washed twice with 1%BSA and 0.1%TritonX-100 in PBS.

8. Samples are incubated with the appropriate secondary antibody for one hour at room temperature.

9. They are washed twice with 0.1%TritonX-100 in PBS and once with PBS.

10. For visualization, slides were mounted in Mowiol (475904 Calbiochem-Novabiochem) containing 0.2 ng/ml DAPI (D9542, Sigma).

Finally, samples are analysed in a Leica SPE confocal microscope equipped with LAS/AF software. Images are acquired and processed using ImageJ (http://imagej.nih.gov/ij/)and Adobe Photoshop software. Mean grey intensities are calculated using ImageJ macros on thresholded images at DAPI-masked regions of interest running analysed particles to plugin on the FeatureJLaplacian (http://imagescience.org/meijering/software/featurej/).

2.6.2   Coverslips coated with concanavalin.

Immunostaining protocol with impact cells previously treated with MAC does not allow to properly evaluating elements that are found outside from the nucleoplasm. Moreover, we get a 2D image of the cell losing its 3D structure perspective. In order to overcome these issues and preserve an intact cell structure to properly evaluate the NE morphology cells are plated in well plates containing cover slips that have been previously treated with Concanavalin A promoting that the cells are glued at the top of the cover slip. The immunostaining protocol is the following:

1. Cells are plated at $1.2 \cdot 10^6$cells/ml in 24 well plates containing cover slips coated with 0.5 mg/ml Concanavalin A (C2010, Sigma). After 6 hours, cells are processed for immunostaining

2. Medium from the well is removed and washed with PBS for 10 minutes with very slow agitation.

3. Cells are fixed in 4% paraformaldehyde for 15minutes, washed

with PBS and permeabilized by incubating them 10minutes twice in 3%BSA, 0.5%TritonX-100 in PBS.

4. Cover slips are incubated with 100-150µl of the appropriate antibody dilution in 1%BSA and 0.1%TritonX-100 PBS solution (for antibodies used see *Materials*) and left 1hour at room temperature and then overnight at 4ºC in a humid chamber.

5. The following day samples are washed three times with 1%BSA and 0.1%TritonX-100 in PBS.

6. Samples are incubated with the appropriate secondary antibody for one hour at room temperature.

7. They are washed twice with 0.1%TritonX-100 in PBS and twice with PBS.

8. For visualization, slides were mounted in Mowiol (475904 Calbiochem-Novabiochem) containing 0.2 ng/ml DAPI (D9542, Sigma).

Finally, samples are analysed in a Leica SP5 confocal microscope equipped with LAS/AF software. Images are acquired and processed using ImageJ and Adobe Photoshop software.

2.7 Statistical analysis

Statistical significance of the difference in the proportion of mitoses showing perichromosomal BAF and centromeric Flfl and in the proportion of cells with aberrant NE morphology defects is assessed via two-tailed Fisher's exact test.

Statistical significance of the difference in the proportion of NE-assembled mitoses between GFP::CenpC^R and GFP::CenpCΔFIM^R-expressing cells is assessed via comparative Chi-square test using the

cp.chisq.test function from the DiffXTables package version 0.1.0 using R 3.5.1[216].

Statistical significance of the difference in centromeric intensity of BAF, immunostaining is determined by Kruskal–Wallis test.

Statistical difference in the extent of BAF/CenpC co-IP and the efficiency of protein depletion is determined by two-tailed t-test comparison of the means.

Statistical difference between phosphatases depletions in the post OA recovery is assessed by mixed linear models using Experiment and technical replicate as nested random effects (lme4 1.1-23, multcomp 1.4-9, R-3.5.1). P-values are adjusted for multiple testing using Benjamini-Hochberg.

For each experiment, the number of independent biological replicates (n) and sample sizes (N) are indicated in the corresponding figure legend.

BIBLIOGRAPHY

1. Wenzel ES, Singh ATK. Cell-cycle checkpoints and aneuploidy on the path to cancer. *In Vivo (Brooklyn)*. 2018;32(1):1-5. doi:10.21873/invivo.11197

2. Malumbres M, Barbacid M. Cell cycle, CDKs and cancer: A changing paradigm. *Nat Rev Cancer*. 2009;9(3):153-166. doi:10.1038/nrc2602

3. Alves FDL, Kerr A, Green LC, Hudson DF, Ohta S, Cooke CA. Mitotic chromosomes are compacted laterally by KIF4 and condensin and axially by topoisomerase II α. *J Cell Biol*. 2012;199(5):755-770. doi:10.1083/jcb.201202155

4. Wilkins BJ, Rall NA, Ostwal Y, et al. A Cascade of Histone Modifications Induces Chromatin Condensation in Mitosis. *Science (80-)*. 2014;343(3):77-81.

5. Goodson H V, Jonasson EM. Microtubules and Microtubule-Associated Proteins. *Cold Spring Harb Perspect Biol*. 2018;10.

6. Stephan Güttinger, Laurell E, Kutay U. Orchestrating nuclear envelope disassembly and reassembly during mitosis. *Nat Rev Mol Cell Biol*. 2009;10:178-191. doi:10.1038/nrm2641

7. Marston AL. Dalmatian: spotting the difference in cohesin protectors. *EMBO J*. 2017;36(11):1468-1470. doi:10.15252/embj.201797090

8. Carlton JG, Jones H, Eggert US. Membrane and organelle dynamics during cell division. *Nat Rev Mol Cell Biol*. 2020. doi:10.1038/s41580-019-0208-1

9. Lin DH, Hoelz A. The Structure of the Nuclear Pore Complex (An Update). *Annu Rev Biochem*. 2019;88(18):1-59. doi:10.1146/annurev-biochem-062917-011901

10. Buchwalter A, Kaneshiro JM, Hetzer MW. Coaching from the sidelines : the nuclear periphery in genome regulation. *Nat Rev Genet*. 2019;20(January). doi:10.1038/s41576-018-0063-5

11. Barton LJ, Soshnev AA, Geyer PK. Networking in the nucleus: A spotlight on LEM-domain proteins. *Curr Opin Cell Biol*. 2015;34:1-8. doi:10.1016/j.ceb.2015.03.005

12. Wagner N, Krohne G. LEM-Domain Proteins: New Insights into Lamin-Interacting Proteins. *Int Rev Cytol*. 2007;261(07):1-46. doi:10.1016/S0074-7696(07)61001-8

13. Bione S, Maestrini E, Rivella S, et al. Identification of a novel X-linked gene responsible for Emery-Dreifuss muscular dystrophy. *Nat Genet*. 1994;8(december):323-327. doi:10.1038/ng1294-323

14. Taylor MRG, Slavov D, Gajewski A, et al. Thymopoietin (lamina-associated polypeptide 2) gene mutation associated with dilated cardiomyopathy. *Hum Mutat*. 2005;26(6):566-574. doi:10.1002/humu.20250

15. Hellemans J, Preobrazhenska O, Willaert A, et al. Loss-of-function mutations in LEMD3 result in osteopoikilosis, Buschke-Ollendorff syndrome and melorheostosis. *Nat Genet*. 2004;36(11):1213-1218. doi:10.1038/ng1453

16. Brachner A, Foisner R. Evolvement of LEM proteins as chromatin tethers at the nuclear periphery. 2011:1735-1741. doi:10.1042/BST20110724

17. Mandigo TR, Turcich BD, Anderson AJ, Hussey MR, Folker ES. Drosophila emerins control LINC complex localization and transcription to regulate myonuclear position. *J Cell Sci*.

144

2019;132(20). doi:10.1242/jcs.235580

18. Barton LJ, Pinto BS, Wallrath LL, Geyer PK. Matters Arising The Drosophila Nuclear Lamina Protein Otefin Is Required for Germline Stem Cell Survival. *Dev Cell*. 2013;25(6):645-654. doi:10.1016/j.devcel.2013.05.023

19. Wagner N, Schmitt J, Krohne G. Two novel LEM-domain proteins are splice products of the annotated Drosophila melanogaster gene CG9424 (Bocksbeutel). *Eur J Cell Biol*. 2004;82(12):605-616. doi:10.1078/0171-9335-00350

20. Geyer PK. Tissue-Specific Defects Are Caused by Loss of the Drosophila MAN1 LEM Domain Protein. 2008;145(September):133-145. doi:10.1534/genetics.108.091371

21. Wagner N, Kagermeier B, Loserth S, Krohne G. The Drosophila melanogaster LEM-domain protein MAN1. *Eur J Cell Biol*. 2006;85(2):91-105. doi:10.1016/j.ejcb.2005.10.002

22. de Leeuw R, Gruenbaum Y, Medalia O. Nuclear Lamins: Thin Filaments with Major Functions. *Trends Cell Biol*. 2018;28(1):34-45. doi:10.1016/j.tcb.2017.08.004

23. Dittmer T, Misteli T. The lamin protein family. *Genome Biol*. 2011;12(5). doi:10.1186/gb-2011-12-5-222

24. Machowska M, Piekarowicz K, Rzepecki R. Regulation of lamin properties and functions: Does phosphorylation do it all? *Open Biol*. 2015;5(11). doi:10.1098/rsob.150094

25. Buchwalter A, Kaneshiro JM, Hetzer MW. Coaching from the sidelines: the nuclear periphery in genome regulation. *Nat Rev Genet*. 2019;20(1):39-50. doi:10.1038/s41576-018-0063-5

26. Romero-Bueno, de la Cruz Ruiz, Artal-Sanz, Askjaer, Dobrzynska. Nuclear Organization in Stress and Aging. *Cells*. 2019;8(7):664. doi:10.3390/cells8070664

27. Pałka M, Tomczak A, Grabowska K, et al. Laminopathies: what can humans learn from fruit flies. *Cell Mol Biol Lett*. 2018;23(1):1-12. doi:10.1186/s11658-018-0093-1

28. Alves DB, Silva JM, Menezes TO, et al. Clinical and radiographic features of Hutchinson-Gilford progeria syndrome: A case report. *World J Clin Cases*. 2014;2(3):67. doi:10.12998/wjcc.v2.i3.67

29. Dobrzynska A, Gonzalo S, Shanahan C, Askjaer P. The nuclear lamina in health and disease. *Nucleus*. 2016;7(3):233-248. doi:10.1080/19491034.2016.1183848

30. Lee MS, Craigie R. Protection of retroviral DNA from autointegration: Involvement of a cellular factor. *Proc Natl Acad Sci U S A*. 1994;91(21):9823-9827. doi:10.1073/pnas.91.21.9823

31. Lee MS, Craigie R. A previously unidentified host protein protects retroviral DNA from autointegration. *Proc Natl Acad Sci U S A*. 1998;95(4):1528-1533. doi:10.1073/pnas.95.4.1528

32. Harris D, Engelman A. Both the structure and DNA binding function of the barrier-to-autointegration factor contribute to reconstitution of HIV type 1 integration in vitro. *J Biol Chem*. 2000;275(50):39671-39677. doi:10.1074/jbc.M002626200

33. Suzuki Y, Craigie R. Regulatory Mechanisms by Which Barrier-to-Autointegration Factor Blocks Autointegration and Stimulates Intermolecular Integration of Moloney Murine Leukemia Virus

Preintegration Complexes. *J Virol*. 2002;76(23):12376-12380. doi:10.1128/jvi.76.23.12376-12380.2002

34.   Lin C-W, Engelman A. The Barrier-to-Autointegration Factor Is a Component of Functional Human Immunodeficiency Virus Type 1 Preintegration Complexes. *J Virol*. 2003;77(8):5030-5036. doi:10.1128/jvi.77.8.5030-5036.2003

35.   Jacque JM, Stevenson M. The inner-nuclear-envelope protein emerin regulates HIV-1 infectivity. *Nature*. 2006;441(7093):641-645. doi:10.1038/nature04682

36.   Ibrahim N, Wicklund A, Jamin A, Wiebe MS. Barrier to autointegration factor (BAF) inhibits vaccinia virus intermediate transcription in the absence of the viral B1 kinase. *Virology*. 2013;444(1-2):363-373. doi:10.1016/j.virol.2013.07.002

37.   Ibrahim N, Wicklund A, Wiebe MS. Molecular Characterization of the Host Defense Activity of the Barrier to Autointegration Factor against Vaccinia Virus. *J Virol*. 2011;85(22):11588-11600. doi:10.1128/jvi.00641-11

38.   Jamin A, Wiebe MS. Barrier to Autointegration Factor (BANF1): Interwoven roles in nuclear structure, genome integrity, innate immunity, stress responses and progeria. *Curr Opin Cell Biol*. 2015. doi:10.1016/j.ceb.2015.05.006

39.   Mansharamani M, Graham DRM, Monie D, et al. Barrier-to-Autointegration Factor BAF Binds p55 Gagand Matrix and Is a Host Component of Human ImmunodeficiencyVirus Type 1Virions. *J Virol*. 2003;77(24):13084-13092. doi:10.1128/jvi.77.24.13084-13092.2003

40.   Bar DZ, Davidovich M, Lamm AT, Zer H, Wilson KL, Magin TM.

BAF-1 mobility is regulated by environmental stresses. *Mol Biol Cell*. 2014;25:1127-1136. doi:10.1091/mbc.E13-08-0477

41. Haraguchi T, Koujin T, Osakada H, et al. Nuclear localization of barrier-to-autointegration factor is correlated with progression of S phase in human cells. *J Cell Sci*. 2007;120(1967-1977). doi:10.1242/jcs.03461

42. Jamin A, Wicklund A, Wiebe MS. Cell-and Virus-Mediated Regulation of the Barrier-to-Autointegration Factor's Phosphorylation State Controls Its DNA Binding, Dimerization, Subcellular Localization, and Antipoxviral Activity. *J Virol*. 2014;88(10):5342-5355. doi:10.1128/JVI.00427-14

43. Segura-Totten M, Wilson KL. BAF: Roles in chromatin, nuclear structure and retrovirus integration. *Trends Cell Biol*. 2004. doi:10.1016/j.tcb.2004.03.004

44. Marcelot A, Petitalot A, Ropars V, et al. Di-phosphorylated BAF shows altered structural dynamics and binding to DNA , but interacts with its nuclear envelope partners. *Nucleic Acids Res*. 2021:1-15. doi:10.1093/nar/gkab184

45. Samson C, Petitalot A, Celli F, et al. Structural analysis of the ternary complex between lamin A/C, BAF and emerin identifies an interface disrupted in autosomal recessive progeroid diseases. *Nucleic Acids Res*. 2018;46(19):10460-10473. doi:10.1093/nar/gky736

46. Haraguchi T, Koujin T, Segura-Totten M, et al. BAF is required for emerin assembly into the reforming nuclear envelope. *J Cell Sci*. 2001;114(24):4575-4585.

47. Wang X, Xu S, Rivolta C, et al. Barrier to autointegration factor

interacts with the cone-rod homeobox and represses its transactivation function. *J Biol Chem*. 2002;277(45):43288-43300. doi:10.1074/jbc.M207952200

48.   Nili E, Cojocaru GS, Kalma Y, et al. Nuclear membrane protein LAP2β mediates transcriptional repression alone and together with its binding partner GCL (germ-cell-less). *J Cell Sci*. 2001;114(18):3297-3307.

49.   Montes De Oca R, Andreassen PR, Wilson KL. Barrier-to-Autointegration Factor influences specific histone modifications. *nucleus*. 2011;2(6):1-11. doi:10.4161/nucl.2.6.17960

50.   Montes De Oca R, Lee KK, Wilson KL. Binding of barrier to autointegration factor (BAF) to histone H3 and selected linker histones including H1.1. *J Biol Chem*. 2005;280(51):42252-42262. doi:10.1074/jbc.M509917200

51.   Bolderson E, Burgess JT, Li J, et al. Barrier-to-autointegration factor 1 (Banf1) regulates poly [ADP-ribose] polymerase 1 (PARP1) activity following oxidative DNA damage. *Nat Commun*. 2019;10(1):1-12. doi:10.1038/s41467-019-13167-5

52.   Tifft KE, Segura-Totten M, Lee KK, Wilson KL. Barrier-to-autointegration factor-like (BAF-L): A proposed regulator of BAF. *Exp Cell Res*. 2006;312(4):478-487. doi:10.1016/j.yexcr.2005.11.013

53.   Cai M, Huang Y, Suh JY, et al. Solution NMR structure of the barrier-to-autointegration factor-emerin complex. *J Biol Chem*. 2007;282(19):14525-14535. doi:10.1074/jbc.M700576200

54.   Lee KK, Haraguchi T, Lee RS, Koujin T, Hiraoka Y, Wilson KL. Distinct functional domains in emerin bind lamin A and DNA-

bridging protein BAF. *J Cell Sci*. 2001;114(24):4567-4573.

55.   Holaska JM, Lee KK, Kowalski AK, Wilson KL. Transcriptional repressor germ cell-less (GCL) and barrier to autointegration factor (BAF) compete for binding to emerin in vitro. *J Biol Chem*. 2003;278(9):6969-6975. doi:10.1074/jbc.M208811200

56.   Haraguchi T, Kojidani T, Koujin T, et al. Live cell imaging and electron microscopy reveal dynamic processes of BAF-directed nuclear envelope assembly. *J Cell Sci*. 2008;121(15):2540-2554. doi:10.1242/jcs.033597

57.   Shimi T, Koujin T, Segura-Totten M, Wilson KL, Haraguchi T, Hiraoka Y. Dynamic interaction between BAF and emerin revealed by FRAP, FLIP, and FRET analyses in living HeLa cells. *J Struct Biol*. 2004;147(1):31-41. doi:10.1016/j.jsb.2003.11.013

58.   Dechat T, Gajewski A, Korbei B, et al. LAP2α and BAF transiently localize to telomeres and specific regions on chromatin during nuclear assembly. *J Cell Sci*. 2004;117(25):6117-6128. doi:10.1242/jcs.01529

59.   Cai M, Huang Y, Ghirlando R, Wilson KL, Craigie R, Clore GM. Solution structure of the constant region of nuclear envelope protein LAP2 reveals two LEM-domain structures: One binds BAF and the other binds DNA. *EMBO J*. 2001;20(16):4399-4407. doi:10.1093/emboj/20.16.4399

60.   Shumaker DK, Lee KK, Tanhehco YC, Craigie R, Wilson KL. LAP2 binds to BAF·DNA complexes: Requirement for the LEM domain and modulation by variable regions. *EMBO J*. 2001;20(7):1754-1764. doi:10.1093/emboj/20.7.1754

61. Furukawa K. LAP2 binding protein 1 (L2BP1/BAF) is a candidate mediator of LAP2-chromatin interaction. *J Cell Sci*. 1999;112(15):2485-2492.

62. Mansharamani M, Wilson KL. Direct binding of nuclear membrane protein MAN1 to emerin in vitro and two modes of binding to barrier-to-autointegration factor. *J Biol Chem*. 2005;280(14):13863-13870. doi:10.1074/jbc.M413020200

63. Brachner A, Reipert S, Foisner R, Gotzmann J. LEM2 is a novel MAN1-related inner nuclear membrane protein associated with A-type lamins. *J Cell Sci*. 2005;118(24):5797-5810. doi:10.1242/jcs.02701

64. Brachner A, Braun J, Ghodgaonkar M, et al. The endonuclease Ankle1 requires its LEM and GIY-YIG motifs for DNA cleavage in vivo. *J Cell Sci*. 2012;125(4):1048-1057. doi:10.1242/jcs.098392

65. Asencio C, Davidson IF, Santarella-Mellwig R, et al. Coordination of kinase and phosphatase activities by Lem4 enables nuclear envelope reassembly during mitosis. *Cell*. 2012;150(1):122-135. doi:10.1016/j.cell.2012.04.043

66. Mamada H, Takahashi N, Taira M. Involvement of an inner nuclear membrane protein, Nemp1, in Xenopus neural development through an interaction with the chromatin protein BAF. *Dev Biol*. 2009;327(2):497-507. doi:10.1016/j.ydbio.2008.12.038

67. Montes de Oca R, Shoemaker CJ, Gucek M, Cole RN, Wilson KL. Barrier-to-autointegration factor proteome reveals chromatin-regulatory partners. *PLoS One*. 2009;4(9). doi:10.1371/journal.pone.0007050

68. Capanni C, Squarzoni S, Cenni V, et al. Familial partial lipodystrophy, mandibuloacral dysplasia and restrictive dermopathy feature barrier-to-autointegration factor (BAF) nuclear redistribution. *Cell Cycle*. 2012;11(19):3568-3577. doi:10.4161/cc.21869

69. Capanni C, Cenni V, Haraguchi T, et al. Lamin A precursor induces barrier-to-autointegration factor nuclear localization. *Cell Cycle*. 2010;9(13):2600-2610. doi:10.4161/cc.9.13.12080

70. Margalit A, Neufeld E, Feinstein N, Wilson KL, Podbilewicz B, Gruenbaum Y. Barrier to autointegration factor blocks premature cell fusion and maintains adult muscle integrity in C. elegans. *J Cell Biol*. 2007;178(4):661-673. doi:10.1083/jcb.200704049

71. Huang Y, Cai M, Clore GM, Craigie R. No interaction of barrier-to-autointegration factor (BAF) with HIV-1 MA, cone-rod homeobox (CRX) or MAN1-C in absence of DNA. *PLoS One*. 2011;6(9):2-7. doi:10.1371/journal.pone.0025123

72. Cox JL, Mallanna SK, Ormsbee BD, Desler M, Wiebe MS, Rizzino A. Banf1 is required to maintain the self-renewal of both mouse and human embryonic stem cells. *J Cell Sci*. 2011;124(15):2654-2665. doi:10.1242/jcs.083238

73. Nichols RJ, Wiebe MS, Traktman P. The Vaccinia-related Kinases Phosphorylate the N¯Terminus of BAF, Regulating Its Interaction with DNA and Its Retention in the Nucleus. *Mol Biol Cell*. 2006;17:2451-2464. doi:10.1091/mbc.E05–12–1179

74. Tyá S Gorjá Ná Cz M, Klerkx EP, Galy V, et al. Caenorhabditis elegans BAF-1 and its kinase VRK-1 participate directly in post-mitotic nuclear envelope assembly. *EMBO J*. 2007;26:132-143. doi:10.1038/sj.emboj.7601470

75. Molitor TP, Traktman P. Depletion of the protein kinase VRK1 disrupts nuclear envelope morphology and leads to BAF retention on mitotic chromosomes. *Mol Biol Cell*. 2014;25(6):891-903. doi:10.1091/mbc.E13-10-0603

76. Zhuang X, Semenova E, Maric D, Craigie R. Dephosphorylation of barrier-to-autointegration factor by protein phosphatase 4 and its role in cell mitosis. *J Biol Chem*. 2014;289(2):1119-1127. doi:10.1074/jbc.M113.492777

77. Sears RM, Roux KJ. Diverse cellular functions of barrier-to-autointegration factor and its roles in disease. *J Cell Sci*. 2020;133(16). doi:10.1242/jcs.246546

78. Umland TC, Wei SQ, Craigie R, Davies DR. Structural basis of DNA bridging by Barrier-to-autointegration factor. *Biochemistry*. 2000;39(31):9130-9138. doi:10.1021/bi000572w

79. Segura-Totten M, Kowalski AK, Craigie R, Wilson KL. Barrier-to-autointegration factor: Major roles in chromatin decondensation and nuclear assembly. *J Cell Biol*. 2002;158(3):475-485. doi:10.1083/jcb.200202019

80. Bradley CM, Ronning DR, Ghirlando R, Craigie R, Dyda F. Structural basis for DNA bridging by barrier-to-autointegration factor. *Nat Struct Mol Biol*. 2005;12(10):935-936. doi:10.1038/nsmb989

81. Skoko D, Li M, Huang Y, et al. Barrier-to-autointegration factor (BAF) condenses DNA by looping. *Proc Natl Acad Sci U S A*. 2009;106(39):16610-16615. doi:10.1073/pnas.0909077106

82. Samwer M, Schneider MWG, Hoefler R, et al. DNA Cross-Bridging Shapes a Single Nucleus from a Set of Mitotic

Chromosomes. *Cell*. 2017;170(5):956-972.e23. doi:10.1016/j.cell.2017.07.038

83. Cabanillas R, Cadiñanos J, Villameytide JAF, et al. Néstor-Guillermo progeria syndrome: A novel premature aging condition with early onset and chronic development caused by BANF1 mutations. *Am J Med Genet Part A*. 2011;155(11):2617-2625. doi:10.1002/ajmg.a.34249

84. Puente XS, Quesada V, Osorio FG, et al. Exome sequencing and functional analysis identifies BANF1 mutation as the cause of a hereditary progeroid syndrome. *Am J Hum Genet*. 2011;88(5):650-656. doi:10.1016/j.ajhg.2011.04.010

85. Paquet N, Box JK, Ashton NW, et al. Néstor-Guillermo Progeria Syndrome: A biochemical insight into Barrier-to-Autointegration Factor 1, alanine 12 threonine mutation. *BMC Mol Biol*. 2014;15(1):1-11. doi:10.1186/s12867-014-0027-z

86. Li J, Wang T, Pei L, et al. Expression of VRK1 and the downstream gene BANF1 in esophageal cancer. *Biomed Pharmacother*. 2017;89:1086-1091. doi:10.1016/j.biopha.2017.02.095

87. Li J, Hu B, Fang LEI, et al. Barrier-to-autointegration factor 1: A novel biomarker for gastric cancer. *Oncol Lett*. 2018;16(5):6488-6494. doi:10.3892/ol.2018.9432

88. Zhang G. Expression and prognostic significance of BANF1 in triple-negative breast cancer. *Cancer Manag Res*. 2020;12:145-150. doi:10.2147/CMAR.S229022

89. Furukawa K. Barrier-to-autointegration factor plays crucial roles in cell cycle progression and nuclear organization in Drosophila.

J Cell Sci. 2003;116(18):3811-3823. doi:10.1242/jcs.00682

90. Duan T, Kitzman SC, Geyer PK. Survival of Drosophila germline stem cells requires the chromatin-binding protein Barrier-to-autointegration factor. *Dev*. 2020;147(9). doi:10.1242/dev.186171

91. Lancaster OM, Cullen CF, Ohkura H. NHK-1 phosphorylates BAF to allow karyosome formation in the Drosophila oocyte nucleus. *J Cell Biol*. 2007. doi:10.1083/jcb.200706067

92. Torras-Llort M, Medina-Giró S, Escudero-Ferruz P, et al. A fraction of barrier-to-autointegration factor (BAF) associates with centromeres and controls mitosis progression. *Commun Biol*. 2020;3(1):1-13. doi:10.1038/s42003-020-01182-y

93. Makarova M, Oliferenko S. Mixing and matching nuclear envelope remodeling and spindle assembly strategies in the evolution of mitosis. *Curr Opin Cell Biol*. 2016;41:43-50. doi:10.1016/j.ceb.2016.03.016

94. De Magistris P, Antonin W. The Dynamic Nature of the Nuclear Envelope. *Curr Biol*. 2018;28(8):R487-R497. doi:10.1016/j.cub.2018.01.073

95. Katsani KaR, Karess RE, Dostatni N, Doye V. In Vivo Dynamics of Drosophila Nuclear Envelope Components. *Mol Biol Cell*. 2008;19(September):3652-3666. doi:10.1091/mbc.E07

96. Hayashi H, Kimura K, Kimura A. Localized accumulation of tubulin during semi-open mitosis in the Caenorhabditis elegans embryo. *Mol Biol Cell*. 2012;23(9):1688-1699. doi:10.1091/mbc.E11-09-0815

97. Moura M, Conde C. Phosphatases in Mitosis: Roles and

regulation. *Biomolecules*. 2019;9(2):1-51. doi:10.3390/biom9020055

98. Laurell E, Beck K, Krupina K, et al. Phosphorylation of Nup98 by Multiple Kinases Is Crucial for NPC Disassembly during Mitotic Entry. *Cell*. 2011;144(4):539-550. doi:10.1016/j.cell.2011.01.012

99. Foisner R, Gerace L. Integral Membrane Proteins of the Nuclear Envelope Interact with Lamins and Chromosomes , and Binding Is Modulated by Mitotic Phosphorylation. 1993;73:1267-1279. doi:10.1016/0092-8674(93)90355-t

100. Gerlich D, Daigle N, Eils R, Ellenberg J. Nuclear Envelope Breakdowns Proceeds by Microtubule-Induced Tearing of the Lamina. 2002;108:83-96.

101. Schlaitz A, Thompson J, Wong CCL, Iii JRY, Heald R. REEP3/4 Ensure Endoplasmic Reticulum Clearance from Metaphase Chromatin and Proper Nuclear Envelope Architecture. *Dev Cell*. 2013;26(3):315-323. doi:10.1016/j.devcel.2013.06.016

102. Anderson DJ, Vargas JD, Hsiao JP, Hetzer MW. Recruitment of functionally distinct membrane proteins to chromatin mediates nuclear envelope formation in vivo. 2009;186(2):183-191. doi:10.1083/jcb.200901106

103. Clever M, Mimura Y, Funakoshi T, Imamoto N. Regulation and coordination of nuclear envelope and nuclear pore complex assembly. *Nucleus*. 2013;4(2):105-114. doi:10.4161/nucl.23796

104. Schellhaus AK, De Magistris P, Antonin W. Nuclear Reformation at the End of Mitosis. *J Mol Biol*. 2016;428(10 Pt A):1962-1985. doi:10.1016/j.jmb.2015.09.016

105. Bengtsson L, Wilson KL. Barrier-to-Autointegration Factor

Phosphorylation on Ser-4 Regulates Emerin Binding to Lamin A In Vitro and Emerin Localization In Vivo. *Mol Biol Cell*. 2005. doi:10.1091/mbc.E05

106. Nasa I, Kettenbach AN. Coordination of protein kinase and phosphoprotein phosphatase activities in mitosis. *Front Cell Dev Biol*. 2018;6(MAR):1-14. doi:10.3389/fcell.2018.00030

107. Margalit A, Segura-Totten M, Gruenbaum Y, Wilson KL. Barrier-to-autointegration factor is required to segregate and enclose chromosomes within the nuclear envelope and assemble the nuclear lamina. *Proc Natl Acad Sci*. 2005;102(9):3290-3295. doi:10.1073/pnas.0408364102

108. Gorjánácz M. LEM-4 promotes rapid dephosphorylation of BAF during mitotic exit. *Nucleus*. 2013;4(1):14-17. doi:10.4161/nucl.22961

109. Mehsen H, Boudreau V, Garrido D, et al. PP2A-B55 promotes nuclear envelope reformation after mitosis in Drosophila. *J Cell Biol*. 2018;217(12):4106-4123. doi:10.1083/jcb.201804018

110. Halfmann CT, Sears RM, Katiyar A, et al. Repair of nuclear ruptures requires barrier-to-autointegration factor. *J Cell Biol*. 2019;218(7):2136-2149. doi:10.1083/jcb.201901116

111. Guo X, Ni J, Liang Z, Xue J, Fenech MF, Wang X. The molecular origins and pathophysiological consequences of micronuclei: New insights into an age-old problem. *Mutat Res - Rev Mutat Res*. 2019;779:1-35. doi:10.1016/j.mrrev.2018.11.001

112. Rao X, Zhang Y, Yi Q, et al. Multiple origins of spontaneously arising micronuclei in HeLa cells: Direct evidence from long-term

live cell imaging. *Mutat Res - Fundam Mol Mech Mutagen*. 2008;646(1-2):41-49. doi:10.1016/j.mrfmmm.2008.09.004

113. Liu S, Kwon M, Mannino M, et al. Nuclear envelope assembly defects link mitotic errors to chromothripsis. *Nature*. 2018;561(7724):551-555. doi:10.1038/s41586-018-0534-z

114. Ly P, Cleveland DW. Rebuilding Chromosomes After Catastrophe: Emerging Mechanisms of Chromothripsis. *Trends Cell Biol*. 2017;27(12):917-930. doi:10.1016/j.tcb.2017.08.005

115. Ly P, Brunner SF, Shoshani O, et al. Chromosome segregation errors generate a diverse spectrum of simple and complex genomic rearrangements. *Nat Genet*. 2019;51(4):705-715. doi:10.1038/s41588-019-0360-8

116. Stephens PJ, Greenman CD, Fu B, et al. Massive genomic rearrangement acquired in a single catastrophic event during cancer development. *Cell*. 2011;144(1):27-40. doi:10.1016/j.cell.2010.11.055

117. Moorhead GBG, Trinkle-Mulcahy L, Ulke-Lemée A. Emerging roles of nuclear protein phosphatases. *Nat Rev Mol Cell Biol*. 2007;8(3):234-244. doi:10.1038/nrm2126

118. Kataria M, Yamano H. Interplay between Phosphatases and the Anaphase-Promoting Complex/Cyclosome in Mitosis. *Cells*. 2019;8(8):1-33. doi:10.3390/cells8080814

119. McCloy RA, Parker BL, Rogers S, et al. Global Phosphoproteomic Mapping of Early Mitotic Exit in Human Cells Identifies Novel Substrate Dephosphorylation Motifs. *Mol Cell Proteomics*. 2015;14(8):2194-2212. doi:10.1074/mcp.m114.046938

120. Grallert A, Boke E, Hagting A, et al. A PP1-PP2A phosphatase relay controls mitotic progression. *Nature*. 2015;517(7532):94-98. doi:10.1038/nature14019

121. Chen F, Archambault V, Kar A, et al. Multiple Protein Phosphatases Are Required for Mitosis in Drosophila. *Curr Biol*. 2007;17(4):293-303. doi:10.1016/j.cub.2007.01.068

122. Trinkle-Mulcahy L, Andersen J, Yun WL, Moorhead G, Mann M, Lamond AI. Repo-Man recruits PP1γ to chromatin and is essential for cell viability. *J Cell Biol*. 2006;172(5):679-692. doi:10.1083/jcb.200508154

123. Nijenhuis W, Vallardi G, Teixeira A, Kops GJPL, Saurin AT. Negative feedback at kinetochores underlies a responsive spindle checkpoint signal. *Nat Cell Biol*. 2014;16(12):1257-1264. doi:10.1038/ncb3065

124. Yamashiro S, Yamakita Y, Totsukawa G, et al. Myosin phosphatase targeting subunit1 regulates mitosis by antagonizing polo-like kinase 1. *Dev Cell*. 2008;14(5):787-797. doi:10.1038/jid.2014.371

125. Wang W, Stukenberg PT, Brautigan DL. Phosphatase Inhibitor-2 Balances Protein Phosphatase 1 and Aurora B Kinase for Chromosome Segregation and Cytokinesis in Human Retinal Epithelial Cells. *Mol Biol Cell*. 2009;20(November):2673-2683. doi:10.1091/mbc.E08

126. Hendrickx A, Beullens M, Ceulemans H, et al. Docking Motif-Guided Mapping of the Interactome of Protein Phosphatase-1. *Chem Biol*. 2009;16(4):365-371. doi:10.1016/j.chembiol.2009.02.012

127. Nasa I, Rusin SF, Kettenbach AN, Moorhead GB. Aurora B opposes PP1 function in mitosis by phosphorylating the conserved PP1-binding RVxF motif in PP1 regulatory proteins. *Sci Signal*. 2018;11(530). doi:10.1126/scisignal.aai8669

128. Wu JQ, Guo JY, Tang W, et al. PP1-mediated dephosphorylation of phosphoproteins at mitotic exit is controlled by inhibitor-1 and PP1 phosphorylation. *Nat Cell Biol*. 2009;11(5):644-651. doi:10.1038/ncb1871

129. Wlodarchak N, Xing Y. PP2A as a master regulator of the cell cycle. *Biochem Mol Biol*. 2016;51(3):162-184. doi:10.3109/10409238.2016.1143913.PP2A

130. Mayer-Jaekel RE, Ohkura H, Gomes R, et al. The 55 kd regulatory subunit of Drosophila protein phosphatase 2A is required for anaphase. *Cell*. 1993;72(4):621-633. doi:10.1016/0092-8674(93)90080-A

131. Yu J, Fleming SL, Williams B, et al. Greatwall kinase: A nuclear protein required for proper chromosome condensation and mitotic progression in Drosophila. *J Cell Biol*. 2004;164(4):487-492. doi:10.1083/jcb.200310059

132. Mochida S, Maslen SL, Skehel M, Hunt T. Greatwall phosphorylates an inhibitor of protein phosphatase 2A that is essential for mitosis. *Science (80-)*. 2010;330(6011):1670-1673. doi:10.1126/science.1195689

133. Rangone H, Wegel E, Gatt MK, et al. Suppression of scant identifies endos as a substrate of greatwall kinase and a negative regulator of protein phosphatase 2a in mitosis. *PLoS Genet*. 2011;7(8). doi:10.1371/journal.pgen.1002225

134. Mochida S. PP1 inactivates Greatwall to release PP2A-B55 from mitotic confinement. *EMBO Rep*. 2015;16(11):1411-1412. doi:10.15252/embr.201541290

135. Castro A, Lorca T. Greatwall kinase at a glance. *J Cell Sci*. 2018;131(20):1-6. doi:10.1242/jcs.222364

136. Hégarat N, Vesely C, Vinod PK, et al. PP2A/B55 and Fcp1 Regulate Greatwall and Ensa Dephosphorylation during Mitotic Exit. *PLoS Genet*. 2014;10(1). doi:10.1371/journal.pgen.1004004

137. Mochida S. Regulation of α-endosulfine, an inhibitor of protein phosphatase 2A, by multisite phosphorylation. *FEBS J*. 2014;281(4):1159-1169. doi:10.1111/febs.12685

138. Heim A, Konietzny A, Mayer TU. Protein phosphatase 1 is essential for Greatwall inactivation at mitotic exit. *EMBO Rep*. 2015;16(11):1501-1510. doi:10.15252/embr.201540876

139. Cundell MJ, Hutter LH, Bastos RN, et al. A PP2A-B55 recognition signal controls substrate dephosphorylation kinetics during mitotic exit. *J Cell Biol*. 2016;214(5):539-554. doi:10.1083/jcb.201606033

140. Pereira G, Schiebel E. Mitotic exit: Determining the PP2A dephosphorylation program. *J Cell Biol*. 2016;214(5):499-501. doi:10.1083/JCB.201608019

141. Vallardi G, Allan LA, Crozier L, Saurin AT. Division of labour between pp2a-b56 isoforms at the centromere and kinetochore. *Elife*. 2019;8:1-25. doi:10.7554/eLife.42619

142. Hertz EPT, Kruse T, Davey NE, et al. A Conserved Motif Provides Binding Specificity to the PP2A-B56 Phosphatase. *Mol*

Cell. 2016;63:686-695. doi:10.1016/j.molcel.2016.06.024

143. Foley EA, Maldonado M, Kapoor TM. Formation of stable attachments between kinetochores and microtubules depends on the B56-PP2A phosphatase. *Nat Cell Biol*. 2011;13(10):1265-1271. doi:10.1038/ncb2327

144. Suijkerbuijk SJE, Vleugel M, Teixeira A, Kops GJPL. Integration of Kinase and Phosphatase Activities by BUBR1 Ensures Formation of Stable Kinetochore-Microtubule Attachments. *Dev Cell*. 2012;23(4):745-755. doi:10.1016/j.devcel.2012.09.005

145. Xu Z, Cetin B, Anger M, et al. Structure and Function of the PP2A-Shugoshin Interaction. *Mol Cell*. 2009;35(4):426-441. doi:10.1016/j.molcel.2009.06.031

146. Peterson FC, Volkman BF. Diversity of polyproline recognition by EVH1 domains. *Front Biosci*. 2009;14(3):833-846. doi:10.2741/3281

147. Ueki Y, Kruse T, Weisser MB, et al. A Consensus Binding Motif for the PP4 Protein Phosphatase. *Mol Cell*. 2019;76(6):953-964.e6. doi:10.1016/j.molcel.2019.08.029

148. Karman Z, Rethi-Nagy Z, Abraham E, et al. Novel perspectives of target-binding by the evolutionarily conserved PP4 phosphatase. *Open Biol*. 2020;10(12):200343. doi:10.1098/rsob.200343

149. Voss M, Campbell K, Saranzewa N, et al. Protein phosphatase 4 is phosphorylated and inactivated by Cdk in response to spindle toxins and interacts with γ-tubulin. *Cell Cycle*. 2013;12(17):2876-2887. doi:10.4161/cc.25919

150. Toyo-oka K, Mori D, Yano Y, et al. Protein phosphatase 4

catalytic subunit regulates Cdk1 activity and microtubule organization via NDEL1 dephosphorylation. *J Cell Biol*. 2008;180(6):1133-1147. doi:10.1083/jcb.200705148

151. Lipinszki Z, Lefevre S, Savoian MS, Singleton MR, Glover DM, Przewloka MR. Centromeric binding and activity of Protein Phosphatase 4. *Nat Commun*. 2015;6(5894). doi:10.1038/ncomms6894

152. Zeng K, Bastos RN, Barr FA, Gruneberg U. Protein phosphatase 6 regulates mitotic spindle formation by controlling the T-loop phosphorylation state of Aurora A bound to its activator TPX2. *J Cell Biol*. 2010;191(7):1315-1332. doi:10.1083/jcb.201008106

153. Kettenbach AN, Schlosser KA, Lyons SP, et al. Global assessment of its network dynamics reveals that the kinase Plk1 inhibits the phosphatase PP6 to promote Aurora A activity. *Sci Signal*. 2018;11(530):1-13. doi:10.1126/scisignal.aaq1441

154. Potapova T, Gorbsky GJ. The Consequences of Chromosome Segregation Errors in Mitosis and Meiosis. *Mol Divers Preserv Int*. 2017;6(12):1-33. doi:10.3390/biology6010012

155. Holland AJ, Cleveland DW. Boveri revisited: Chromosomal instability, aneuploidy and tumorigenesis. *Nat Rev Mol Cell Biol*. 2009;10(7):478-487. doi:10.1038/nrm2718.Boveri

156. McKinley KL, Cheeseman IM. The molecular basis for centromere identity and function. *Nat Rev Mol Cell Biol*. 2016;17(1):16-29. doi:10.1038/nrm.2015.5

157. Henikoff S, Ahmad K, Platero JS, Steensel B Van. Heterochromatic deposition of centromeric histone H3-like

proteins. *Proc Natl Acad Sci*. 2000;97(2):716-721. doi:10.1073/pnas.97.2.716

158. Sullivan BA, Blower MD, Karpen GH. Determining centromere identity: cyclical storeis and forking paths. *Nat Rev Genet*. 2001;2(August):584-596.

159. Torras-Llort M, Moreno-Moreno O, Azorín F. Focus on the centre: The role of chromatin on the regulation of centromere identity and function. *EMBO J*. 2009;28(16):2337-2348. doi:10.1038/emboj.2009.174

160. Moreno-Moreno O, Torras-Llort M, Azorín F. Variations on a nucleosome theme: The structural basis of centromere function. *BioEssays*. 2017;39(4):1-7. doi:10.1002/bies.201600241

161. Milks KJ, Moree B, Straight AF. Dissection of CENP-C–directed Centromere and Kinetochore Assembly. *Mol Biol Cell*. 2009;20:4246-5255. doi:10.1091/mbc.E09

162. Carroll CW, Milks KJ, Straight AF. Dual recognition of CENP-A nucleosomes is required for centromere assembly. *J Cell Biol*. 2010;189(7):1143-1155. doi:10.1083/jcb.201001013

163. Mellone BG, Grive KJ, Shteyn V, Bowers SR, Oderberg I, Karpen GH. Assembly of drosophila centromeric chromatin proteins during mitosis. *PLoS Genet*. 2011;7(5). doi:10.1371/journal.pgen.1002068

164. Chen CC, Mellone BG. Chromatin assembly: Journey to the CENter of the chromosome. *J Cell Biol*. 2016;214(1):13-24. doi:10.1083/jcb.201605005

165. Foltz DR, Jansen LET, Bailey AO, et al. Centromere-Specific Assembly of CENP-A Nucleosomes Is Mediated by HJURP.

Cell. 2009;137(3):472-484. doi:10.1016/j.cell.2009.02.039

166. Chen CC, Dechassa ML, Bettini E, et al. CAL1 is the Drosophila CENP-A assembly factor. *J Cell Biol*. 2014;204(3):313-329. doi:10.1083/jcb.201305036

167. Schalch T, Steiner FA. Structure of centromere chromatin: from nucleosome to chromosomal architecture. *Chromosoma*. 2017;126(4):443-455. doi:10.1007/s00412-016-0620-7

168. Allshire RC, Karpen GH. Epigenetic regulation of centromeric chromatin: Old dogs, new tricks? *Nat Rev Genet*. 2008;9(12):923-937. doi:10.1038/nrg2466

169. Rošić S, Erhardt S. No longer a nuisance: Long non-coding RNAs join CENP-A in epigenetic centromere regulation. *Cell Mol Life Sci*. 2016;73(7):1387-1398. doi:10.1007/s00018-015-2124-7

170. Rošić S, Köhler F, Erhardt S. Repetitive centromeric satellite RNA is essential for kinetochore formation and cell division. *J Cell Biol*. 2014. doi:10.1083/jcb.201404097

171. Gascoigne KE, Cheeseman IM. T time for point centromeres. *Nat Cell Biol*. 2012;14(6):559-561. doi:10.1038/ncb2509

172. V Mi-Sun Kwon, Tetsuya Hori, Masahiro Okada and TF, Department. CENP-C Is Involved in Chromosome Segregation, Mitotic Checkpoint Function, and Kinetochore Assembly. *Mol Biol Cell*. 2007;18(June):2155–2168. doi:10.1091/mbc.E07

173. Tanaka K, Li Chang H, Kagami A, Watanabe Y. CENP-C Functions as a Scaffold for Effectors with Essential Kinetochore Functions in Mitosis and Meiosis. *Dev Cell*. 2009;17(3):334-343. doi:10.1016/j.devcel.2009.08.004

174. Przewloka MR, Venkei Z, Bolanos-Garcia VM, Debski J, Dadlez M, Glover DM. CENP-C is a structural platform for kinetochore assembly. *Curr Biol*. 2011;21(5):399-405. doi:10.1016/j.cub.2011.02.005

175. Talbert PB, Bryson TD, Henikoff S. Adaptive evolution of centromere proteins in plants and animals. *J Biol*. 2004;3(18). doi:10.1186/jbiol11

176. Yang CH, Tomkiel J, Saitoh H, Johnson DH, Earnshaw WC. Identification of overlapping DNA-binding and centromere-targeting domains in the human kinetochore protein CENP-C. *Mol Cell Biol*. 1996;16(7):3576-3586. doi:10.1128/mcb.16.7.3576

177. Zhou X, Zheng F, Wang C, et al. Phosphorylation of CENP-C by Aurora B facilitates kinetochore attachment error correction in mitosis. *Proc Natl Acad Sci U S A*. 2017;114(50):E10667-E10676. doi:10.1073/pnas.1710506114

178. Watanabe R, Hara M, Okumura EI, et al. CDK1-mediated CENP-C phosphorylation modulates CENP-A binding and mitotic kinetochore localization. *J Cell Biol*. 2019;218(12):4042-4062. doi:10.1083/JCB.201907006

179. Varma D, Salmon ED. The KMN protein network – chief conductors of the kinetochore orchestra. *J Cell Sci*. 2012;125:5927-5936. doi:10.1242/jcs.093724

180. Hara M, Ariyoshi M, Okumura E, Hori T, Fukagawa T. Multiple phosphorylations control recruitment of the KMN network onto kinetochores. *Nat Cell Biol*. 2018;20(December). doi:10.1038/s41556-018-0230-0

181. Dorner D, Vlcek S, Foeger N, et al. Lamina-associated polypeptide 2α regulates cell cycle progression and differentiation via the retinoblastoma-E2F pathway. *J Cell Biol*. 2006;173(1):83-93. doi:10.1083/jcb.200511149

182. Lara-gonzalez P, Westhorpe FG. The Spindle Assembly Checkpoint. *Curr Biol*. 2012;22(22):R966-R980. doi:10.1016/j.cub.2012.10.006

183. Sacristan C, Kops GJPL. Joined at the hip: Kinetochores, microtubules, and spindle assembly checkpoint signaling. *Trends Cell Biol*. 2015;25(1):21-28. doi:10.1016/j.tcb.2014.08.006

184. Musacchio A, Salmon ED. The spindle-assembly checkpoint in space and time. *Nat Rev Mol Cell Biol*. 2007;8(5):379-393. doi:10.1038/nrm2163

185. Saurin AT. Kinase and Phosphatase Cross-Talk at the Kinetochore. *Front Cell Dev Biol*. 2018;6(June):1-23. doi:10.3389/fcell.2018.00062

186. Espert A, Uluocak P, Bastos RN, Mangat D, Graab P, Gruneberg U. PP2A-B56 opposes Mps1 phosphorylation of Knl1 and thereby promotes spindle assembly checkpoint silencing. *J Cell Biol*. 2014;206(7):833-842. doi:10.1083/jcb.201406109

187. Liu S, Pellman D. The coordination of nuclear envelope assembly and chromosome segregation in metazoans. *Nucleus*. 2020;11(1):35-52. doi:10.1080/19491034.2020.1742064

188. Afonso O, Matos I, Maiato H. Spatial control of the anaphase-telophase transition. *Cell Cycle*. 2014;13(19):2985-2986. doi:10.4161/15384101.2014.959853

189. Afonso O, Castellani CM, Cheeseman LP, et al. Spatiotemporal control of mitotic exit during anaphase by an aurora B-Cdk1 crosstalk. *Elife*. 2019;8:1-31. doi:10.7554/eLife.47646

190. Maiato H, Afonso O, Matos I. A chromosome separation checkpoint: A midzone Aurora B gradient mediates a chromosome separation checkpoint that regulates the anaphase-telophase transition. *BioEssays*. 2015;37(3):257-266. doi:10.1002/bies.201400140

191. Fuller BG, Lampson MA, Foley EA, et al. Midzone activation of aurora B in anaphase produces an intracellular phosphorylation gradient. *Nature*. 2008;453(7198):1132-1136. doi:10.1038/nature06923

192. Afonso O, Matos I, Pereira AJ, Aguiar P, Lampson MA, Maiato H. Feedback control of chromosome separation by a midzone Aurora B gradient. *Science (80-)*. 2014;345(6194):332-336. doi:10.1126/science.1251121

193. Norden C, Mendoza M, Dobbelaere J, Kotwaliwale C V., Biggins S, Barral Y. The NoCut Pathway Links Completion of Cytokinesis to Spindle Midzone Function to Prevent Chromosome Breakage. *Cell*. 2006;125(1):85-98. doi:10.1016/j.cell.2006.01.045

194. Steigemann P, Wurzenberger C, Schmitz MHA, et al. Aurora B-Mediated Abscission Checkpoint Protects against Tetraploidization. *Cell*. 2009;136(3):473-484. doi:10.1016/j.cell.2008.12.020

195. Ohta S, Wood L, Bukowski-Wills JC, Rappsilber J, Earnshaw WC. Building mitotic chromosomes. *Curr Opin Cell Biol*. 2011;23(1):114-121. doi:10.1016/j.ceb.2010.09.009

196. Yasuda Y, Maul GG. A nucleolar auto-antigen is part of a major chromosomal surface component. *Chromosoma*. 1990;99(2):152-160. doi:10.1007/BF01735332

197. Van Hooser AA, Yuh P, Heald R. The perichromosomal layer. *Chromosoma*. 2005;114(6):377-388. doi:10.1007/s00412-005-0021-9

198. Callaini G, Riparbelli MG, Cintorino M, et al. The proliferating cell marker monoclonal antibody Ki-67 recognizes specific antigens associated with the nuclear envelope of the early Drosophila embryo. *Biol Cell*. 1994;81(1):39-45. doi:10.1016/0248-4900(94)90053-1

199. Booth DG, Beckett AJ, Molina O, et al. 3D-CLEM Reveals that a Major Portion of Mitotic Chromosomes Is Not Chromatin. *Mol Cell*. 2016;64(4):790-802. doi:10.1016/j.molcel.2016.10.009

200. Whitfield ML, George LK, Grant GD, Perou CM. Common markers of proliferation. *Nat Rev Cancer*. 2006;6(2):99-106. doi:10.1038/nrc1802

201. Sobecki M, Mrouj K, Camasses A, et al. The cell proliferation antigen Ki-67 organises heterochromatin. *Elife*. 2016;5(MARCH2016):1-33. doi:10.7554/eLife.13722

202. Matheson TD, Kaufman PD. The p150N domain of Chromatin Assembly Factor-1 regulates Ki-67 accumulation on the mitotic pericrhomosomal layer. *Mol Biol Cell*. 2017;28(1):1-29. doi:10.1091/mbc.E16-09-0659

203. Booth DG, Takagi M, Sanchez-Pulido L, et al. Ki-67 is a PP1-interacting protein that organises the mitotic chromosome periphery. *Elife*. 2014;3:1-22. doi:10.7554/elife.01641

204. Takagi M, Ono T, Natsume T, et al. Ki-67 and condensins support the integrity of mitotic chromosomes through distinct mechanisms. *J Cell Sci*. 2018;131(6). doi:10.1242/jcs.212092

205. Takagi M, Natsume T, Kanemaki MT, Imamoto N. Perichromosomal protein Ki67 supports mitotic chromosome architecture. *Genes to Cells*. 2016;21(10):1113-1124. doi:10.1111/gtc.12420

206. Cuylen S, Blaukopf C, Politi AZ, et al. Ki-67 acts as a biological surfactant to disperse mitotic chromosomes. *Nature*. 2016;535(7611):308-312. doi:10.1038/nature18610

207. Cuylen-Haering S, Petrovic M, Hernandez-Armendariz A, et al. Chromosome clustering by Ki-67 excludes cytoplasm during nuclear assembly. *Nature*. 2020;587(7833):285-290. doi:10.1038/s41586-020-2672-3

208. Bonner AM, Hawley RS. A Nucleoporin at the Meiotic Kinetochore. *Dev Cell*. 2016;38(5):447-448. doi:10.1016/j.devcel.2016.08.018

209. Hattersley N, Cheerambathur D, Moyle M, et al. A Nucleoporin Docks Protein Phosphatase 1 to Direct Meiotic Chromosome Segregation and Nuclear Assembly. *Dev Cell*. 2016;38(5):463-477. doi:10.1016/j.devcel.2016.08.006.A

210. Gómez-saldivar G, Fernandez A, Hirano Y, Mauro M. Identification of Conserved MEL-28 / ELYS Domains with Essential Roles in Nuclear Assembly and Chromosome Segregation. 2016:1-27. doi:10.1371/journal.pgen.1006131

211. Hertz EPT, Nilsson J. Localization of PP2A-B56 to centromeres in Drosophila. *Cell Cycle*. 2017;16(15):1385-1386.

doi:10.1080/15384101.2017.1337986

212. Wurzenberger C, Gerlich DW. Phosphatases: Providing safe passage through mitotic exit. *Nat Rev Mol Cell Biol*. 2011;12(8):469-482. doi:10.1038/nrm3149

213. Nilsson J. Protein phosphatases in the regulation of mitosis. *J Cell Biol*. 2019;218(2):395-409. doi:10.1083/jcb.201809138

214. Schneider I. Cell lines derived from late embryonic stages of Drosophila melanogaster. *J Embryol Exp Morphol*. 1972;27(2):353-365. doi:10.1091/mbc.E16-09-0659

215. Xing Y, Xu Y, Chen Y, et al. Structure of Protein Phosphatase 2A Core Enzyme Bound to Tumor-Inducing Toxins. *Cell*. 2006;127(2):341-353. doi:10.1016/j.cell.2006.09.025

216. Song M, Zhang Y, Katzaroff AJ, Edgar BA, Buttitta L. Hunting complex differential gene interaction patterns across molecular contexts. *Nucleic Acids Res*. 2014;42(7):1-11. doi:10.1093/nar/gku086

ANNEX

COMMUNICATIONS BIOLOGY

ARTICLE

Check for updates

A fraction of barrier-to-autointegration factor (BAF) associates with centromeres and controls mitosis progression

Mònica Torras-Llort [1,2,6✉], Sònia Medina-Giró[1,2,6], Paula Escudero-Ferruz[1,2,6], Zoltan Lipinszki [3,4], Olga Moreno-Moreno[1,2], Zoltan Karman[3,4], Marcin R. Przewloka [5] & Fernando Azorín [1,2✉]

Barrier-to-Autointegration Factor (BAF) is a conserved nuclear envelope (NE) component that binds chromatin and helps its anchoring to the NE. Cycles of phosphorylation and dephosphorylation control BAF function. Entering mitosis, phosphorylation releases BAF from chromatin and facilitates NE-disassembly. At mitotic exit, PP2A-mediated dephosphorylation restores chromatin binding and nucleates NE-reassembly. Here, we show that in *Drosophila* a small fraction of BAF (cenBAF) associates with centromeres. We also find that PP4 phosphatase, which is recruited to centromeres by CENP-C, prevents phosphorylation and release of cenBAF during mitosis. cenBAF is necessary for proper centromere assembly and accurate chromosome segregation, being critical for mitosis progression. Disrupting cenBAF localization prevents PP2A inactivation in mitosis compromising global BAF phosphorylation, which in turn leads to its persistent association with chromatin, delays anaphase onset and causes NE defects. These results suggest that, together with PP4 and CENP-C, cenBAF forms a centromere-based mechanism that controls chromosome segregation and mitosis progression.

[1] Institute of Molecular Biology of Barcelona, CSIC, Barcelona, Spain. [2] Institute for Research in Biomedicine (IRB Barcelona), The Barcelona Institute of Science and Technology, Barcelona, Spain. [3] MTA SZBK Lendület Laboratory of Cell Cycle Regulation and Institute of Biochemistry, Biological Research Centre, Szeged, Hungary. [4] Doctoral School of Biology, Faculty of Science and Informatics, University of Szeged, Szeged, Hungary. [5] School of Biological Sciences, Institute for Life Sciences, University of Southampton, Southampton SO17 1BJ, UK. [6] These authors contributed equally: Mònica Torras-Llort, Sònia Medina-Giró, Paula Escudero-Ferruz. ✉email: mtlbmc@ibmb.csic.es; fambmc@ibmb.csic.es

C ell division involves major architectural rearrangements. Metazoa generally undergo open mitosis, which implies that the nuclear envelope (NE) disassembles at prometaphase and reassembles in telophase, after chromosome segregation is completed. A principal player in the regulation of NE dynamics during mitosis is barrier-to-autointegration factor (BAF)[1–7]. BAF is an essential 10 kDa chromatin-binding protein that is highly conserved in metazoan, being involved in multiple pathways including nuclear envelope reassembly (NER), chromatin epigenetics, DNA damage response, and defense against viral DNA infection (reviewed in ref. [8]). Of great importance for its role in the regulation of NE dynamics, BAF interacts with the LEM-domain containing proteins LAP2, EMERIN, and MAN1[9–15] that, together with lamins, form the nuclear lamina (reviewed in ref. [16]). These interactions help anchoring chromatin to the NE in interphase and, in late mitosis, are essential for the recruitment of membranes to the ensemble of decondensing chromosomes[1,2,4]. A still poorly understood contribution of BAF to chromosome segregation has also been reported, since loss of BAF leads to strong chromosome segregation defects and high embryonic lethality in both *C. elegans* and *Drosophila*[1,2,17].

Phosphorylation plays a key role in regulating BAF localization and function. The mitotic kinase VRK1/NHK1 phosphorylates BAF in mitosis and meiosis[1,18–20]. This phosphorylation weakens the binding of BAF to both chromatin and the LEM-domain proteins[21], and is required for NE disassembly[1,22]. BAF plays also a crucial role in postmitotic NER[1–7]. At mitotic exit, BAF is dephosphorylated and reassociates with chromatin and the LEM-domain proteins, concentrating at the "core region" that surrounds the bulk of decondensing chromosomes, where its mobility and the mobility of the LEM-domain proteins decrease[3], and nucleates NER. Two protein phosphatases, PP2A and PP4, have been shown to dephosphorylate BAF in different species[5,6,23]. In *C. elegans* and HeLa cells, PP2A is targeted to BAF by the LEM-domain protein Ankle2/LEM4, which is required for BAF dephosphorylation[5]. Ankle2/LEM4 also associates with VRK1/NHK1 and inhibits its activity, which enhances BAF dephosphorylation[5]. PP2A-mediated BAF dephosphorylation regulates BAF reassociation with chromatin at mitotic exit and is required for NER[5,6]. PP4 has also been shown to regulate BAF dephosphorylation during mitosis in HEK293 cells[23].

Here we show that in *Drosophila* BAF is also a centromere-associated protein that is required for proper centromere assembly and function. Centromeric BAF (cenBAF) localization depends on the PP4 regulatory subunit Falafel (Flfl), which is recruited to centromeres by the constitutive centromeric protein CENP-C[24]. Our results suggest that, together with PP4/Flfl and CENP-C, cenBAF forms a centromeric network that controls phosphorylation and association with chromatin of the bulk of BAF, and regulates mitosis progression.

Results

BAF associates with centromeres. Others and we identified BAF amongst the proteins co-purifying with centromeric chromatin enriched in the histone H3 variant CENP-A^CID[25] (Supplementary Table 1) (see also "Methods" section). BAF also co-purified with canonical H3 containing chromatin[25] and its binding to bulk chromatin has been reported[26,27]. Indeed, in interphase cells, we observed that BAF preferentially associated with heterochromatin, since it strongly co-localized with the heterochromatic HP1a variant (Fig. 1a, left), being largely excluded from regions enriched in the euchromatic HP1c isoform (Fig. 1a, center). However, unexpectedly, in metaphase chromosomes, BAF strongly overlapped with the constitutive centromeric protein

CENP-C (Fig. 1b; see also Fig. 4d, e), suggesting that, in mitosis, chromosomal BAF localization was restricted to centromeres. The αBAF immunostaining detected in both interphase cells and metaphase chromosomes was specific, since it strongly decreased upon RNAi-mediated depletion of BAF (Supplementary Fig. 1). Chromatin fibers analysis confirmed centromeric localization of BAF since we detected BAF in ~80% of CENP-C-containing regions ($N = 38$) (one-tailed binomial test, p-value < 0.001) (Fig. 1c). This strong co-localization suggests that BAF localizes at centromeres also in interphase since mitotic cells accounted only for <5% of the total cells used in these analyses.

Co-immunoprecipitation experiments were consistent with the association of BAF with centromeres since αBAF antibodies immunoprecipitated CENP-C (Fig. 1d, left) and, vice versa, αCENP-C antibodies immunoprecipitated BAF (Fig. 1d, right). This interaction was resistant to treatment of the extract with DNAse I prior to immunoprecipitation (Supplementary Fig. 2a, b), suggesting that it was not mediated by chromatin binding. Along the same lines, we did not detect co-immunoprecipitation with the centromeric H3 variant CENP-A^CID, which is an intrinsic structural component of the nucleosome and, hence, is tightly bound to centromeric chromatin. Endogenous CENP-A^CID was difficult to detect by WB in co-IP experiments. Thus, for these experiments, we used a stable S2 cell line expressing a CENP-A^CID::YFP fusion protein that showed strong centromeric localization (Supplementary Fig. 2c). We observed that αBAF antibodies did not immunoprecipitate CENP-A^CID::YFP (Supplementary Fig. 2d, lane 4) and, similarly, neither BAF nor CENP-C could be immunoprecipitated with αGFP (Supplementary Fig. 2d, lane 3). The lack of CENP-C co-immunoprecipitation with CENP-A^CID has been previously reported[28].

Altogether these results suggest that a fraction of BAF (cenBAF) stays associated with centromeres throughout the cell cycle.

BAF is required for functional centromere assembly. We observed that depletion of BAF decreased centromeric CENP-C and CENP-A^CID levels in both metaphase chromosomes (Fig. 2a–c) and interphase cells (Supplementary Fig. 3a, b). We observed that reduction of CENP-A^CID levels was markedly weaker than that observed for CENP-C (Fig. 2c and Supplementary Fig. 3b), suggesting that BAF primarily affects centromeric CENP-C levels. Along the same lines, we observed that expression of a BAF::YFP construct decreased CENP-C levels, without significantly affecting centromeric CENP-A^CID levels (Kruskal–Wallis test, p-value = 0.215) (Supplementary Fig. 3c, d). Localization of BAF::YFP largely mimicked the pattern of immunolocalization of endogenous BAF since, in interphase cells, BAF::YFP overlapped with HP1a (Supplementary Fig. 4a), while it localized at centromeric regions in metaphase chromosomes (Supplementary Fig. 4b, c) and strongly overlapped with CENP-C in chromatin fibers (64%; $N = 37$) (one-tailed binomial test, p-value < 0.05) (Supplementary Fig. 4d). However, in contrast to endogenous BAF, BAF::YFP localization in metaphase chromosomes extended to pericentromeric heterochromatin (Supplementary Fig. 4c). Genetic analysis showed that BAF::YFP acts as a dominant negative mutation. In these experiments, *baf^RNAi* knockdown flies, which carry a UAS_GAL4-construct expressing a synthetic hairpin from the *baf*-coding region, were crossed to *nub*-GAL4 flies to specifically induced BAF depletion in the pouch region of wing imaginal disks. BAF depletion resulted in a strong wing phenotype in adult flies (Supplementary Fig. 3e, bottom left panel). This phenotype was partially rescued by expression of RNAi-resistant untagged BAF^R (Supplementary Fig. 3e, bottom center panel), but not by expression of an RNAi-resistant BAF::YFP^R construct (Supplementary Fig. 3e, bottom right
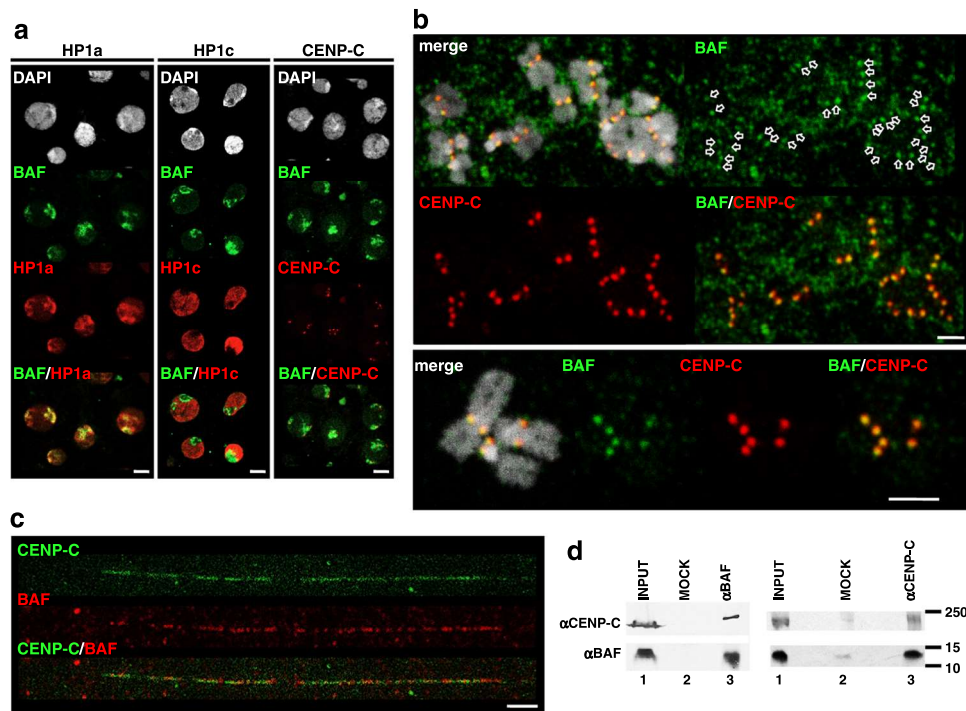
Fig. 1 BAF associates with the centromere. a The patterns of immunolocalization with αBAF antibodies (green), and αHP1a (left), αHP1c (center), and αCENP-C (right) antibodies (red) are presented in interphase S2 cells. DNA was stained with DAPI. Scale bars correspond to 5 µm. **b** The patterns of immunolocalization with αBAF (green) and αCENP-C (red) antibodies are presented in metaphase chromosomes from S2 cells. Enlarged images are presented in the bottom. Arrows indicate αBAF signals that overlap with αCENP-C signals at centromeres. DNA was stained with DAPI. Scale bars correspond to 2.5 µm. **c** Immunostainings with αBAF (red) and αCENP-C (green) antibodies are presented in extended chromatin fibers prepared from S2 cells. Scale bar corresponds to 5 µm. **d** BAF/CENP-C co-immunoprecipitation. IPs were performed with αBAF or αCENP-C antibodies (lanes 3) and control preimmune serum (MOCK) (lanes 2) using S2 cells extracts. IP-materials were analyzed by WB using αCENP-C and αBAF antibodies. Lanes 1 correspond to 3% of the input material. The position of MW markers (in kDa) is indicated.

panel). Moreover, while overexpression of untagged BAF caused no detectable wing defects (Supplementary Fig. 3e, top center panel), overexpression of BAF::YFP in control wild-type flies mimicked the loss-of-function phenotype observed upon BAF depletion (Supplementary Fig. 3e, top right panel). In this regard, we observed that expression of BAF::YFP strongly reduced the levels of endogenous BAF, whereas several other chromosomal proteins were not affected (i.e., CENP-C, CENP-A^{CID}, HP1a) (Supplementary Fig. 3f). On the other hand, as discussed below, BAF::YFP showed an aberrant pattern of phosphorylation (Supplementary Fig. 5b). Impaired phosphorylation is likely affecting BAF::YFP function since phosphorylation regulates binding of BAF to both chromatin and the LEM-domain proteins[21]. Hence, the negative dominant character of BAF::YFP is likely associated with destabilization and replacement of endogenous BAF by a non-functional BAF::YFP form of altered chromatin-binding dynamics due to abnormal phosphorylation.

CENP-A^{CID} and CENP-C are conserved constitutive centromeric proteins that are essential for centromere/kinetochore assembly and chromosome segregation (reviewed in ref. [29]). Hence, their decrease upon BAF depletion suggest a contribution of BAF to centromere function. Consistent with this hypothesis, depletion of BAF increased the frequency of chromosome segregation defects (Fig. 2d, e). In particular, the frequency of mitoses showing misaligned metaphase chromosomes strongly increased from ~7% in control dsRNA^{LacZ} cells to ~31% in BAF-depleted cells (Fig. 2e). The frequency of anaphase chromatin bridges and lagging chromosomes also increased, though to a lesser extent (Fig. 2e). Expression of the dominant negative BAF::YFP form also induced strong segregation defects (~86%) ($N = 14$; two-tailed Fisher's test, p-value < 0.0001) (Supplementary Fig. 3g). These results are in agreement with previous reports showing a

high incidence of chromosome segregation defects upon BAF depletion in *C. elegans*[1,2] and in *baf* null mutant flies[17].

Altogether these observations suggest that BAF stabilizes centromeric association of the essential centromeric components CENP-A^{CID} and CENP-C and, thus, it is required for accurate chromosome segregation.

cenBAF localization depends on PP4 phosphatase. It has been shown that BAF is phosphorylated at mitosis by the mitotic kinase VRK1/NHK1[1,5,19,20]. Phos-tag gel electrophoretic analyses confirmed BAF phosphorylation since we detected mono-(1pBAF) and di-phosphorylated (2pBAF) BAF species that migrated slower than non-phosphorylated BAF and were sensitive to treatment with alkaline phosphatase (AP) (Supplementary Fig. 5a). VRK1/NHK1 overexpression increased the proportion of 2pBAF, whereas VRK1/NHK1 depletion increased non-phosphorylated BAF (Supplementary Fig. 5a). Previous studies showed that, at mitosis, phosphorylation resolves the interaction of BAF with chromatin as well as with the NE LEM-domain proteins[1,5,19,20]. In this regard, we observed that mitotic spreads had high non-chromosomal αBAF reactivity (Fig. 1b and Supplementary Fig. 1b, top panel), which likely reflects the bulk of free pBAF that exists during mitosis since this background was strongly reduced upon BAF depletion (Supplementary Fig. 1b, bottom panel). Noteworthy, the dominant negative BAF::YFP form showed an aberrant phosphorylation pattern (Supplementary Fig. 5b), suggesting that it was not properly phosphorylated by VRK1/NHK1. Impaired VRK1/NHK1 phosphorylation is likely responsible for the persistent binding of BAF::YFP to heterochromatin observed in mitosis (Supplementary Fig. 4c).
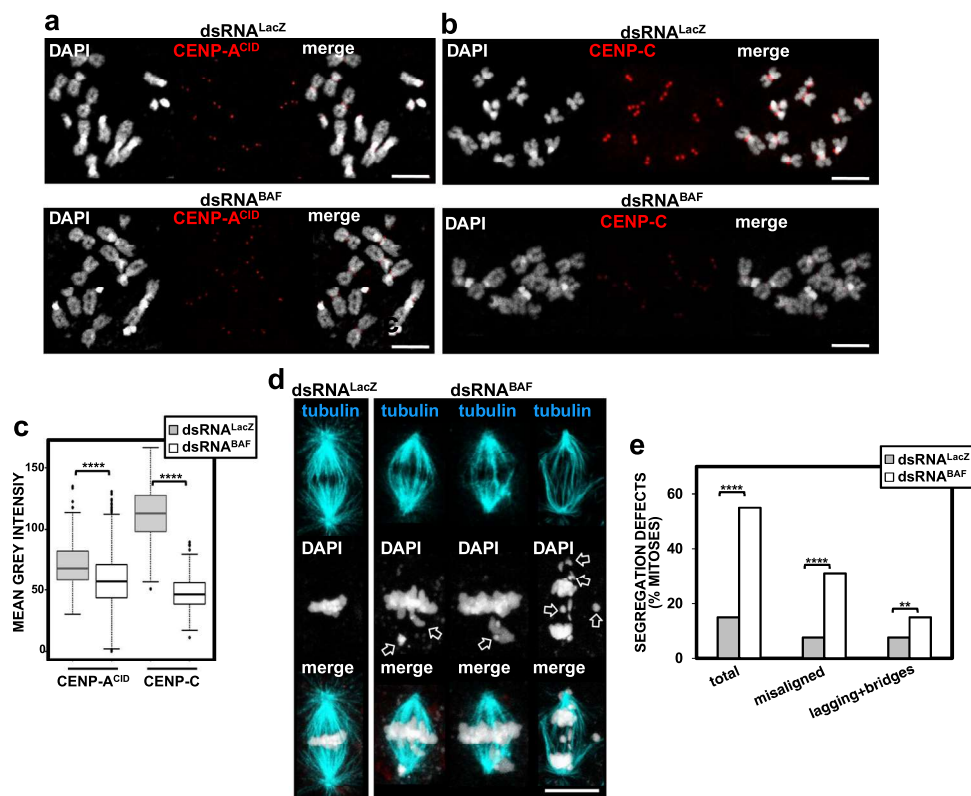
Fig. 2 BAF depletion impairs centromere assembly and chromosome segregation. a and **b** The patterns of immunolocalization with αCENP-A[CID] **a** and αCENP-C **b** antibodies (red) are presented in metaphase chromosomes from S2 cells upon RNAi-mediated depletion of BAF (dsRNA[BAF]) and in control cells treated with dsRNA against LacZ (dsRNA[LacZ]). DNA was stained with DAPI. Scale bars correspond to 5 μm. **c** Quantitative analyses of the results shown in **a** and **b**. The mean grey values per centromere of αCENP-A[CID] and αCENP-C fluorescence are shown for dsRNA[BAF] and control dsRNA[LacZ] cells. Values correspond to a representative experiment out of five independent experiments showing equivalent results ($N > 382$; Kruskal–Wallis test, ****p-value < 0.0001. **d** Metaphase figures from dsRNA[BAF] and control dsRNA[LacZ] cells. The spindle was stained with αTubulin antibodies (blue). DNA was stained with DAPI. Arrows indicate chromosome segregation defects (metaphase misalignment, lagging and fragmented chromosomes, and chromatin bridges). Scale bar corresponds to 5 μm. **e** The percentages of mitoses showing segregation defects are presented for dsRNA[BAF] and control dsRNA[LacZ] cells. Results are presented for total defects, misaligned metaphase chromosomes, and anaphase chromatin bridges and lagging chromosomes. Values are the sum of two independent experiments showing equivalent results ($N > 104$; two-tailed Fisher's test, **p < 0.01, ****p < 0.0001).

In light of these observations, we hypothesized that the fraction of BAF that remained bound to centromeres during mitosis was likely non-phosphorylated. In this regard, protein phosphatase 4 (PP4), which has been previously shown to regulate BAF phosphorylation[23], is known to associate with centromeres through the interaction of its conserved regulatory 3 subunit, Flfl, with CENP-C[24]. A short sequence-motif in CENP-C (Falafel Interacting Motif (FIM)) mediates this interaction[24]. Notably, deletion of this motif, which disrupts binding of PP4 to centromeres[24], strongly reduced the levels of centromeric BAF (cenBAF). In these experiments, stable cell lines expressing RNAi-resistant GFP-tagged CENP-C constructs, lacking the FIM motif (GFP::CENP-CΔFIM[R]) or not (GFP::CENP-C[R]), were subjected to depletion of endogenous CENP-C that did not affect centromeric localization of the RNAi-resistant constructs (Fig. 3a). Upon depletion of endogenous CENP-C, Flfl recruitment to centromeres was impaired in cells expressing GFP::CENP-CΔFIM[R24] (Supplementary Fig. 6a, center and b) and, concomitantly, we observed that cenBAF levels were strongly reduced as determined by both IF (Fig. 3a, b) and co-IP experiments (Fig. 3c, d). As expected, in control GFP::CENP-C[R]-expressing cells, depletion of endogenous CENP-C did not affect Flfl recruitment to centromeres (two-tailed Fischer's test, p-value = 0.58) (Supplementary Fig. 6a, left and b) and, consequently, cenBAF levels were not significantly affected (Fig. 3a–d). In addition, we observed that Flfl depletion decreased

cenBAF levels (Supplementary Fig. 7c–f), without affecting total BAF levels (Supplementary Fig. 7a, b). These results suggest that PP4 is required for centromeric localization of cenBAF.

We also analyzed localization of FLAG::BAF phosphomutants, in which the three putative VRK1/NHK1 phosphorylation sites (S2, T4, and S5)[18–20,23] were mutated to A (phosphonull) and E (phosphomimetic) (Supplementary Fig. 5c, d). As expected, we observed that the phosphomimetic FLAG::BAF3E construct was not binding chromosomes ($N = 238$) (Fig. 3e), while the phosphonull FLAG::BAF3A mutant showed persistent binding to chromosomes in mitosis (Fig. 3f). Noteworthy, although FLAG::BAF3A was generally binding across the entire chromosome (Fig. 3f, left), we observed that its localization was restricted to centromeres in ~15% of the mitoses ($N = 123$) (two-tailed binomial test, p-value < 0.0001) (Fig. 3f, right), which is consistent with cenBAF not being phosphorylated. In addition, BAF phosphorylation impaired BAF/CENP-C co-immunoprecipitation, since VRK1/NHK1 overexpression decreased co-immunoprecipitation of CENP-C with αBAF, whereas VRK1/NHK1 depletion increased it (Fig. 3g, h). Altogether these results suggest that, during mitosis, cenBAF is maintained non-phosphorylated by the action of PP4.

cenBAF prevents PP2A-dependent BAF dephosphorylation. Normally, in mitosis, the bulk of BAF stays phosphorylated and
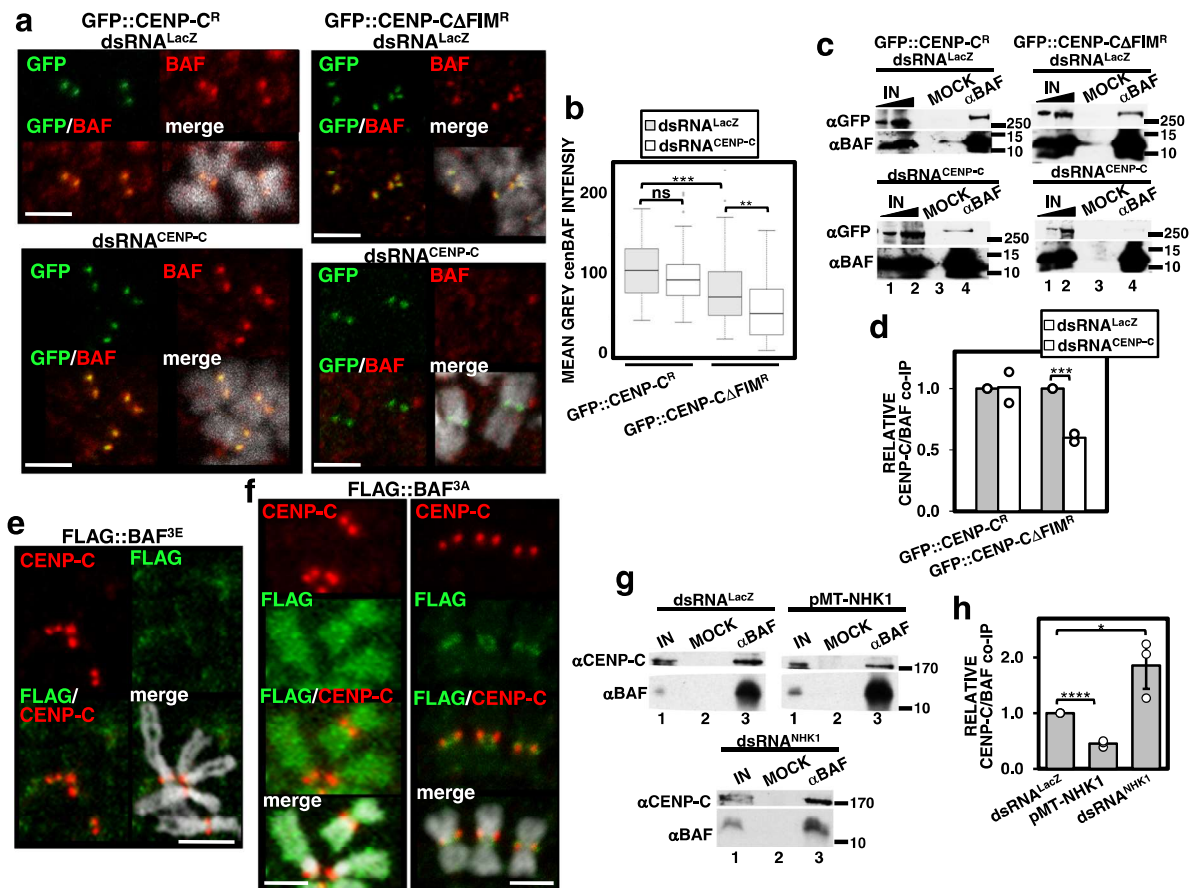
Fig. 3 Centromeric cenBAF localization depends on FIfl. a Immunostainings with αBAF antibodies (red) are presented in cells expressing GFP::CENP-C[R] (left) and GFP::CENP-CΔFIM[R] (right) upon CENP-C depletion (dsRNA[CENP-C]) and in control dsRNA[LacZ] cells. GFP signals are direct fluorescence. DNA was stained with DAPI. Scale bars are 2.5 μm. **b** Quantitative analysis of the results shown in **a**. Mean grey values per centromere of αBAF fluorescence are presented for control dsRNA[LacZ] and dsRNA[CENP-C] cells expressing the indicated constructs. Values correspond to a representative experiment out of five independent experiments showing equivalent results ($N > 48$; Kruskal–Wallis test, p-value: ns > 0.05, **$p < 0.01$, ***$p < 0.001$). **c** co-IP experiments with αBAF antibodies in extracts from control dsRNA[LacZ] and dsRNA[CENP-C] cells expressing GFP::CENP-C[R] (left) and GFP::CENP-CΔFIM[R] (right) (lanes 4). Lanes 3 are mock IPs with preimmune serum. Lanes 1 and 2 are 2% and 5% of the input, respectively. IPs were analyzed by WB using αGFP and αBAF antibodies. The position of MW markers (in kDa) is indicated. **d** Quantitative analysis of the results shown in **c**. The ratio of αCENP-C and αBAF signals normalized with respect to the corresponding control dsRNA[LacZ] cells is presented for dsRNA[CENP-C] cells expressing the indicated constructs. Results are the average of two independent experiments (two-tailed t-test, ***p-value < 0.001). **e** Immunostaining with αFLAG antibodies (green) in metaphase chromosomes from cells transiently expressing FLAG::BAF[3E]. Immunostaining with αCENP-C antibodies (red) is also presented. DNA was stained with DAPI. Scale bar is 5 μm. **f** As in **e** but for cells transiently expressing FLAG::BAF[3A]. **g** co-IP experiments with αBAF antibodies in extracts from control dsRNA[LacZ] cells, VRK1/NHK1-depleted dsRNA[NHK1] cells and pMT-NHK1 cells overexpressing VRK1/NHK1 (lanes 3). Lanes 2 are mock IPs with preimmune serum. Lanes 1 correspond to 3% of the input. IPs were analyzed by WB using αCENP-C and αBAF antibodies. The position of MW markers (in kDa) is indicated. **h** Quantitative analyses of the results shown in **g**. The ratio of αCENP-C and αBAF signals normalized respect to control dsRNA[LacZ] cells is presented for pMT-NHK1 and dsRNA[NHK1] cells. Results are the average of three independent experiments (error bars are SD; two-tailed t-test, *$p < 0.05$, ****$p < 0.0001$).

free in the cytoplasm, reassociating with chromatin only after chromosomes start to decondense in telophase, an event that marks the formation of the "core region" and the initiation of NER[3,5–7]. However, we observed that, concomitant to decreased cenBAF, CENP-C depletion in GFP::CENP-CΔFIM[R]-expressing cells induced intense perichromosomal αBAF immunostaining in ~50% of the mitosis, which was infrequent when CENP-C depletion was performed in control GFP::CENP-C[R]-expressing cells (Fig. 4a, left and center, and 4b). WB analysis showed that total BAF levels did not change upon CENP-C depletion in both GFP::CENP-CΔFIM[R]-expressing cells and control GFP::CENP-C[R]-expressing cells (Supplementary Fig. 8). The presence of perichromosomal BAF correlated with the reduction of cenBAF since, in CENP-C-depleted GFP::CENP-CΔFIM[R]-expressing cells, mitoses showing perichromosomal αBAF immunostaining

had lower cenBAF levels than mitoses without perichromosomal BAF (Fig. 4c). We also observed that, in comparison to control GFP::CENP-C[R]-expressing cells, cells expressing GFP::CENP-CΔFIM[R] had reduced cenBAF levels even without depletion of endogenous CENP-C in control dsRNA[LacZ] cells (Fig. 3a, b) and, concomitantly, they showed increased perichromosomal BAF (Fig. 4b). Super-resolution microscopy analysis confirmed these results. In control CENP-C-depleted GFP::CENP-C[R]-expressing cells, the distribution of BAF was largely restricted to the centromere, showing a well-defined maximum that strongly overlapped with GFP::CENP-C (Fig. 4d, e). Instead, in CENP-C-depleted GFP::CENP-CΔFIM[R]-expressing cells, the distribution of BAF was radically different with the maximum in the perichromosomal layer surrounding the chromosome and a much-reduced overlapping with CENP-C at the centromere (Fig. 4f, g).
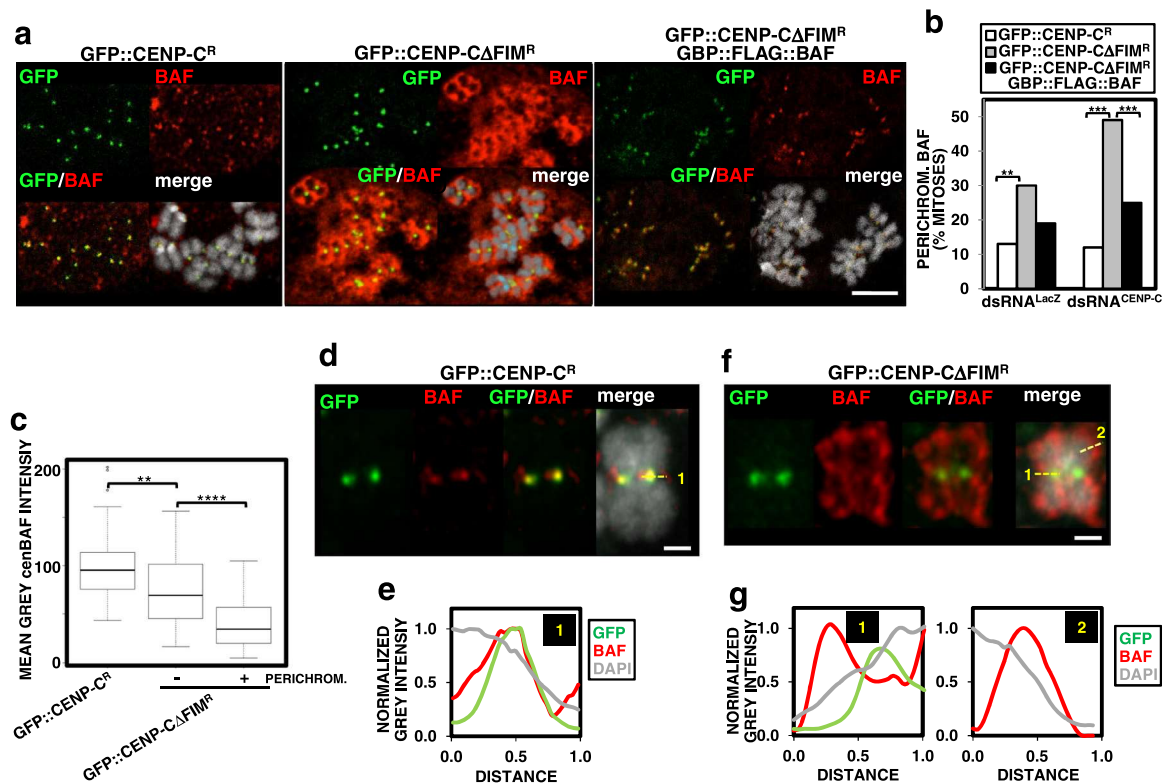
Fig. 4 cenBAF prevents the accumulation of perichromosomal BAF in mitosis. a The patterns of immunolocalization with αBAF antibodies (red) are presented in dsRNA[CENP-C] cells expressing the indicated constructs. GFP signals are direct fluorescence (green). DNA was stained with DAPI. Scale bar corresponds to 5 μm. **b** The percentages of mitoses showing perichromosomal BAF are presented for control dsRNA[LacZ] and dsRNA[CENP-C] cells expressing the indicated constructs. Values correspond to the sum of 3-4 independent experiments showing equivalent results ($N > 73$; two-tailed Fischer's test, $**p < 0.01$, $***p < 0.001$). **c** The mean grey values per centromere of αBAF fluorescence are presented for dsRNA[CENP-C] cells expressing GFP::CENP-C[R] (left) and dsRNA[CENP-C] cells expressing GFP::CENP-CΔFIM[R] showing perichromosomal BAF (right) or not (center). Values correspond to a representative experiment out of five independent experiments showing equivalent results ($N > 33$; Kruskal–Wallis test, $**p < 0.01$, $****p < 0.0001$). **d** Super-resolution microscopy analysis of a representative chromosome from dsRNA[CENP-C] cells expressing GFP::CENP-C[R]. The pattern of immunolocalization with αBAF antibodies is shown in red. GFP signals are direct fluorescence (green). DNA was stained with DAPI. Scale bar corresponds to 1 μm. **e** The profiles of αBAF (red), GFP (green), and DAPI (light grey) fluorescence along the line indicated in **d** are presented. Distance increases from left to right. **f** As in **d** but for a representative chromosome from dsRNA[CENP-C] cells expressing GFP::CENP-CΔFIM[R] showing perichromosomal BAF. **g** The profiles of αBAF (red), GFP (green), and DAPI (light grey) fluorescence along the lines indicated in **f** are presented. Distance increases from left to right.

Within this perichromosomal layer, BAF was in direct association with the chromosome, though the maximum BAF concentration was detected beyond its surface (Fig. 4g).

Results reported above suggest that disrupting cenBAF localization induces the accumulation of BAF in a perichromosomal layer that wraps around chromosomes in mitosis. This phenotype depends on cenBAF since constitutive targeting of BAF to centromeres prevents the accumulation of perichromosomal BAF. For these experiments, we used a GBP::FLAG::BAF construct that was tethered to centromeres by specifically recognizing the GFP-moiety of the GFP::CENP-C[R] and GFP::CENP-CΔFIM[R] constructs via the GFP-binding protein (GBP)[30] (Supplementary Fig. 9a, b). Importantly, expression of GBP::FLAG::BAF in control GFP::CENP-C[R]-expressing cells caused no detectable defects (Supplementary Fig. 9c–h). Notably, we observed that expression of GBP::FLAG::BAF in CENP-C-depleted GFP::CENP-CΔFIM[R]-expressing cells strongly reduced perichromosomal BAF (Fig. 4a, right and b). Expression of GBP::FLAG::BAF also tended to reduce perichromosomal BAF in control dsRNA[LacZ] GFP::CENP-CΔFIM[R]-expressing cells (two-tailed Fischer's test, p-value = 0.07) (Fig. 4b).

The association of BAF with chromatin is regulated by PP2A phosphatase that, at mitotic exit, dephosphorylates free pBAF and restores its binding to chromatin[1,5,6,20]. In this regard, we

observed that formation of the perichromosomal BAF layer depended on PP2A. In these experiments, we used Flfl-depleted cells that, similar to CENP-C-depleted GFP::CENP-CΔFIM[R]-expressing cells, showed impaired cenBAF localization (Supplementary Fig. 7c–f) and, consequently, high perichromosomal BAF (Fig. 5a, b). Depletion of the *Drosophila* PP2A catalytic subunit Microtubule star (MTS) in Flfl-depleted cells strongly reduced perichromosomal BAF (Fig. 5a, b), while, on the other hand, MTS depletion alone did not induce perichromosomal BAF (two-tailed Fischer's test, p-value = 0.86) (Fig. 5a, b). Note that MTS depletion was carried out for only 3 days since longer depletion times resulted in high cell death. In Flfl-depleted cells, MTS depletion was carried out simultaneously to Flfl-depletion during the last 3 days of the 6 days of treatment with dsRNA[Flfl] (see "Methods" section). The efficiency of the knockdowns was confirmed by WB (Supplementary Fig. 10). Altogether these results suggest that the accumulation of perichromosomal BAF observed when cenBAF localization is impaired involves dephosphorylation of free pBAF by PP2A in mitosis. Consistent with this, perichromosomal BAF was not reactive with an αBAFpS5 antibody (Fig. 5c, d), which specifically recognized pBAF (Supplementary Fig. 5e) (see "Methods" section).

Phos-tag gel electrophoresis analysis confirmed the role of PP2A in BAF dephosphorylation since MTS depletion
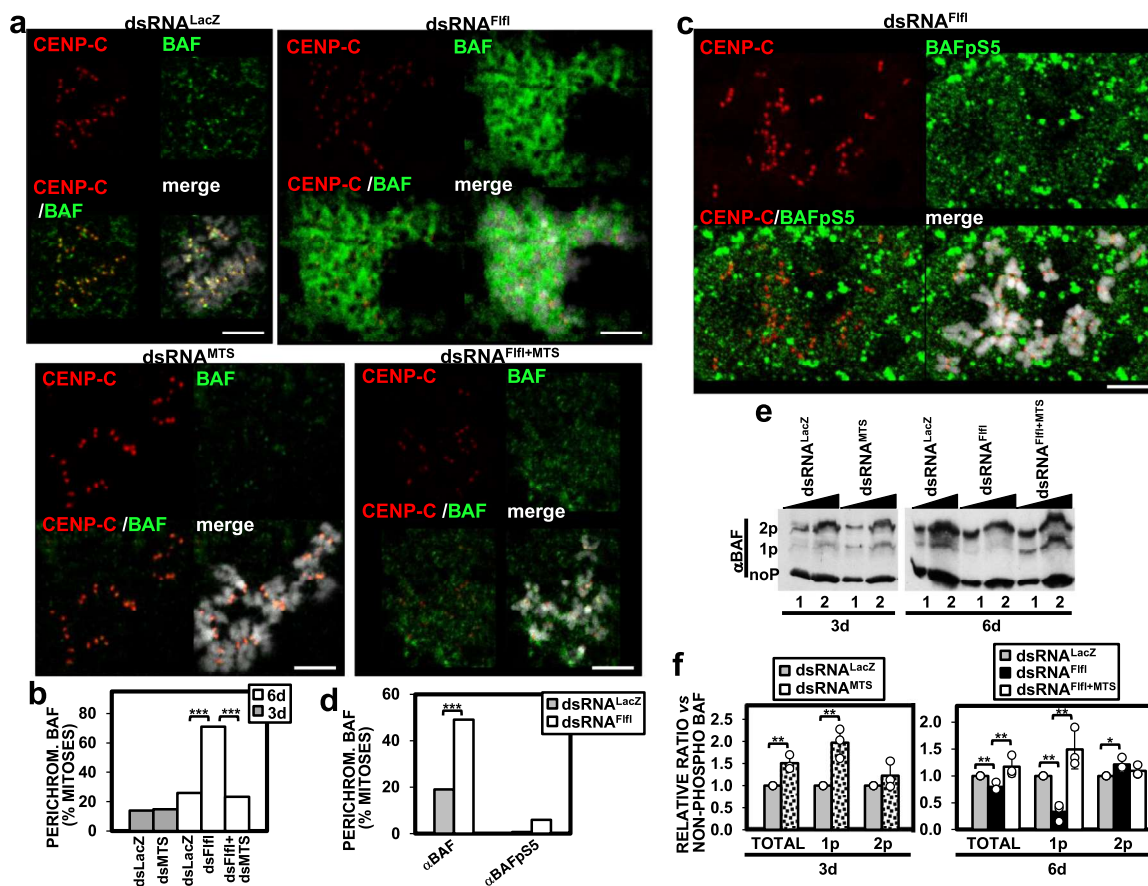
Fig. 5 Perichromosomal BAF requires PP2A-mediated dephosphorylation of pBAF. a The patterns of immunolocalization with αBAF (green) and αCENP-C (red) antibodies are presented for control dsRNA^{LacZ} cells and cells treated with dsRNA against Flfl (dsRNA^{Flfl}), MTS (dsRNA^{MTS}), and both Flfl and MTS (dsRNA$^{Flfl+MTS}$). DNA was stained with DAPI. Scale bars correspond to 5 μm. **b** The percentages of mitoses showing perichromosomal BAF are presented for the indicated RNAi-treated cells. Depletion was carried out for 3 or 6 days as indicated. Values are the sum of 5–9 independent experiments showing equivalent results ($N > 165$; two-tailed Fischer's test, ****$p < 0.0001$). **c** The patterns of immunolocalization with αBAFpS5 (green) and αCENP-C (red) antibodies are presented for cells treated with dsRNA against Flfl (dsRNA^{Flfl}). DNA was stained with DAPI. Scale bar corresponds to 5 μm. **d** The percentages of mitoses showing perichromosomal αBAF and αBAFpS5 signals in control dsRNA^{LacZ} and dsRNA^{Flfl} cells are compared. Values are the sum of three independent experiments showing equivalent results ($N > 86$ for αBAF and $N > 28$ for αBAFpS5; two-tailed Fischer's test, ***$p < 0.001$). **e** The pattern of BAF phosphorylation is analyzed by phos-tag gel electrophoresis of increasing amounts of extracts (lanes 1 and 2) prepared from control dsRNA^{LacZ} cells and cells treated with dsRNA against Flfl (dsRNA^{Flfl}), MTS (dsRNA^{MTS}), and both Flfl and MTS (dsRNA$^{Flfl+MTS}$). Extracts are analyzed by WB using αBAF antibodies. The positions corresponding to non-phosphorylated (noP), and mono- (1pBAF), and di-phosphorylated (2pBAF) species are indicated. **f** Quantitative analysis of the results shown in **e**. The relative proportions with respect to non-phosphorylated BAF of total pBAF, and 1pBAF and 2pBAF species are presented for the indicated RNAi-treated cells. Results are the average of three independent experiments (error bars are SD; two-tailed t-test, *$p < 0.05$, **$p < 0.01$).

significantly increased total pBAF levels (Fig. 5e, f). Interestingly, this effect was mainly constrained to 1pBAF (Fig. 5e, f), since the levels of 2pBAF were not significantly affected (two-tailed t-test, p-value = 0.268) (Fig. 5e, f). These results suggest that PP2A preferentially dephosphorylates 1pBAF. Conversely, and opposite to what would be expected, Flfl depletion decreased total pBAF levels (Fig. 5e, f), strongly reducing 1pBAF levels (Fig. 5e, f), which suggests that Flfl depletion enhanced PP2A-mediated dephosphorylation of 1pBAF. Consistent with this, depletion of MTS in Flfl-depleted cells restored 1pBAF levels (Fig. 5e, f). We also observed that Flfl depletion slightly increased 2pBAF levels (Fig. 5e, f).

cenBAF regulates progression through mitosis. Next, we analyzed the effects of disrupting cenBAF localization on mitosis progression. For this purpose, we performed live image analysis in cells expressing the nuclear pore component Nup-107::mRFP to label the NE. We observed that, in comparison to control

dsRNA^{LacZ} cells, depletion of CENP-C in GFP::CENP-CΔFIM^R-expressing cells significantly increased the overall duration of mitosis (Fig. 6a, b, and Supplementary Movies 1 and 2). No such effect was observed in GFP::CENP-C^R-expressing cells, where the length of mitosis was similar in control dsRNA^{LacZ} cells and after CENP-C depletion (Fig. 6b). These results suggest that impairing cenBAF localization delays mitosis progression. In particular, the time from NEBD to AO was significantly increased (Fig. 6a, b, and Supplementary Movies 1 and 2). The time from AO to NER also showed a clear tendency to increase (Kruskal–Wallis test, p-value = 0.057) (Fig. 6a, b, and Supplementary Movies 1 and 2).

In CENP-C-depleted GFP::CENP-CΔFIM^R-expressing cells, we often observed that Nup-107::mRFP signal persisted through mitosis (Supplementary Movies 2–4), suggesting incomplete NE disassembly. Nuclear pore disassembly is a very early step in NEBD. Thus, to further analyze the effects on NE assembly, we performed IF experiments using αPS10 antibodies, which recognize H3S10P in mitotic cells, and αLaminB antibodies to
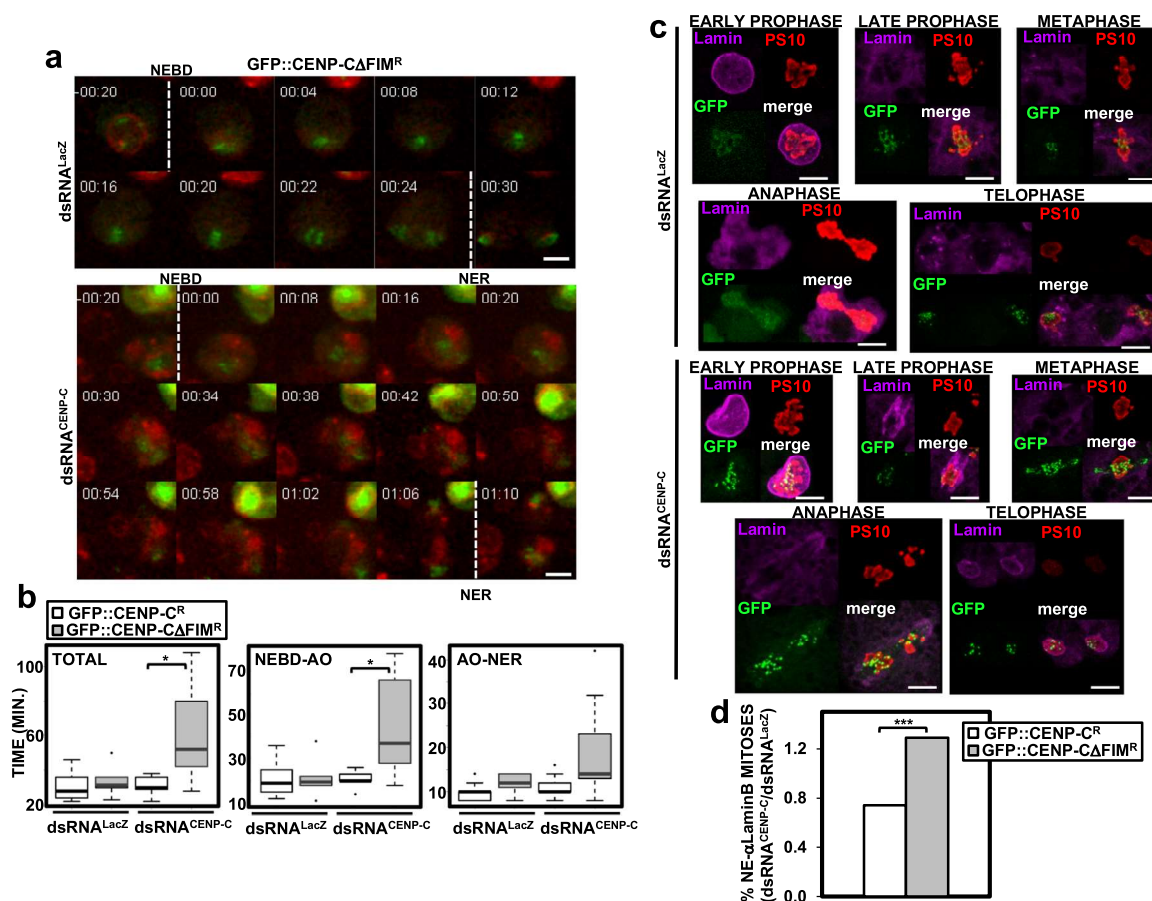
Fig. 6 cenBAF regulates mitosis progression. a In vivo time-lapse recordings of control dsRNA^LacZ (top) and dsRNA^CENP-C (bottom) Nup-107::mRFP cells expressing GFP::CENP-CΔFIM^R. mRFP (red) and GFP (green) signals are direct fluorescence. NEBD and NER are indicated. Times are minutes before/after NEBD. Scale bars correspond to 5 μm. **b** Quantitative analysis of the results shown in **a**. The total duration of mitosis (left), and the times from NEBD to anaphase onset (AO) (center) and from AO to NER (right) are presented for control dsRNA^LacZ and dsRNA^CENP-C Nup-107::mRFP cells expressing the indicated constructs ($n = 3$; $N > 5$; Kruskal–Wallis test, *$p < 0.05$). **c** Immunostainings with αLaminB antibodies (magenta) and αPS10 (red) of control dsRNA^LacZ and CENP-C-depleted dsRNA^CENP-C cells expressing GFP::CENP-CΔFIM^R. Mitotic phases are indicated. GFP (green) is direct fluorescence. Scale bars correspond to 5 μm. **d** The effect of CENP-C depletion on the proportion of mitoses showing NE-assembled αLaminB immunostaining is shown with respect to control dsRNA^LacZ cells for GFP::CENP-C^R and GFP::CENP-CΔFIM^R-expressing cells. Values are the sum of 5–8 independent experiments showing equivalent results ($N > 92$; Chi-square test, ***$p < 0.001$).

monitor NE status. In control dsRNA^LacZ cells, αLaminB immunostaining marked the NE in interphase, became diffuse through the cytoplasm after NEBD in late prophase to relocate to the NE during NER in telophase (Fig. 6c, top). However, in CENP-C-depleted GFP::CENP-CΔFIM^R-expressing cells, we often detected less diffuse αLaminB immunostaining in late prophase (Fig. 6c, bottom). Moreover, the proportion of αPS10-positive cells showing NE-assembled αLaminB immunostaining increased upon CENP-C depletion in GFP::CENP-CΔFIM^R-expressing cells in comparison with control GFP::CENP-C^R-expressing cells (Fig. 6d). Altogether these results suggest that, upon disrupting cenBAF localization, the NE remains partially assembled during mitosis.

In addition, in comparison to control GFP::CENP-C^R-expressing cells, we observed an increased frequency of NE morphology defects in CENP-C-depleted GFP::CENP-CΔFIM^R-expressing cells (two-tailed Fischer's test, p-value < 0.0001) (Fig. 7a, b). These defects ranged from nuclear budding and the formation of micronuclei (Fig. 7c, image 3), to multinucleated cells (Fig. 7c, image 4) and cells with enlarged nucleus of irregular NE (Fig. 7c, images 5–7). In this regard, in CENP-C-depleted GFP::CENP-CΔFIM^R-expressing cells, we detected aberrant mitoses that generated cells with abnormal nuclear morphology, often

multinucleated (Supplementary Movies 3–6). Notably, these defects were significantly rescued when BAF was constitutively targeted to centromeres in cells expressing GBP::FLAG::BAF (Fig. 7a, b).

cenBAF, CENP-C, and PP4 localization is interdependent. Results reported above suggest a model by which CENP-C mediates recruitment of PP4 to centromeres, PP4 retains cenBAF at centromeres in mitosis, which in turn stabilizes CENP-C (Fig. 8a). Consistent with these interdependences, Flfl depletion, which reduced centromeric cenBAF levels (Supplementary Fig. 7c–f), also decreased centromeric CENP-C (Fig. 8b) (see also Supplementary Fig. 7c, bottom panel), and, along with CENP-C, BAF depletion reduced centromeric levels of Flfl (Fig. 8c). Moreover, depletion of CENP-C abolished centromeric localization of both Flfl (Fig. 8d) and cenBAF (Fig. 8e). Noteworthy, like when cenBAF localization is disturbed in CENP-C-depleted GFP::CENP-CΔFIM^R-expressing cells (Fig. 4a) or upon Flfl-depletion (Fig. 5a), depletion of CENP-C induced the accumulation of perichromosomal BAF too (Supplementary Fig. 11). Altogether these results indicate that CENP-C, PP4, and BAF are interdependent for centromeric localization in mitotic chromosomes.
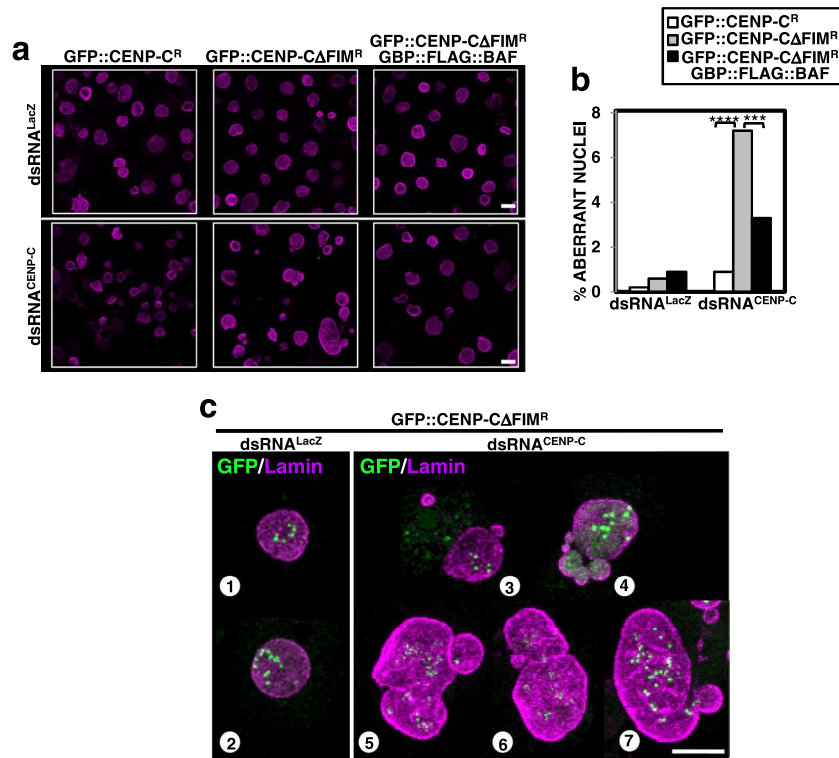
Fig. 7 Disrupting cenBAF localization causes NE morphology defects. a Immunostainings with αLaminB antibodies (magenta) of control dsRNA[LacZ] and CENP-C-depleted dsRNA[CENP-C] cells expressing the indicated constructs. Scale bars correspond to 10 μm. **b** Quantitative analysis of the results are shown in **a**. The percentage of cells showing altered nuclear morphology is presented for control dsRNA[LacZ] and dsRNA[CENP-C] cells expressing the indicated constructs. Values are the sum of 3–4 independent experiments showing equivalent results ($N > 334$; two-tailed Fischer's test, ***$p < 0.001$, ****$p < 0.0001$). **c** Enlarged images of immunostainings with αLaminB antibodies (magenta) of dsRNA[CENP-C] cells (images 3–7) and control dsRNA[LacZ] cells (images 1 and 2) expressing GFP::CENP-CΔFIM[R]. GFP signals are direct fluorescence. Scale bar corresponds to 5 μm.

Interestingly, we also observed that targeting of GBP::FLAG::BAF to centromeres in CENP-C-depleted GFP::CENP-CΔFIM[R]-expressing cells significantly rescued centromeric Flfl levels (Supplementary Fig. 6a, b), without affecting depletion of endogenous CENP-C (Supplementary Fig. 6c), suggesting that BAF also stabilizes centromeric PP4 independently of CENP-C.

Discussion

Here we have unveiled a novel centromere-based mechanism that controls mitosis progression. Central to this mechanism is the NE component BAF. We have shown that a fraction of BAF (cenBAF) associates with centromeres. BAF is known to bind across chromatin in interphase[26,27], but, in mitosis, VRK1/NHK1 phosphorylates BAF[1,18–20], resulting in its release from chromatin. Our results suggest that, at the centromere, PP4 prevents phosphorylation and release of cenBAF in mitosis. cenBAF is a very small proportion of total BAF. In this regard, the vast majority of BAF is phosphorylated and free in mitosis, resulting in high non-chromosomal background that likely precluded the identification of cenBAF in previous IF studies.

cenBAF forms a functional network with PP4 and CENP-C, as all three factors are interdependent for their centromeric localization. Whether they physically interact to form a centromeric complex remains to be determined. In favor of this possibility, CENP-C interacts directly with Flfl in vitro[24] and, moreover, BAF and CENP-C co-immunoprecipitate, suggesting that, either directly or indirectly, CENP-C also interacts with BAF. Along the same lines, constitutive targeting of BAF to centromeres stabilizes centromeric Flfl as well as CENP-C.

Our results suggest that cenBAF stabilizes CENP-C at centromeres and, thus, it is required for accurate chromosome segregation. CENP-C connects centromeric chromatin with the outer kinetochore[31,32] and loss-of-function mutations induce strong chromosome segregation defects, mostly chromosome misalignment in metaphase[33,34]. Interestingly, metaphase misalignment is the most frequent chromosome segregation defect observed in BAF-depleted cells, supporting that destabilization of CENP-C is their principal cause. The mechanism by which BAF stabilizes CENP-C at centromeres remains unknown. It is possible that cenBAF modifies centromeric chromatin in a way that stabilizes CENP-C, since BAF has been shown to affect histone modifications and higher-order chromatin organization[2,3,15,17,26]. It is also possible that the stabilization is through the action of PP4, since cenBAF is required for centromeric localization of Flfl. On the other hand, CENP-C destabilization at centromeres likely involves tension exerted by spindle microtubules since, when centromeric localization of cenBAF and PP4 are impaired in CENP-CΔFIM-expressing cells, CENP-C delocalizes to centrosomes and across the spindle in metaphase chromosomes[24] (see also Fig. 6c, metaphase in bottom panel). Our results also show that cenBAF is reciprocally stabilized by CENP-C via the recruitment of Flfl. Altogether these observations suggest that the network of interactions between CENP-C, PP4, and cenBAF forms a positive feedback loop that reinforces assembly of centromeric chromatin and, hence, ensures faithful chromosome segregation. BAF depletion also affected centromeric CENP-A[CID] levels. This effect is likely a consequence of CENP-C destabilization, since CENP-A[CID] was reduced to a much lesser extent than CENP-C and it is known that CENP-A[CID] and CENP-C are interdependent for their centromeric localization[35–37].

The small fraction of cenBAF regulates the behavior of the large pool of free pBAF in mitosis. Disrupting cenBAF localization
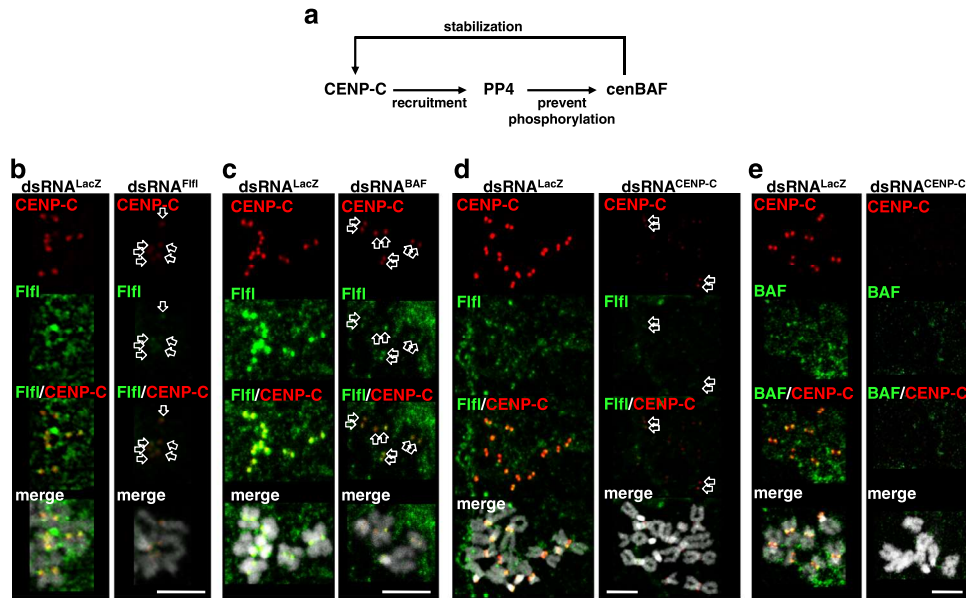
Fig. 8 cenBAF, PP4, and CENP-C are interdependent for centromeric localization. a Schematic representation of the interdependences for centromeric localization between cenBAF, PP4, and CENP-C. CENP-C mediates centromeric recruitment of PP4, which is required to retain cenBAF at centromeres during mitosis. cenBAF stabilizes CENP-C at centromeres. **b** Immunostainings with αFlfl (green) and αCENP-C antibodies (red) are presented for mitotic chromosomes from dsRNA^Flfl (right) and control dsRNA^LacZ (left) cells. DNA was stained with DAPI. Arrows in dsRNA^Flfl cells indicate centromeric αCENP-C signals. Scale bar corresponds to 5 μm. **c** Immunostainings with αFlfl (green) and αCENP-C antibodies (red) are presented for mitotic chromosomes from dsRNA^BAF (right) and control dsRNA^LacZ (left) cells. DNA was stained with DAPI. Arrows indicate αFlfl signals in dsRNA^BAF cells overlapping with αCENP-C at centromeres. Scale bar corresponds to 5 μm. **d** Immunostainings with αFlfl (green) and αCENP-C antibodies (red) are presented for mitotic chromosomes from dsRNA^CENP-C (right) and control dsRNA^LacZ (left) cells. DNA was stained with DAPI. Scale bar corresponds to 5 μm. **e** Immunostainings with αBAF (green) and αCENP-C antibodies (red) are presented for mitotic chromosomes from dsRNA^CENP-C (right) and control dsRNA^LacZ (left) cells. DNA was stained with DAPI. Scale bar corresponds to 5 μm.
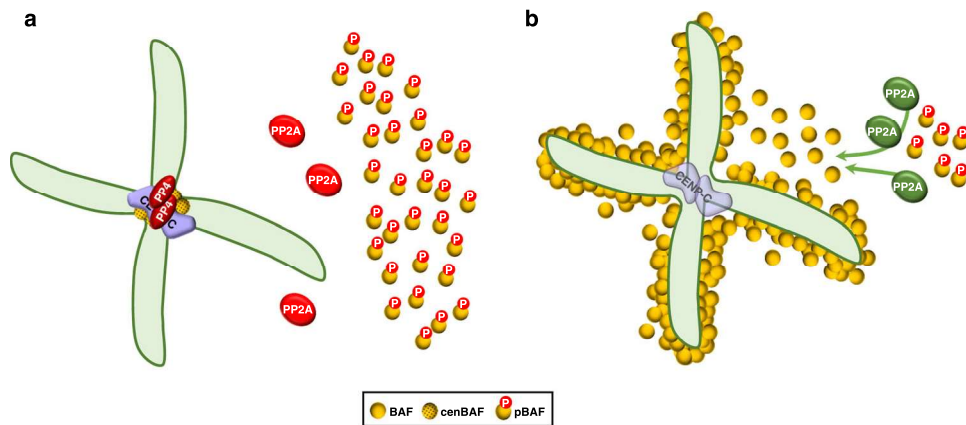

Fig. 9 cenBAF, PP4, and CENP-C form a centromeric network that prevents PP2A-mediated dephosphorylation and perichromosomal accumulation of BAF in mitosis. a Normally, centromeric localization of cenBAF and PP4, which depends on CENP-C, maintains PP2A inactive (in red) during mitosis and, consequently, the bulk of BAF stays phosphorylated and free. **b** Disrupting centromeric localization of cenBAF and PP4 causes ectopic PP2A activation (in green) in mitosis, which results in dephosphorylation of pBAF and the accumulation of perichromosomal BAF. Centromeric CENP-C is also destabilized. See text for details.

induces PP2A-mediated dephosphorylation of free pBAF in mitosis and the accumulation of BAF in a perichromosomal layer that surrounds chromosomes (Fig. 9). Normally, PP2A is inactivated at the entry into mitosis (reviewed in ref. [38]). Thus, our results suggest that in the absence of cenBAF, PP2A remains active in mitosis. How might cenBAF regulate PP2A activity in mitosis remains to be determined. In this regard, PP4 could play a central role, since our results suggest that it regulates PP2A-mediated pBAF dephosphorylation. Whether the centromere-bound fraction of PP2A[39] participates in this regulatory mechanism remains to be determined too.

PP2A selectively dephosphorylates 1pBAF, but not 2pBAF, suggesting that various phosphatases specifically target pBAF. In this regard, in *Drosophila*, a second unidentified phosphatase has been proposed to dephosphorylate pBAF at the exit from mitosis[6]. PP4 might be involved in 2pBAF dephosphorylation since, though weakly, Flfl depletion increased 2pBAF levels. Further work is required to clarify the actual phospho-sites in 1pBAF and

2pBAF and the potential site-specific activity of the various phosphatases involved in BAF dephosphorylation.

cenBAF disruption compromises progression through mitosis, delaying AO and increasing total mitosis duration. Several factors could contribute to these effects. On one hand, defects in centromere and kinetochore assembly are known to delay or arrest mitosis progression, particularly before AO. Furthermore, altering PP2A activity could impact mitosis in many different ways. In this regard, impaired BAF phosphorylation was shown to affect mitosis progression, since VRK1 depletion in mammalian cells, which also prevents BAF phosphorylation and its release from chromatin during mitosis, delays AO and increases mitosis duration too[22]. Delayed AO could reflect a defect in NEBD since BAF phosphorylation is important to weaken anchoring of chromatin to the NE[1,21,22]. On the other hand, exiting mitosis, pBAF dephosphorylation is crucial for NER[3,5,6,23]. Thus, it is also possible that, due to the ectopic activation of PP2A in mitosis, cenBAF disruption induces premature pBAF dephosphorylation and NER. The increased proportion of mitotic cells showing assembled NE, and the persistence of Nup-107::mRFP signal through mitosis, support a contribution of cenBAF to NE disassembly/reassembly. Along the same lines, cenBAF disruption induces strong NE morphological defects. Altered nuclear morphology is widely associated with generic mitotic problems. However, the defects observed upon impairing cenBAF localization are rescued by constitutive targeting of BAF to centromeres, indicating that they are linked to cenBAF disruption. Moreover, BAF mutations that affect its ability to polymerize and crossbridge distant DNA sites[7], or when BAF phosphorylation is impeded by VRK1 depletion[1,22], induce similar nuclear morphology defects. Altogether these results suggest that cenBAF, although localized at centromeres, participates in the global regulation of the structural rearrangements that the NE undergoes during mitosis. Further work is required to reach a better understanding of this contribution.

In summary, our results suggest that, together with PP4 and CENP-C, cenBAF forms a functional centromeric network that is required for accurate chromosome segregation and controls mitosis progression by regulating PP2A-mediated BAF dephosphorylation. It is tempting to speculate that this network helps to coordinate chromosome segregation with the crucial NE rearrangements that mark mitosis progression. Interestingly, other NE components have also been reported to associate with the centromere/kinetochore during mitosis and contribute to spindle assembly[40–42], revealing the strong functional links that exist between the NE and the centromere/kinetochore.

Methods

DNAs, protein constructs, cell lines, and antibodies. cDNA encoding BAF was obtained from *Drosophila* Genomics Resource Center (clone GH06291). Plasmids expressing BAF::YFP and CENP-A[CID]::YFP under the control of their own promoters were obtained by cloning the appropriate constructs into pEYFP (Clontech). BAF[R] constructs resistant to RNAi knockdown were obtained by modifying codon usage following the *Drosophila* RNAi escape strategy construct (RESC). Plasmid expressing GBP::FLAG::BAF under the control of the copper-inducible metallothionein promoter was generated by standard PCR and Gateway cloning methods. Briefly, the GBP[30] encoding sequence was PCR amplified using primers described in Supplementary Table 2 and cloned into the pMT-3xFlag-DEST vector upstream to and in frame with the 3xFlag-tag. This new product was used in LR reaction with the BAF-entry clone to generate pMT-GBP::FLAG::BAF. Plasmid expressing FLAG::BAF under the control of its own promoter was obtained by cloning BAF into pEYFP plasmid (Clontech) and replacing the YFP tag by the FLAG-tag. Plasmids FLAG::BAF[S5A], FLAG::BAF[3A], and FLAG::BAF[3E] were obtained from plasmid FLAG::BAF mutating S5 to A and S2, T4 and S5 to A or E, respectively. Plasmid expressing CENP-A[CID]::TAP under the control of its own promoter was obtained by cloning the appropriate construct into plasmid pMK33-C::TAP (Clontech). Plasmid pMT-NHK1 expressing VRK1/NHK1::FLAG::HA construct was obtained from BDGP (clone FMO02828). Plasmid pMT-Nup-107::mRFP was a gift from Dr. Helder Maiato and is described in ref. [43].

Cultured cells used in these experiments were Schneider's *Drosophila* Line 2 [D. Mel. (2), SL2] (ATCC® CRL-1963™). To generate cell lines stably expressing RNAi-resistant ([R]) GFP::CENP-C[R] and GFP::CENP-CΔFIM[R] constructs, we replaced the Acc65I-EcoRI (420 bps) fragment in GFP::CENP-C and GFP::CENP-CΔFIM constructs[24] to a codon modified version of the fragment (GeneArt gene synthesis) that encodes the same amino acids but is insensitive to RNAi targeting endogenous CENP-C. Stable lines expressing CENP-A[CID]::TAP, YFP::CENP-A[CID], BAF::YFP, GBP::FLAG::BAF/GFP::CENP-C[R], GBP::FLAG::BAF/GFP::CENP-CΔFIM[R], Nup-107::mRFP/GFP::CENP-C[R], and Nup-107::mRFP/GFP::CENP-CΔFIM[R] were obtained according to standard procedures.

Rabbit polyclonal αBAF, and rat and rabbit polyclonal αCENP-C antibodies were raised against bacterially expressed full length *Drosophila* BAF and a *Drosophila* CENP-C fragment (aa 505–1227), respectively. Specificity of the antibodies was determined by WB and/or immunostaining (IF) (Supplementary Figs. 1 and Fig. 8d). Rabbit polyclonal αCID, and rat polyclonal αHP1a and αHP1c antibodies are described in refs. [44,45]. Rat polyclonal αFlfl antibodies are described in ref. [24]. Rabbit polyclonal αBAFpS5 antibodies raised against a phospho-peptide spanning the N-terminal region of human BAF and are described in ref. [23]. Specificity of αBAFpS5 antibodies for *Drosophila* pBAF was determined by phostag gel electrophoresis analysis, in which αBAFpS5 antibodies recognized pBAF, but not non-phosphorylated BAF, and a S5A mutation abolished this reactivity (Supplementary Fig. 5e). The rest of antibodies used were commercially available: rabbit polyclonal αTAP (Open Biosystems, CAB1001), mouse monoclonal αMTS (BD-Transduction Laboratories, 610555), mouse monoclonal αFLAG (Sigma F3165), rabbit purified αFLAG (Sigma F7425), mouse monoclonal αTubulin (Millipore, MAB3408), mouse monoclonal αLaminB (DSHB ADL67.10), mouse monoclonal αGFP (Roche 1181446001), rabbit polyclonal αGFP (Invitrogen A11122), rabbit polyclonal αH3 (Cell Signaling 9715), and rabbit polyclonal αPS10 (Millipore 06-570).

Fly stocks and genetic procedures. nub-*GAL4* flies were obtained from Bloomington Stock Center. *baf*[RNAi] corresponds to 102,013 stock from the Vienna *Drosophila* RNAi Center. Transgenic flies carrying the various UAS-dBAF constructs described in the text were obtained by site-directed integration of the corresponding pUASTattb plasmids into chromosome 3 using 3R-86Fb embryos.

For experiments with knockdown *baf*[RNAi] flies, crosses were left at 25 °C until third-instar larvae stage. For overexpression experiments, homozygous transgenic lines carrying the corresponding UAS-constructs were crossed to homozygous nub-GAL4 flies. To analyze the effects on wing development, flies were kept in 75% ethanol, 25% glycerol solution for at least 24 h at room temperature and washed in PBS. Then, wings were dissected and immediately mounted in Fauré's medium under gentle pressure. Images were collected using a ×4 objective lens on a Nikon E-600 microscope equipped with an Olympus DP72 camera and CellF software.

Identification of CENP-A[CID] chromatin-associated proteins. For the identification of proteins associated with CENP-A[CID]-enriched chromatin, a stable S2 cell line expressing CENP-A[CID]::TAP under the control of the CENP-A[CID] promoter was used. The pattern of CENP-A[CID]::TAP localization was determined by immunostaining with αTAP antibodies (Supplementary Fig. 12a, b). TAP-affinity purification of proteins associated with CENP-A[CID]::TAP containing chromatin was performed as described in ref. [46]. Briefly, nuclei were purified and digested with micrococcal nuclease (MNase) (Sigma). After digestion was stopped, the soluble chromatin fraction (SN1), which accounted for ~66% of total chromatin, was prepared by centrifugation at 10,000×g for 15 min at 4 °C. The remaining insoluble material was extracted at increasing EDTA concentration from 2 to 200 mM. Nucleosomal composition of each fraction was analyzed by agarose gel electrophoresis (Supplementary Fig. 12c). CENP-A[CID]::TAP and CENP-C content were determined by WB (Supplementary Fig. 12d, e). Then, the SN1, 2 and 20 mM EDTA fractions were subjected to conventional TAP-affinity purification using IgG-Dynabeads (Invitrogen). Bound proteins were eluted and analyzed by standard LC/MS at the Proteomics Unit of the "Institut de Recerca de la Vall d'Hebron" (Barcelona). Supplementary Table 1 summarizes the proteins identified in these studies, which included BAF (mascot score: 97; sequence coverage: 16.7%).

RNAi knockdown experiments. For RNAi-mediated BAF knockdown experiments, dsRNA encompassing the entire BAF-coding region was prepared using the MEGAscript T7 kit (Ambion). Then, cells were incubated with 20 μg of dsRNA at a concentration of 5×10^5 cells/ml and, after 3 days, cells were diluted 1:2 and treated with a second dose of 20 μg of dsRNA for 4 days. CENP-C, VRK1/NHK1, and Flfl knockdown experiments were performed as for BAF using 40–50 μg (CENP-C) and 30 μg (VRK1/NHK1 and Flfl) of the corresponding dsRNA. MTS knockdown was performed with a single dose of 30 μg of dsRNA for 3 days. When MTS depletion was combined with Flfl knockdown, dsRNA against MTS was added with the second dose of dsRNA against Flfl. The extent of BAF, CENP-C, MTS, and Flfl depletion were determined by WB and/or IF. The extent of VRK1/NHK1 depletion was assessed from the effects on BAF phosphorylation (Supplementary Fig. 5a). Primers used in these experiments are indicated in Supplementary Table 2.

Immunostaining experiments. Immunostaining experiments were performed as described elsewhere[44]. Briefly, cells were treated for 6 h with 25 μM colchicine (Sigma), immobilized onto a slide by centrifugation for 10 min at 500 rpm with low acceleration in a TermoShandon Cytospin using a single-chamber Cytofunnel and, then, fixed in 4% paraformaldehyde for 10 min, washed with PBS and blocked in 3% BSA, 0.5% TritonX-100 in PBS. Samples were then immunostained with αBAF (1:300), αBAFpS5 (1:200), rat αCENP-C (1:500), rabbit αCENP-C (1:300), αCENP-A[CID] (1:500), αHP1a (1:200), αHP1c (1:500), αFlfl (1:1000), αFLAG (1:2000), αTubulin (1:10,000), αTAP (1:300), and αLaminB (1:1500) antibodies. For visualization, slides were mounted in Mowiol (Calbiochem-Novabiochem) containing 0.2 ng/ml DAPI (Sigma) and analyzed in a Leica TCS/SPE confocal microscope equipped with LAS/AF software. Images were acquired and processed identically using ImageJ (http://imagej.nih.gov/ij/) and Adobe Photoshop software. Mean grey intensities were calculated using ImageJ macros[47] on thresholded images at DAPI-masked regions of interest running analyzed particles to plugin on the FeatureJ Laplacian (http://imagescience.org/meijering/software/featurej/).

For super-resolution microscopy, samples were mounted in Vectashield antifade mounting medium containing DAPI (Vector Laboratories). Images were taken with a Zeiss 880 confocal microscope equipped with Airyscan for image acquisition. A ×100 magnification 1.46 NA oil-immersion lens with a digital zoom of ×3 was used. The Z-step between the stacks was set at 167.9 nm. Airyscan raw data were preprocessed with the automatic setting of Zen Black. For the generation of the intensity profile plots a segmented line was manually drawn on a single z-stack and analyzed on ImageJ. The intensity profile was calculated for each staining separately.

Live cell imaging. Stable cell lines expressing Nup-107::mRFP/GFP::CENP-C[R] and Nup-107::mRFP/GFP::CENP-CΔFIM[R] were treated with dsRNA against CENP-C as described above. Cells were plated 24 h before live imaging in poly-D-lysine dishes (MatTek Corporation P35GC-1.5-14C). Expression of the tagged constructs was induced by adding 500 μM CuSO$_4$ to the media 20 h before live imaging. Live imaging was performed on an Ultraview ERS6 spinning disc system mounted on a Zeiss Axiovert 200M inverted microscope and equipped with a Hamamatsu C9100-50 electron-multiplied camera and a Plan-Neofluar ×40/1.3NA oil objective. z-stacks covering the entire volume of the mitotic cell were collected every 2 min at a step size of 8 nm, using the acquisition software Volocity 6.1. Images and movies were processed and analyzed in ImageJ. Merged images represent maximum intensity projections of all z-stacks.

Chromatin fibers. For fiber analyses, extended chromatin fibers were prepared essentially as described in ref. [48]. Briefly, fibers were extended in 450 mM NaCl and immunostained with αBAF (1:200) and αCENP-C (1:300) antibodies. Images were acquired with a ×63 objective on a SP5 Leica confocal microscope equipped with LAS/AF software and analyzed with Image J and Adobe Photoshop software.

NE and chromosome segregation defects. For these experiments, cells were plated at 0.5 × 10^6 cells/ml in well plates containing cover slips coated with Con-canavalin A (0.5 mg/ml; Sigma) and, after 18 h, cells were processed for immunostaining. To monitor nuclear morphology and chromosome segregation defects, cells were stained with αLamin (1:1000) and αTubulin (1:5000) antibodies, respectively. To analyze NE assembly in mitosis, cells were co-stained with αLamin (1:1000) and αPS10 (1:3000) antibodies.

Co-IP experiments. For Co-IP experiments, cell extracts were obtained in 50 mM Tris–HCl pH 8, 150 mM NaCl, 5 mM EDTA, 0.5% NP-40, 0.1 mM PMSF, Protease Inhibitor Cocktail and, after homogenization with Dounce (B pestle), supplemented to 300 mM NaCl and centrifuged at 14,000 rpm for 15 min at 4 °C. The supernatant was incubated overnight at 4 °C with the indicated antibodies or preimmune serum as control (mock). Then, Protein A Sepharose beads (GE Healthcare) were added and incubated at 4 °C for 2 h. After incubation, beads were pelleted by centrifugation, washed and eluted in PLB 1X, 10% β-mercaptoethanol, and analyzed by WB. For treatment with DNAse I, extracts were supplemented with 20 mM MgCl$_2$ and 3 mM CaCl$_2$ and incubated at 37 °C for 30 min with Turbo™ DNAse I (Ambion) at a final concentration of 0.4 units/μl. Digestion was stopped by adding 10 mM EDTA. Before DNAse I treatment, 30 μg of pUC19 were added to monitor the efficiency of digestion.

Analysis of BAF phosphorylation. To analyze BAF phosphorylation, total cell extracts were obtained in PLB and analyzed by Phos-tag gel electrophoresis according to manufacturers' instructions (Wako Chemicals Inc.). Briefly, 50 μM of acrylamide-pendant Phos-tag™ (AAL-107) and 100 μM of MnCl$_2$ were added to 10% polyacrylamide resolving gel solution before polymerization. After electrophoresis, gels were incubated 15 min in transfer buffer with 1 mM EDTA and 15 min in transfer buffer without EDTA, and analyzed by WB. For alkaline phosphatase (AP) treatment, cell extracts were obtained in 150 mM NaCl, 50 mM Tris–HCl pH 8, 10% glycerol, 0.1% SDS, 1% NP40, 1 mM PMSF, protease inhibitor cocktail, 50 mM NaF, 2 mM Na$_3$VO$_4$, and 10 mM glycerol phosphate. AP treatment was performed with calf intestine AP (Roche) for 1 h at 37 °C in 150 mM NaCl, 50 mM Tris–HCl pH 8, 10 mM MgCl$_2$, and 1 mM DTT.

Western blot analysis. Western blot analysis was performed according to standard procedures using the following antibody dilutions: αBAF (1:2500), αBAFpS5 (1:1000), αCENP-C (1:3000), αFLFL (1:10,000), αMTS (1:5000), αCENP-A[CID] (1:2000), αHP1a (1:10,000), αH3 (1:2500), αTubulin (1:5000), αGFP (1:2000), αFLAG (1:2500), αTAP (1:2500). For all WBs presented in main and supplementary figures, uncropped images are presented in Supplementary Fig. 13.

Statistics and reproducibility. Statistical significance of the difference in the proportion of mitoses showing segregation defects, perichromosomal BAF and centromeric Flfl, and in the proportion of cells with aberrant NE morphology was assessed via two-tailed Fisher's exact test. Statistical significance of the difference in the proportion of NE-assembled mitoses between GFP::CENP-C[R] and GFP::CENP-CΔFIM[R]-expressing cells was assessed via comparative Chi-square test using the cp.chisq.test function from the DiffXTables package version 0.1.0 using R 3.5.1[49]. One-tailed binomial test was used to assess the probability to find BAF and BAF-YFP co-localizing with CENP-C on the same chromatin fiber. Statistical significance of the centromeric localization of BAF phosphomutants was assessed by two-tailed binomial test. Statistical significance of the difference in centromeric intensity of BAF, CENP-C, and CENP-A[CID] immunostaining was determined by Kruskal–Wallis test. Statistical difference in the extent of BAF/CENP-C co-IP and the changes in BAF phosphorylation was determined by two-tailed t-test comparison of the means. For each experiment, the number of independent biological replicates and sample sizes are indicated in the corresponding figure legend.

Data availability

All data and unique materials in this paper are available from the corresponding authors upon reasonable request. All data underlying the graphs described in the main and supplementary figures are presented in Supplementary Data 1.

References

1. Gorjánácz, M. et al. *Caenorhabditis elegans* BAF-1 and its kinase VRK-1 participate directly in post-mitotic nuclear envelope assembly. *EMBO J.* **26**, 132–143 (2007).
2. Margalit, A., Segura-Totten, M., Gruenbaum, Y. & Wilson, K. L. Barrier-to-autointegration factor is required to segregate and enclose chromosomes within the nuclear envelope and assemble the nuclear lamina. *Proc. Natl Acad. Sci. USA* **102**, 3290–3295 (2005).
3. Haraguchi, T. et al. Live cell imaging and electron microscopy reveal dynamic processes of BAF-directed nuclear envelope assembly. *J. Cell Sci.* **121**, 2540–2554 (2008).
4. Haraguchi, T. et al. BAF is required for emerin assembly into the reforming nuclear envelope. *J. Cell Sci.* **114**, 4575–4585 (2001).
5. Asencio, C. et al. Coordination of kinase and phosphatase activities by Lem4 enables nuclear envelope reassembly during mitosis. *Cell* **150**, 122–135 (2012).
6. Mehsen, H. et al. PP2A-B55 promotes nuclear envelope reformation after mitosis in *Drosophila*. *J. Cell Biol.* **217**, 4106–4123 (2018).
7. Samwer, M. et al. DNA cross-bridging shapes a single nucleus from a set of mitotic chromosomes. *Cell* **170**, 956–972 (2017).
8. Jamin, A. & Wiebe, M. S. Barrier to autointegration factor (BANF1): interwoven roles in nuclear structure, genome integrity, innate immunity, stress responses and progeria. *Curr. Opin. Cell Biol.* **34**, 61–68 (2015).
9. Berk, J. M. et al. The molecular basis of emerin–emerin and emerin–BAF interactions. *J. Cell Sci.* **127**, 3956–3969 (2014).
10. Cai, M. et al. Solution structure of the constant region of nuclear envelope protein LAP2 reveals two LEM-domain structures: one binds BAF and the other binds DNA. *EMBO J.* **20**, 4399–4407 (2001).
11. Cai, M. et al. Solution NMR structure of the barrier-to-autointegration factor–Emerin complex. *J. Biol. Chem.* **282**, 14525–14535 (2007).
12. Furukawa, K. LAP2 binding protein 1 (L2BP1/BAF) is a candidate mediator of LAP2–chromatin interaction. *J. Cell Sci.* **112**, 2485–2492 (1999).
13. Lee, K. K. et al. Distinct functional domains in emerin bind lamin A and DNA-bridging protein BAF. *J. Cell Sci.* **114**, 4567–4573 (2001).
14. Mansharamani, M. & Wilson, K. L. Direct binding of nuclear membrane protein MAN1 to emerin in vitro and two modes of binding to barrier-to-autointegration factor. *J. Biol. Chem.* **280**, 13863–13870 (2005).
15. Segura-Totten, M., Kowalski, A. K., Craigie, R. & Wilson, K. L. Barrier-to-autointegration factor: major roles in chromatin decondensation and nuclear assembly. *J. Cell Biol.* **158**, 475–485 (2002).

16. Barton, L. J., Soshnev, A. A. & Geyer, P. K. Networking in the nucleus: a spotlight on LEM-domain proteins. *Curr. Opin. Cell Biol.* **34**, 1–8 (2015).

17. Furukawa, K. et al. Barrier-to-autointegration factor plays crucial roles in cell cycle progression and nuclear organization in Drosophila. *J. Cell Sci.* **116**, 3811–3823 (2003).

18. Bengtsson, L. & Wilson, K. L. Barrier-to-autointegration factor phosphorylation on Ser-4 regulates emerin binding to lamin A *in vitro* and emerin localization *in vivo*. *Mol. Biol. Cell* **17**, 1154–1163 (2006).

19. Lancaster, O. M., Cullen, C. F. & Ohkura, H. NHK-1 phosphorylates BAF to allow karyosome formation in the *Drosophila* oocyte nucleus. *J. Cell Biol.* **179**, 817–824 (2007).

20. Nichols, R. J., Wiebe, M. S. & Traktman, P. The vaccinia-related kinases phosphorylate the N' terminus of BAF, regulating its interaction with DNA and its retention in the nucleus. *Mol. Biol. Cell* **17**, 2451–2464 (2006).

21. Margalit, A., Brachner, A., Gotzmann, J., Foisner, R. & Gruenbaum, Y. Barrier-to-autointegradtion factor—a BAFfling little protein. *Trends Cell Biol.* **17**, 202–208 (2007).

22. Molitor, T. P. & Traktman, P. Depletion of the protein kinase VRK1 disrupts nuclear envelope morphology and leads to BAF retention on mitotic chromosomes. *Mol. Biol. Cell* **25**, 891–903 (2014).

23. Zhuang, X., Semenova, E., Maric, D. & Craigie, R. Dephosphorylation of barrier-to-autointegration factor by protein phosphatase 4 and its role in cell mitosis. *J. Biol. Chem.* **289**, 1119–1127 (2014).

24. Lipinszki, Z. et al. Centromeric binding and activity of protein phosphatase 4. *Nat. Commun.* **6**, 5894 (2015).

25. Barth, T. K. et al. Identification of novel *Drosophila* centromere-associated proteins. *Proteomics* **14**, 2167–2178 (2014).

26. Montes de Oca, R., Andreassen, P. R. & Wilson, K. L. Barrier-to-autointegration factor influences specific histone modifications. *Nucleus* **2**, 580–590 (2011).

27. Kind, J. & van Steensel, B. Stochastic genome–nuclear lamina interactions: modulating roles of Lamin A and BAF. *Nucleus* **5**, 124–130 (2014).

28. Mellone, B. G. et al. Assembly of *Drosophila* centromeric chromatin proteins during mitosis. *PLoS Genet.* **7**, e1002068 (2011).

29. Westermann, S. & Scheleiffer, A. Family matters: structural and functional conservation of centromere-associated proteins from yeast to humans. *Trends Cell Biol.* **23**, 260–269 (2013).

30. Rothbauer, U. et al. Targeting and tracing antigens in live cells with fluorescent nanobodies. *Nat. Methods* **3**, 887–889 (2006).

31. Przewloka, M. R. et al. CENP-C is a structural platform for kinetochore assembly. *Curr. Biol.* **21**, 399–405 (2011).

32. Screpanti, E. et al. Direct binding of Cenp-C to the Mis12 complex joins the inner and outer kinetochore. *Curr. Biol.* **21**, 391–398 (2011).

33. Kalitsis, P., Fowler, K. J., Earle, E., Hill, J. & Choo, K. H. Targeted disruption of mouse centromere protein C gene leads to mitotic disarray and early embryo death. *Proc. Natl Acad. Sci. USA* **95**, 1136–1141 (1998).

34. Kwon, M. S., Hori, T., Okada, M. & Fukagawa, T. CENP-C is involved in chromosome segregation, mitotic checkpoint function, and kinetochore assembly. *Mol. Biol. Cell* **18**, 2155–2168 (2007).

35. Erhardt, S. et al. Genome-wide analysis reveals a cell cycle-dependent mechanism controlling centromere propagation. *J. Cell Biol.* **183**, 805–818 (2008).

36. Goshima, G. et al. Genes required for mitotic spindle assembly in *Drosophila* S2 cells. *Science* **316**, 417–421 (2007).

37. Heeger, S. et al. Genetic interactions of separase regulatory subunits reveal the diverged *Drosophila* Cenp-C homolog. *Genes Dev.* **19**, 2041–2053 (2005).

38. Castro, A. & Lorca, T. Greatwall kinase at a glance. *J. Cell Sci.* **131**, pii: jcs222364 (2018).

39. Vallardi, G., Allan, L. A., Crozier, L. & Saurin, A. T. Division of labour between PP2A-B56 isoforms at the centromere and kinetochore. *Elife* **8**, pii: e42619 (2019).

40. Güttinger, S., Laurell, E. & Kutay, U. Orchestrating nuclear envelope disassembly and reassembly during mitosis. *Nat. Rev. Mol. Cell Biol.* **10**, 178–191 (2009).

41. Kutay, U. & Hetzer, M. W. Reorganization of the nuclear envelope during open mitosis. *Curr. Opin. Cell Biol.* **20**, 669–677 (2008).

42. Batzenschlager, M. et al. Arabidopsis MZT1 homologs GIP1 and GIP2 are essential for centromere architecture. *Proc. Natl Acad. Sci. USA* **112**, 8656–8660 (2015).

43. Afonso, O. et al. Feedback control of chromosome separation by a midzone Aurora B gradient. *Science* **345**, 332–336 (2014).

44. Moreno-Moreno, O., Torras-Llort, M. & Azorín, F. Proteolysis restricts localization of CID, the centromere-specific histone H3 variant of *Drosophila*, to centromeres. *Nucleic Acids Res.* **34**, 6247–6255 (2006).

45. Font-Burgada, J., Rossell, D., Auer, H. & Azorín, F. *Drosophila* HP1c isoform interacts with the zinc-finger proteins WOC and relative-of-WOC (ROW) to regulate gene expression. *Genes Dev.* **22**, 3007–3023 (2008).

46. Foltz, D. R. et al. The human CENP—a centromeric nucleosome-associated complex. *Nat. Cell Biol.* **8**, 427–429 (2006).

47. Schindelin, J. et al. Fiji: an open-source platform for biological-image analysis. *Nat. Methods* **9**, 676–682 (2012).

48. Sullivan, B. A. Optical mapping of protein–DNA complexes on chromatin fibers. *Methods Mol. Biol.* **659**, 99–115 (2010).

49. Song, M., Zhang, Y., Katzaroff, A. J., Edgar, B. A. & Buttitta, L. Hunting complex differential gene interaction patterns across molecular contexts. *Nucleic Acids Res.* **42**, e57 (2014).

Acknowledgements

Author contributions

M.T.-L., S.M.-G., P.E.-F., Z.L., Z.K., and O.M.-M. performed the experiments. Z.L. and M.R.P. provided materials. M.T.-L., S.M.-G., P.E.-F., Z.L., O.M.-M., M.R.P. and F.A. designed the experiments, analyzed the data, and wrote the paper.

Competing interests

The authors declare no competing interests.

Additional information

Supplementary information is available for this paper at https://doi.org/10.1038/s42003-020-01182-y.

Correspondence and requests for materials should be addressed to M.T.-L. or F.A.

Reprints and permission information is available at http://www.nature.com/reprints

Publisher's note Springer Nature remains neutral with regard to jurisdictional claims in published maps and institutional affiliations.